The effect of kimberlite weathering on the behaviour of waste material at Cullinan diamond mine, South Africa.

J Strydom
21212627

Dissertation submitted in fulfillment of the requirements for the degree *Magister Scientiae* in Environmental Science at the Potchefstroom Campus of the North-West University

Supervisor: Prof MS Coetzee
Assistant supervisor: Dr PW Wade

January 2015

DISCLAIMER

Although all reasonable care was taken in preparing these reports and plans, the North-West University (NWU) and/or the sender is not responsible for the detail information with respect to dates, alterations, roads, boundaries, urban and rural developments, mining activities, change in site conditions or whatever. The integrity of this report and the University and/or sender nevertheless do not give any warranty whatsoever that the report is free of any mis-interpretations of national or Provincial Acts or Regulations, with respect to environmental and/or social issues. The integrity of this communication and the University and/or sender do not give any warranty whatsoever that the report is free of damaging code, viruses, errors, interference or interpretations of any nature. The University and/or the sender do not make any warranties in this regard whatsoever and cannot be held liable for any loss or damages incurred by the recipient or anybody who will use it in any respect. Although all possible care has been taken in the production of the reports, maps and plans, NWU and/or the sender cannot take any liability for perceived inaccuracy or miss-interpretation of the information shown on these plans and maps.

ACKNOWLEDGEMENTS

There are so many “THANK YOU’S” due upon completion of this dissertation but none more than to my Creator, who kindly blessed me with the capabilities and strength to do so when I did not see it possible.

To my supervisors, who guided with respect, encouraged without pressuring, invested valuable time and enthusiastically believed in me.

To my friends, for sharing their experiences, giving words of advice and always finding the time to pick me up when motivation was lacking. In particular I have to single out Angelika Möhr and Chanté Venter.

To each and every member of my dear family, for their interest, support and understanding, when visits were few and far between.

Also to Petra Diamonds and the Cullinan mine for providing financial support to the project. To staff members, Anja van Deventer and Jaco du Toit, for their friendly reception, help and patience with the sampling. In addition, to every researcher, technician and analyst mentioned in the text, without whom there would have been no dissertation.

Lastly I would like to express deep gratitude to Willem Fouché, for every late night discussion, bouncing around ideas, suggestions, support, constant inspiration and just being there.

ABSTRACT

Water quality and space constraints have become major concerns regarding the No. 7 waste water dam at Petra Diamonds' Cullinan mine. The unique location of the dam constrains further development, while unsustainable accumulation of waste water inside the dam increases the risk of potential environmental contamination from seepages and spillages. The dam retains a significant amount of very poor quality water. Its excessively high pH, dissolved salt content, density and extreme turbidity result from the concentration of natural weathering products of the diamond bearing kimberlite ore. The turbidity results from the dispersion of colloidal chlorite, saponite and nontronite clay. Along with the chemistry of the solution, their colloidal shape contributes equally significantly to the non-settlement of these suspended clays. Flocculation of the dispersed clay particles will provide (a) for easy and effective separation of the clay material from the waste water and (b) more convenient options for water treatment (and subsequent redistribution)

This study was aimed at contributing to a better understanding of the dynamic interactions in the No 7 Dam system to contribute towards identifying a suitable means/method for chemical flocculation of the clay particles. The individual components of the system (clays, water quality) and influx contributors (kimberlite and its leachate) were systematically characterized by means of X-Ray Diffraction, X-Ray Fluorescence, petrographic microscopy, electron microscopy, electrophoretic mobility and standard water- and soil quality analyses. The baseline quality of the Cullinan kimberlite leachate was obtained based on ASTM D5744 principles.

It was found that adjusting the pH-level and ionic strength of the waste water to the critical coagulation point (c_K) (as determined by electrophoretic mobility and batch jar experiments) automatically induced coagulation. Higher valence cations were displaced from pH dependent surface charge sites by proton adsorption. The resultant increased ionic strength, in combination with decreased thickness of the ionic double layer, was sufficient for the automatic initiation of high strength disordered face-face and edge-face bonds. During batch Jar tests, flocculation initiated within 4 minutes after the addition of HCl (0.5 M) and total sedimentation completed within 3 hours. The use of commercial flocculants might decrease the sedimentation time. As expected a significant increase in dissolved salt content of the clear supernatant was observed. No re-dispersion of the dried clay occurred.

Throughout the study geochemical modeling was performed with PHREEQC software to identify/determine possible effective experimental conditions, minimizing experimental time and expenses. The program was also used to model outcomes of the possible water treatment options, indicated in literature as viable options for similar situations. These options can be tested to extend upon the current research.

KEY TERMS

Cullinan kimberlite, kimberlite weathering, Cullinan No 7 Dam, clay mineral, suspension, dispersion, coagulation, flocculation, wastewater quality, high humidity leaching, zeta potential.

UITTREKSEL

Die waterkwaliteit en ruimtelike beperkinge rakende die No 7-Dam vir mynafvalwater van Petra Diamonds se Cullinan-myn, is kommerwekkend. Die plasing van die dam beperk verdere ontwikkeling van die myn, terwyl onvolhoubare akkumulasie van mynafvalwater in die dam die risiko wat potensiële verhoogde omgewingsbesoedeling deur sypeling en storting kan inhou. Die dam stoor ‘n groot hoeveelheid swak kwaliteit water. Die uiters hoë pH, opgeloste soutinhoud, digtheid en troebelheid is die gevolg van die konsentrasie van natuurlike verwerinsprodukte van die diamant-draende kimberliet-ertsliggaam. Die troebelheid is ‘n gevolg van dispersiewe kolloïdale chloriet-, nontroniet- en saponietkleiminerale in suspensie. Beide die chemie van die stelsel en die spesifieke vorm van die kleideeltjies gee aanleiding tot sodanige dispergering. Flokkulasie van die gesuspendeerde kleipartikels sal bydra tot (a) effektiewe skeiding van die kleimateriaal en (b) meer gepaste moontlikhede vir waterbehandeling en daaropvolgende herverspreiding.

Hierdie studie was daarop gemik om by te dra tot ‘n beter begripvan die dinamiese interaksiesin die stelsel van die No 7 Dam en om sodoende ‘n geskikte manier/metode vir die chemiese flokkulasie van die kleideeltjies te identifiseer. Die individuele komponente van die damstelsel (klei en water) asook die komponente wat bydra tot invloei in die damstelsel (kimberliet- en loogwater afkomstig van kimberliet), is sistematies gekarakteriseer met behulp van X-straaldiffraksie en -fluoressensie, petrografiese mikroskopie, elektroforetiese mobiliteit, elektronmikroskopi, standaard water- en grondkwaliteitanalises. Basislyn loogwaterkwaliteit van die Cllinan kimberliet is verkry gebasseer op ATSM D5744-beginsels.

Daar is gevind dat die aanpassing van die pH-vlak en ioonsterkte van die mynafvalwater tot by die kritieke koagulasiepunt (c_K), soos bepaal deur elektroforetiese mobiliteit en ‘n stel kleinskaalse houer-eksperimente, flokkulasie outomaties bewerkstellig. Hoër valensie katione is vervang by vanaf pH afhanklike vervangingsposisies op die oppervlakareas van die kleiminerale deur proton-adsorpsie. Die gevolglike verhoogde ioonsterkte van die oplossing, in kombinasie met afname in dikte van die ioniese dubbele laag, was voldoende om die outomatiese inisïering van ho-sterkte ongeordende platvlak-tot-plavlak en rand-tot-platvlak aantrekking tussen die kleideeltjies te bewerkstellig. Gedurende die stel kleinskaalse houertoetse, is flokkulasie reeds binne vier minute na die toevoeging van HCl (0.5 M) waargeneem en totale sedimentasie binne drie uur voltooi. Na verwagting sal die gebruik van kommersiële flokkulante hierdie sedimentasietyd verminder. Soos verwag was daar ‘n beduidende toename in opgeloste sout-inhoud van die helder bowater. Geen her-dispergering van die gedroogde klei het plaasgevind nie.

Gedurende die studie is geochemiese modellering met PHREEQC sagteware aangewend om effektiewiteit van eksperimentele toestande te evalueer asook eksperimentele tyd en kostes te verminder.

SLEUTEL WOORDE

Cullinan-kiemberliet, kimberliet verwering, Cullinan No 7-dam, dispersie, koagulering, flokkulering, stortingswater-kwaliteit, hoëhumiditeitsloging, zetapotensiaal.

Contents

LIST OF TABLES

LIST OF FIGURES

LIST OF ABBREVIATIONS

Å	Angstrom
AEC	Anion Exchange Capacity
B	Leaching factor
BIC	Bushveld Igneous Complex
C.I.	Contamination Index
CEC	Cation Exchange Capacity
c_K	Critical coagulation concentration
COLE	Coefficient of linear extensibility
Cpht	Carats per hundred tonnes
DDL	Diffuse Double Layer
DFK	Diatreme facies kimberlite
DI	De-ionized
EC	Electrical conductivity
E_H	Redox potential
ESP	Exchangeable Sodium Percentage
Ha	Hectare
HFK	Hypabyssal facies kimberlite
HHAWK-test	High Humidity Accelerated Weathering Kinetic test
HSF	High field strenght
JST	Tailings sample site
K_{sp}	Solubility products
L_D	Length of the bar of clay when air dried
L_M	Initial length of the bar of clay at plastic limit
LOI	Loss On Ignition
MARID	Mica-amphibole-rutile-illmenite-diopside
Mt/a	Million tonnes per annum
Nm	Nano meter
NNP	Net neutralisation potential
PL	Plastic Limit
PSD	Particle size distribution analysis
Pzc	Point of zero charge
Px	Pico meter
REE	Rare Earth Element
SAR	Sodium Adsorption Ratio
SEM	Scanning Electron Microscopy
SI	Saturation Index

TEM	Transmission Electron Microscopy
TFK	Transitional facies kimberlite
TDS	Total Dissolved Solids
TSS	Total Suspended Solids
USGS	United States Geological Survey
WDXRF	Wavelength dispersive X-Ray Fluorescence
XRD	X-Ray Diffraction
XRF	X-Ray Fluorescence
ε	Dielectric constant
U_E	Electrophoretic mobility
ζ	Zeta-potential
η	*Viscosity*

LIST OF EQUATIONS

CHAPTER 1

AN INTRODUCTION

1.1 THE OPERATIONS AT CULLINAN

Diamonds were discovered in the Cullinan area in 1902 and open cast mining started in 1903. Intermittent mining continued, dictated by economic fluctuations, but has not paused since underground mining commenced in 1950 (Field *et al*., 2008). The mine is currently operated by Petra Diamonds who took over in 2008. In 2009 the 507 carat Cullinan Heritage diamond was retrieved - a perfect example of the world class gem quality diamonds the Cullinan mine is known for. More than 750 diamonds larger than 100 carats have been produced since mining first started. In 1905 this mine supplied the largest ever found 3 106 carat Cullinan Diamond, from which, amongst other, the Great Star of Africa and Lesser Star of Africa were cut. These are displayed in England's crown jewels. The Cullinan mine is also a substantial supplier of particularly rare blue diamonds.

Diamonds are carried to mineable depths in about 10% of all kimberlite pipes (Janse & Sheahan, 1995). At Cullinan the surface area of the pipe was 32 ha – the biggest pipe, to date, to be found in South Africa. After more than a century it is currently being mined at a depth of 747 m and the surface area of the pipe is now about 16 ha. An expansion plan called the C-Cut project (see Figure 1), aimed at increasing production to 4 million tonnes per annum (Mt/a), should be fully implemented by 2019 as there are an estimated 430 million tonnes of resource available (including waste dumps) that will keep the mine operative for another 50 years (Petra Diamonds Limited, 2014). The mine aims at delivering an overall diamond grade of 50 carats per hundred tonnes (cpht) (currently at 36) (Tasse, 2012). Over the years the diamond grade has varied from 40 to 80 cpht with early reports as high as 170 cpht, which Williams (1932) ascribed to significant surface enrichment.

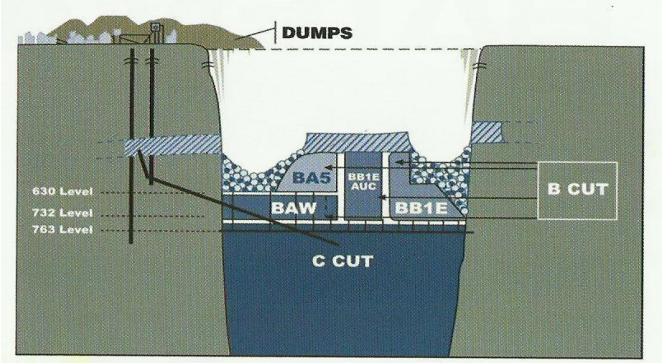

Figure 1: Blocks that are currently being mined and the relative location of the C-cut phase (Tassel, 2012)

Before it is brought up to the processing plant, the mined material is reduced to < 250 mm size at one of two underground jaw crusher stations. It is then conveyed and hoisted to the 27 ha (footprint) plant where crushing continues and state-of-the-art flow-sort X-ray machines contribute to the recovery of the diamonds. The waste material from this process is thereafter deposited on the waste dumps, and the waste water pumped into the adjacent No. 7 waste water dam as shown in Figure 2.

Once exposed to surficial conditions, the kimberlite ore rock weathers relatively quickly. Morkel (2006) states that: “some kimberlites can be totally reduced to fines within minutes of contact with water while others are not prone to weathering degradation at all”. Both physical and chemical mechanisms of weathering influence the breakdown of kimberlite in the mining process and naturally. Smectite group clay minerals are known to form as weathering products. In conjunction with physical slaking, the swelling capacity of these clay minerals also contributes to the rate of kimberlite weathering (Morkel, 2006).

Figure 2: The Cullinan operations as seen from above showing the relation of the open pit to the larger No 7 wastewater dam (Courtesy of Adele Schoeman, 2013)

1.2 PROBLEM STATEMENT

The No 7 Dam has an approximated total volume of 80,000,000 m ^{3} (Miller, Van Den Bossche & Slogrove., 2008) and is close to reaching its maximum capacity. With the planned increase in

production, space for waste water disposal has become a major concern for the mine. To sustain the life of mine 33,000 m^3 of space in the dam is needed (Van Deventer, 2014). In its current state, only an estimated 17 % of the water in the dam, located in the top 5 m of the profile, can be reused in the mining process (Miller *et al.,* 2008). The reason the bulk of the water is unavailable, is due to an unusual change in density of the water below 5 m because of the accumulation and stabilization of the suspended fine clay minerals resulting from the weathering of the kimberlite. Dewatering of the No 7 Dam will provide much needed waste material storage space and potentially supplement surface water resources. South Africa is considered to be a water-stressed country with an average of 1100 m^3 of water available per person per year (DEAT, 2006) (<1000m^3/person/annum is considered water scares). Currently the country relies mostly on surface water sources, although, groundwater consumption is drastically increasing as the surface resources are becoming more susceptible to pollution (Eby, 2004) and the demands of various industries and different socio-economic settings increase (i.e. mining, agriculture, rural developments). Approximately only 50 % of the water required by urban and industrial sectors in South Africa (including mining) is re-used in the various processes as an attempt at more sustainable water management (DEAT, 2006).

Dewatering of the No 7 Dam is inhibited by the stability of the dispersed suspension. Such clay - water suspensions, are complex systems in which the clay minerals present as well as the solutes in the water play a role in isomorphic substitution (in tetrahedrons and octahedrons of crystal structures) and sorption reactions (adsorption, surface precipitation and polymerization) occurring between the solid phases and the solution (Sparks, 2003).

In 2012 the mine initiated a research project in collaboration with the NWU to characterize the kimberlite, the tailings, and the No 7 Dam to contribute to a functional understanding of the integrated geochemical interactions within the system (No 7dam) and with its surrounding environment (the mine). This understanding can then ultimately be applied toward effectively separating the suspended fines from the solution and mitigating the abovementioned concerns.

Ideally clarification of the water would be achieved by coagulation and flocculation as is common in the treatment of waste water. Gilchrist & Hunt (1988) proposed the combination of lime and a commercial anionic polymer in a two stage process to clear kimberlite process water while both Van Deventer (2003) and Potgieter & Green (2006) have experimented with gypsum ($CaSO_4 \cdot 2H_2O$) to ameliorate the observed dispersion. Gypsum is widely used to rehabilitate dispersive soils due to the formation of leachable Na_2SO_4.(thenardite) The approach of Van Deventer (2003) focussed on stabilizing the tailings to establish vegetation while Potgieter & Green (2006) tested gypsum in combination with commercial flocculants to ameliorate the high turbidity of the No 7 Dam water caused by the dispersed fine clay. It was found that long

residence times were needed for sufficient clarity but it could be improved if a second dose of gypsum was applied shortly after the first or by adding more gypsum. This increased the costs of treatment and caused excessive algal growth to occur the second day after treatment. The water qualities after these treatments were questionable, however, as no analyses were reported.

In addition, the waste material produced by the mine, is high in dissolved salt load. Janse van Rensburg & van Blerk (2007) found elevated levels of dissolved SO_4^{2-}, Na^+ and F^-, and suggested a geochemical study of the ore. Na^+ is easily dissolved from primary minerals because of its affinity for water (forming NaOH) and is known to be a major cause of dispersion in soils. Na-solutions are omnipresent in the weathering environment at the surface of the earth (Puntis & Ruiz-Agudo, 2013). Sparks (2003) stated that Na^+ often becomes the dominant ion in soil solutions due to its replacement by exchangeable Mg^{2+} and Ca^{2+} on the exchange phase. The Na^+-ion, also has a smaller enthalpy of hydration than, for instance K^+, therefore more energy is released during ionisation, which means the Na^+-ion can for more easily (Ma, Bruckard &McCallum, 2012). The effect of various cation-anion combinations on the flow behaviour of homogeneous, laboratory prepared clay slurries are studied especially for its application to industrial and ceramic processes. This study will investigate the application of some of these principles with regards to the natural heterogeneous No 7 Dam suspension.

1.3 RESEARCH OBJECTIVES

The aim of this research was therefore to:

(1). Develop an understanding of the cause of dispersion and non-settlement of the fines.

(2). Develop a laboratory treatment for the No 7 Dam suspension based on (1).

These aims were achieved through the following objectives, which systematically guided the research and methodology (see Figure 3) from macroscopic to microscopic scale:

- Characterize the kimberlite (mineralogically and geochemically).
- Characterize the tailings material.
- Characterize the suspended clays in No 7 Dam.
- Establish baseline kimberlite - and tailings material leachate water quality.
- Characterize the current water quality of No 7 Dam.
- Identify and test the ideal coagulant/flocculants based on the specific mineralogy and geochemistry of the system.
- Characterize water quality after the flocculation.
- Characterize the flocculated clay material.

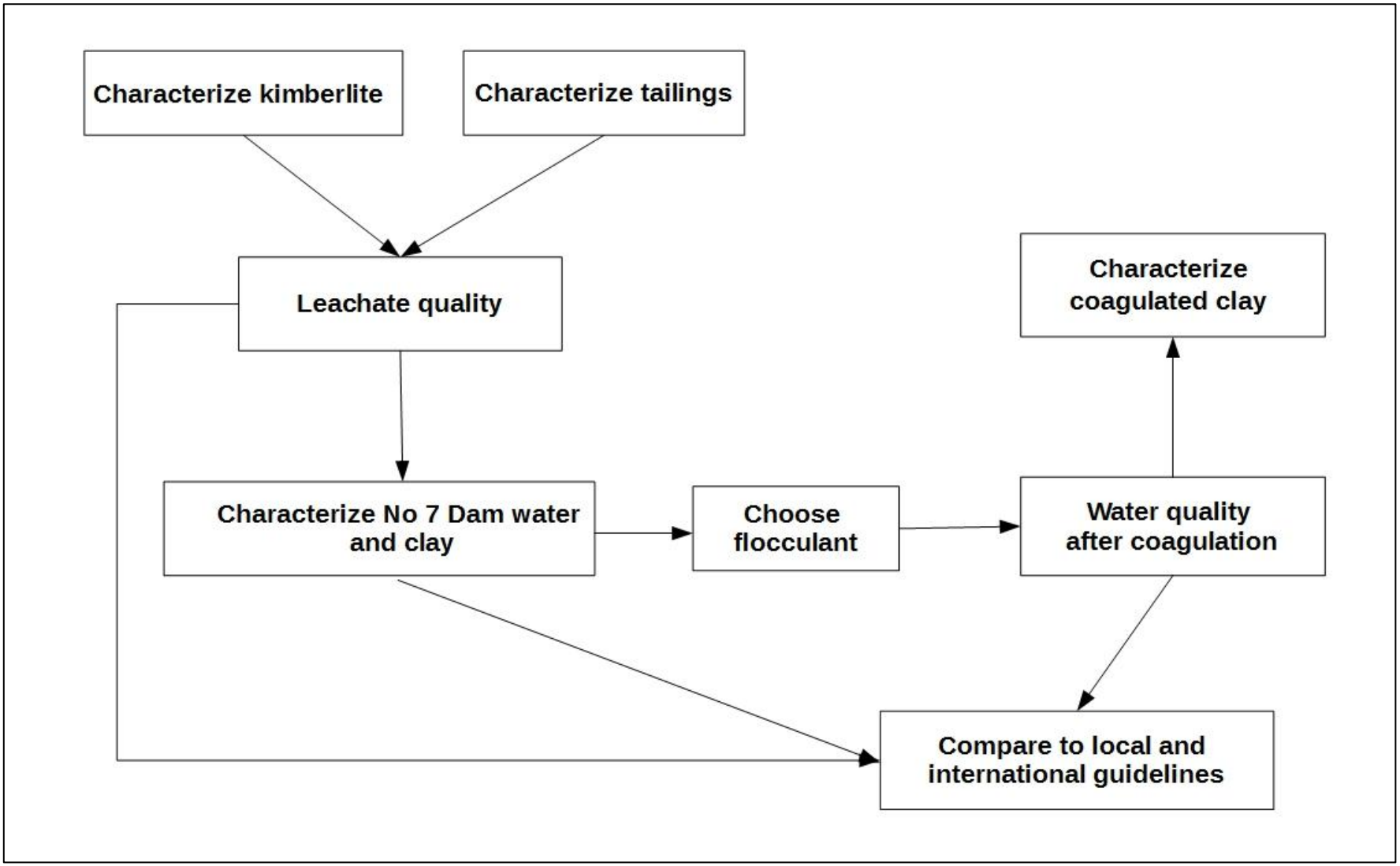

Figure 3: A systematic research design followed to achieve the objectives of the study.

1.4 ORIGINAL HYPOTHESIS

The basic hypothesis constitutes that smectite clay minerals, form as weathering products of the Cullinan kimberlite, whereby this process elevates the sodium content of the waste water. Interparticular repulsive forces between the clay particles, in combination with high sodium levels, influence non-settlement of the dispersed fines at the No 7 waste water dam. A suitable coagulant/flocculent will be dictated by the chemistry of the system and could have a significant effect on the composition of both the clay and treated water that can be retrieved from the dam.

1.5 LIMITATIONS TO THE PROJECT

The scope of this project does not include environmental law and regulations of South Africa nor any other, regarding the management of waste material or water and the disposal thereof. The study is not concerned with any form of environmental monitoring. No distinction and/or comparison are made between No 7 Dam water sampled in succeeding years of the study.

1.6 JUSTIFICATION

Many advantages come from understanding the natural weathering process of kimberlites – one being effective management of waste material and waste water. For example, rehabilitation of kimberlite tailings is challenging due to the osmotic effect induced on plants by high levels of salt. At the high pH-levels observed, certain element deficiencies (such as Fe, Mn, Zn, and Cu) can also potentially occur (Van Deventer, 2003). The need and value of the research therefore is in its application. Once the origin of the above mentioned problems is determined, one can work towards effectively mitigating and managing it.

CHAPTER 2

HISTORIC AND GEOGRAPHIC BACKGROUND OF THE STUDY SITE

This chapter is an assimilation of literature on the Cullinan kimberlite pipe and the wastewater dam associated with the mining of the pipe. The general composition of kimberlites is summarised followed by an overview of the mineralogy and geochemistry of the specific pipe. The setting and underlying geology of both the pipe and the wastewater dam is then investigated.

2.1 A DEFINITION OF KIMBERLITE

Diamond-bearing igneous rock was first identified in South Africa and named after the town Kimberley, where several diamondiferous kimberlite pipes were discovered (Wagner, 1914). The mineralogy and geochemistry of kimberlite can be complex and are pipe specific because of the many variables contributing to its formation including significant influence (contaminations) from the surrounding rocks and groundwater (Mitchell, 1986).

Comparing various definitions of kimberlite, (Mitchell, 1986; Lapidus & Winstanley, 1990; Winter 2001; Skinner & Truswell, 2006; Field *et al.*, 2008) there are some requirements for an intrusive body to be classified as a kimberlite - the classic carrot-shape of the diatreme not being one of them. Kimberlites also occur as dykes or sills.

Kimberlite is a volcanic to hypabyssal ultrabasic rock (< 45 % silica content) that originates from volatile rich (high content of CO_2 and H_2O) magma, which ascends to the Earth's surface at speeds up to 30 km per hour (Eggler, 1989) *from more than 150 km* (Weisburd, 1986) *deep within the mantle where the pressure and temperature conditions are favourable for diamond formation. It ultimately requires an ultramafic composition, meaning more than 90 % of the mineral content is magnesium- and iron rich, but also specifically potassic composition (high K_2O). Phenocrysts (commonly olivine), xenocrysts, and some wall rock xenoliths should be contained in a fine grained matrix. The xenoliths are often also ultramafic in composition – specifically what is known as the MARID (mica-amphibole-rutile-illmenite-diopsite) suite of minerals in Group 1 kimberlites. Apart from olivine (as major component) variable amounts of phlogopite, monticellite, ilmenite, spinel, garnet, serpentine, melilite, apatite, perovskite, ortho- and clinopyroxene, as well as carbonate (calcite) are present.*

Typically the carrot-shaped pipe, or diatreme zone, containing angular xenoliths and often also xenocrysts originates from a hypabyssal feeder dyke, or root zone, with less crustal contamination, and therefore a more crystalline texture, with a more primary ultramafic composition. An upper crater zone, consisting of a tuff ring including lithic fragments, is rarely preserved due to ease of weathering and consequent erosion (see Figure 5 below for an illustration).

2.2 GEOLOGICAL SETTING

The Cullinan pipe outcrops in the Pretoria Group of the Transvaal Supergroup, 25 km east north-east of Pretoria. This post-Waterberg pipe was dated at approximately 1150 Ma (Wu *et al.*, 2013) and is part of 11 diatremes associated with a series of nepheline syenite, trachyte and carbonatite intrusions (Frick, 1970; Dawson, 1980) which concluded the set of events that formed the Pilanesberg Alkaline Province (Verwoerd, 2006). Many authors have associated its emplacement with the major north north-west to south south-east Precambrian fracture system, namely the Franspoort Line, of the Pienaar's Rivier Subprovince (Skinner & Truswell, 2006) which is illustrated in Figure 4. However, the Cullinan pipe is the only one to be diamondiferous.

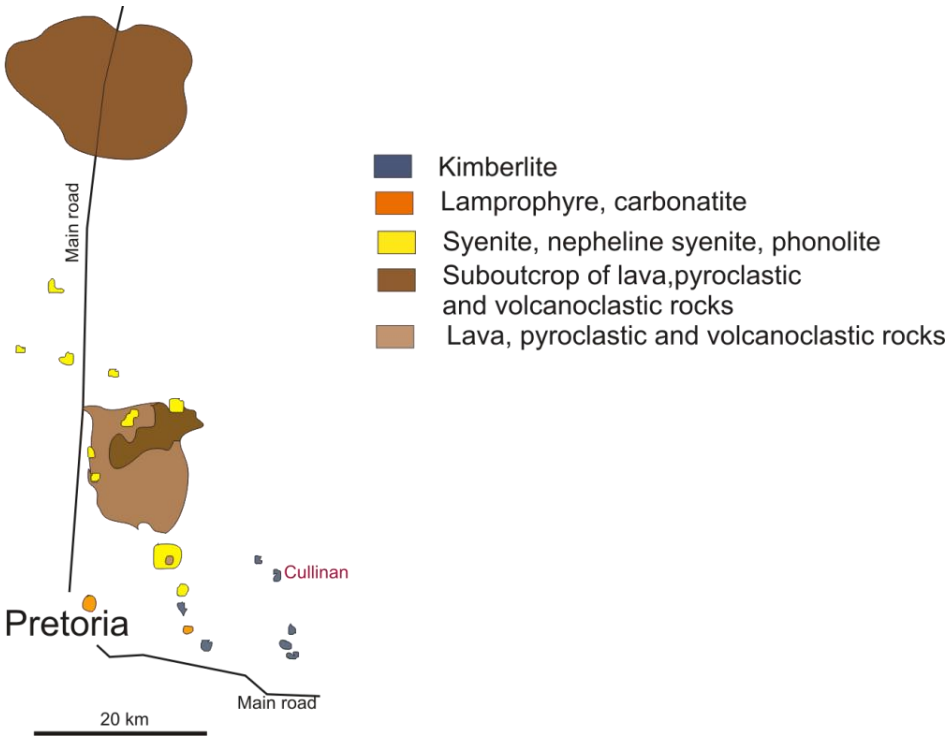

Figure 4: Alkaline complexes associated with the Pilanesberg series of events. Note that Cullinan, in the bottom right was one of the last events in this series (modified after Verwoerd, 2006).

At surface, the pipe is fairly oval shaped with a minor constriction slightly off-centre to the east (see Figure 5). Early on it was recognised that more than one intrusion contributed to the diatreme (Frick, 1970; Dawson, 1980). Frick (1970) recognised four textural-, twelve colour- and three petrographical variations that resulted from four separate intrusions (see Table 1). First, a highly explosive phase, representing the kimberlite in the western and eastern parts of the pipe, followed by less explosive phases, and finally the intrusion of unexplosive veins. An unpublished study by Wiethoff (2000) argued proof for a similar source of the different types of kimberlite.

Table 1: Geology of the Cullinan pipe as classified by (a) Frick (1970), (b) Bartlett (1998), and (c) Skinner & Marsh (2004).

	GENERAL DESCRIPTION	***EMPLACEMENT***
Group I [a] **(*Grey Kimberlite*** [b]**)** **(*DFK** [c]**)**	• Generally grey • High wall rock inclusion • High primary phenocryst content • Low diamond content	Highly explosive, first phase of volcanism.
Group II [a] **(*Kimberlite dykes*** [b]**)**	Only matrix material and no diamonds. (Carbonatite dykes or Massive basaltic kimberlite)	Last phase of volcanism. Placid emplacement.
Group III **Eastern** [a] **(*Brown*** [b]**,) kimberlite (*DFK** [c]**)** **Western** [a] **(*Black*** [b]**) Kimberlite** **(***HFK-**TFK-*DFK** [c]**)**	• Most common in Cullinan pipe • Highest phenocrystal - and diamond content • Unconnected eastern and western kimberlite (contains ultramafic nodules)	Formed “two bulges” of pipe. Injected into solidified group I (indicated by sharp contact).
Group IV [a]	• More wall-rock inclusions and matrix material • Contains some diamonds • Altered (bleached) by intrusion of carbonatite dykes	

*Diatreme facies kimberlite

**Transitional facies kimberlite

***Hypabyssal facies kimberlite

As Bartlett (1998) divided the diatreme facies of Cullinan kimberlite into grey, brown and black, the hypabyssal facies were sub-divided into dark piebald, pale piebald and black by Wiethoff (2000). Skinner (2000) indicated a transitional phase towards the diatreme, based on significant petrographic changes observed.

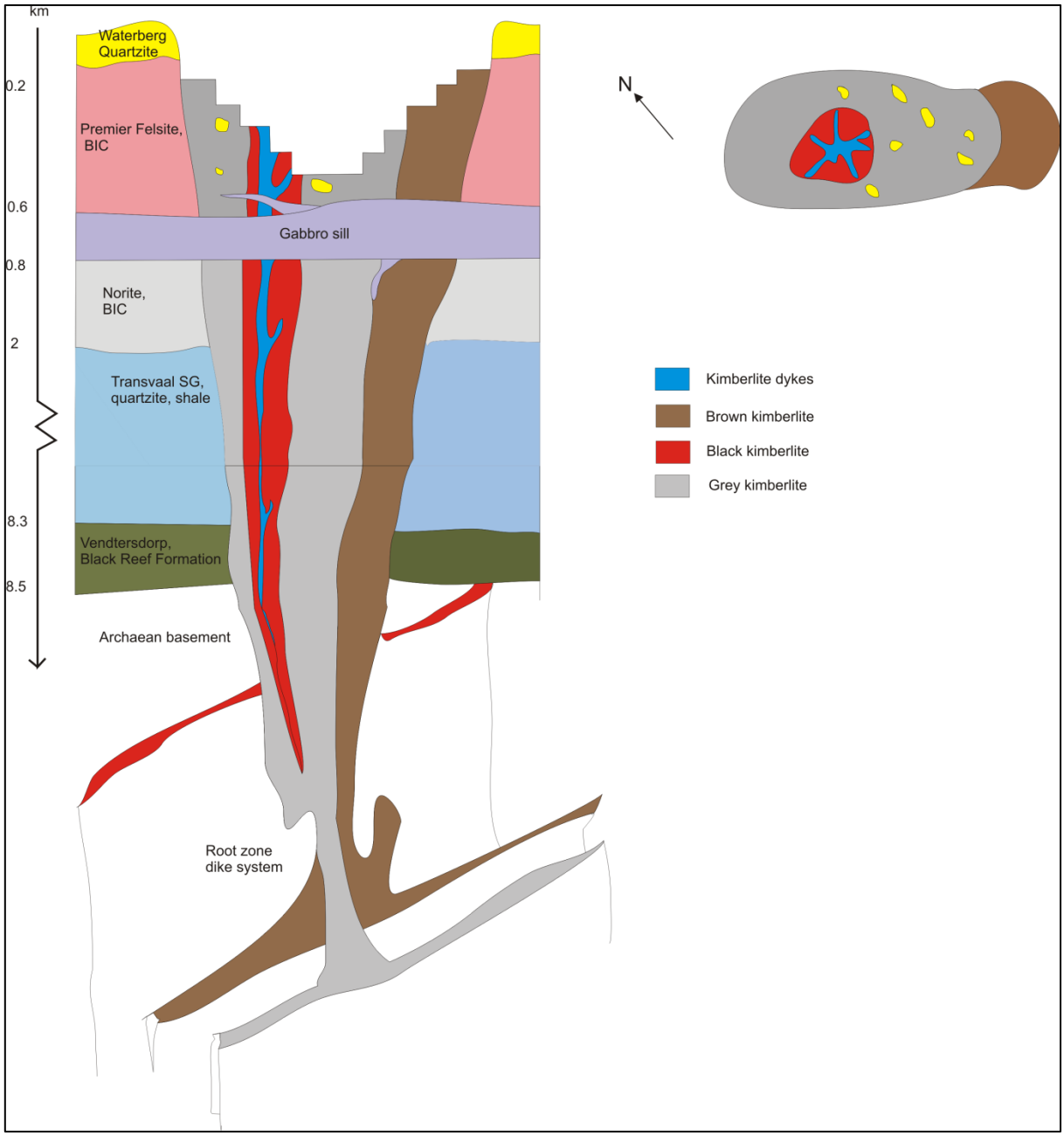

Figure 5: An illustration compiled from Field *et al.* (2008), Frick (1970) and Mitchel (1986) relating the various types of kimberlite as well as the country rock surrounding the Premier pipe. On the right, a plan view is shown. BIC = Bushveld Igneous Complex.

2.3 MINERALOGY

The scope of this study does not include differentiation between the mineralogy of the kimberlite varieties of the pipe. Therefore, Table 2 lists and summarizes the minerals present in all varieties.

Morkel (2006) found mica > chlorite > magnetite > talc > amphibole to be major contributing minerals. Serpentine and pyroxene both contributed < 10 % (mass %) while smectite, olivine and quartz each contributed < 5% to the Cullinan kimberlite composition.

2.4 GEOCHEMISTRY

Being classified as a Group I kimberlite means its Sr-Nd isotopic signatures hint at asthenospheric mantle (Skinner & Truswell, 2006; Becker & Le Roux, 2006) as it is slightly depleted in Sr and enriched in Nd compared to the bulk composition of the earth (Field *et al.*, 2008). Group I kimberlites are considered to be volatile-rich and have primarily olivine as matrix mineral. According to Becker & Le Roux (2006) Group I kimberlites are inclined to higher TiO_2, CaO and CO_2 but lower SiO_2 and K_2O content than Group II. There are also diagnostic differences in trace element and rare earth element (REE) ratios of the two groups, which were interpreted as indication of different source regions.

The Cullinan kimberlite shows some contamination from crustal rocks and/or groundwater, assimilated during the emplacement process. Frick (1970) found the kimberlite to generally be enriched in both sodium (Na) and potassium (K). Fesq, Kable & Gurney (1975) reported the Si/Mg ratio of the brown kimberlite facies as 1.56 and Mitchell (1986) calculated its contamination index (C.I.) as 2.02. The C.I. is an indication of the more felsic silicates (represented by Si, Al and Na content) in relation to olivine and phlogopite (represented by Mg and K content) (see section 3.5.1). Furthermore, Wiethoff (2000) determined that the C.I. decreased with depth, as the diatreme facies transitioned into the hypabyssal facies.

Trace elements in the kimberlites are either compatible (meaning similar to abundances in ultramafic rocks) or incompatible (similar to abundances found in alkaline rocks). Compatible trace elements (Sc, V, Cr, Co, Ni, Cu and Zn) are essentially hosted by spinels and olivine, and to a lesser degree by perovskite, sulphides and diopside (Mitchell, 1986). The incompatible trace elements represent a better overview of the whole-rock/over-all composition of kimberlite as these elements are only consumed in the later stages of crystallisation, *i.e.* the matrix. Phlogopite typically hosts Ba, whereas Sr, Th and U, as well as rare earth elements, can be hosted by phosphates (e.g. apatite) or alternatively titinates (mainly perovskite and ilmenite), which can also host Nb, Ta and Hf (Wiethoff, 2000).

Table 2: Summarised mineralogy of the Cullinan kimberlite from the detailed study by Frick (1970). The underlined minerals were identified as the dominating phases present of a particular mineral group.

MINERALS PRESENT (MICROSCOPY)		*CHEMICAL COMPOSITION*	*AS OBSERVED IN CULLINAN KIMBERLITE*	*ADDITIONAL NOTES*
Prominent in matrix	Olivine	<u>Fosterite</u> (Mg_2SiO_4) Fayalite (Fe_2SiO_4) <u>Monticellite</u> $(CaMgSiO_4)$	• As macrocrysts and phenocrysts and in the matrix • First and second generation phenocrysts are observed • Serpentinized and altered	Possible source of Ni or Mn
	Phlogopite	$KMg_3(AlSi_3O_{10})(F,OH)_2$	• Fine-grained primary phlogopite but secondary in the black kimberlite • Prominent in the matrix but few macrocrysts were observed	Source of F^-
	Serpentine	$(Mg,Fe)_3Si_2O_5(OH)_4$	• Prominent in the residual phase (matrix) • Occupies large areas between phenocrysts (sometimes replaced by secondary calcite) • Many metamorphic minerals (amphibole, diopside, hydroglossular) are contained within these areas • Primary or secondary	
	Perovskite	$CaTiO_3$	• Matrix mineral occurring mostly primary but also secondary in the black kimberlite	Could be rare earth element bearing as well as source of Na. $(Ca,Ce,Na)(Ti,Fe)O_3$
	Calcite	$CaCO_3$	• Primary calcite in residual phase of kimberlite. • Secondary calcite occurs within the matrix of the primary calcite field.	

Table 2 (*cont.*): Summarised mineralogy of the Cullinan kimberlite (Frick, 1970).

MINERALS PRESENT (MICROSCOPY)		*CHEMICAL COMPOSITION*	*AS OBSERVED IN CULLINAN KIMBERLITE*	*ADDITIONAL NOTES*
Mainly but not limited to macrocrysts and phenocrysts	Garnet	<u>Pyrope</u> $(Mg_3Al_2(SiO_4)_3)$ Almandine $(Fe_3Al_2(SiO_4)_3)$ <u>Glossular</u> $(Ca_3Al_2(SiO_4)_{3)}$	• Extensive alteration of primary garnet to light green hydroglossular (also almandine-rich) due to influence of tholeiitic (gabbro) sill • As phenocrysts and in matrix	Possible source of Cr and Ti
	Ilmenite	<u>Ilmenite</u> $(FeTiO_3)$ Geikielite $(MgTiO_3)$	• Often zoned in group I kimberlite • Rims of alteration products from outer rim to center – sphene, perovskite, leucoxene In metamorphosed kimberlite, parallel exsolution lamellae of hematite occur	
	Spinel	Spinel $MgAl_2O_4$ Chromite $FeCr_2O_4$ Magnetite Fe_3O_4	• In small amounts in matrix. • Measured unit cell dimentions rather indicate picotite and magnesiochromite • Small euhedral to subhedral grains in residual phase of kimberlite or peripheries of phenocrystal phase (especially olivine grains) • Some grains are rimmed by sphene • However, kimberlite is reported to be more enriched in spinel	
	Pyroxene	<u>Enstatite</u> $(MgSiO_3)$ Ferrosilite $(FeSiO_3)$ <u>Diopside</u> $(MgCaSi_2O_6)$ Acmite $(NaFeSi_2O_6)$	• No free orthopyroxene in Cullinan kimberlite • Only in peridotite and pyroxenite nodules • Clinopyroxene occur as primary phenocrysts and in ultramafic nodules • Eclogitic inclusions are enriched in jadeite • Microlitic diopside contributes to matrix as well	Clinopyroxene source of both Na^+ and K^+ as well as Cr

Table 2 (*cont.*): Summarized mineralogy of the Cullinan kimberlite (Frick, 1970).

MINERALS PRESENT (MICROSCOPY)		*CHEMICAL COMPOSITION*	*AS OBSERVED IN CULLINAN KIMBERLITE*	*ADDITIONAL NOTES*
Mainly but not limited to macrocrysts and phenocrysts	Pyroxene	Jadeite ($NaAlSi_2O_6$) Hedenbergite ($FeCaSi_2O_6$)		At higher pressure of formation, increasing Na and Al is incorporated in clinopyroxene (White, 1997)
	Apatite	$Ca_5(PO_4)_3(F,Cl,OH)$	• Mostly occurs in residual phase • Considerably more in group II kimberlite • Fluorine-apatite - last mineral to crystallize in phenocrystal phase	
	Pyrite	FeS_2	• Euhedral grains and minute grains in ultramafic nodules (but not eclogite) • Considered to crystalize fairly late in process by interaction of H_2S with volcanic gasses	
	Biotite	$K(Mg,Fe)_3AlSi_3O_{10}(F,OH)_2$	• Residual phase • Occupies large areas between primary phenocrysts with intergranular green chloritic material	
	Amphibole	Tremolite $Ca_2Mg_5Si_8O_{22}(OH)_2$	• Residual phase • Al product of thermal metamorphism (e.g. fibrous masses in serpentine matrix) • Also as coarse grained porphyroblasts	

2.5 BATHYMETRY OF THE NO 7 WASTEWATER DAM

The No. 7 Dam is located north north-east of the pit and is bordered by Cullinan to its south, the Refilwe township to its north and game farms owned by the mine to its west. Jacarandapark is to its east. It is located on geology of the Transvaal Supergroup; almost entirely on the Pretoria Group sediments with some diabase intrusion to the east as shown in Figure 6 below.

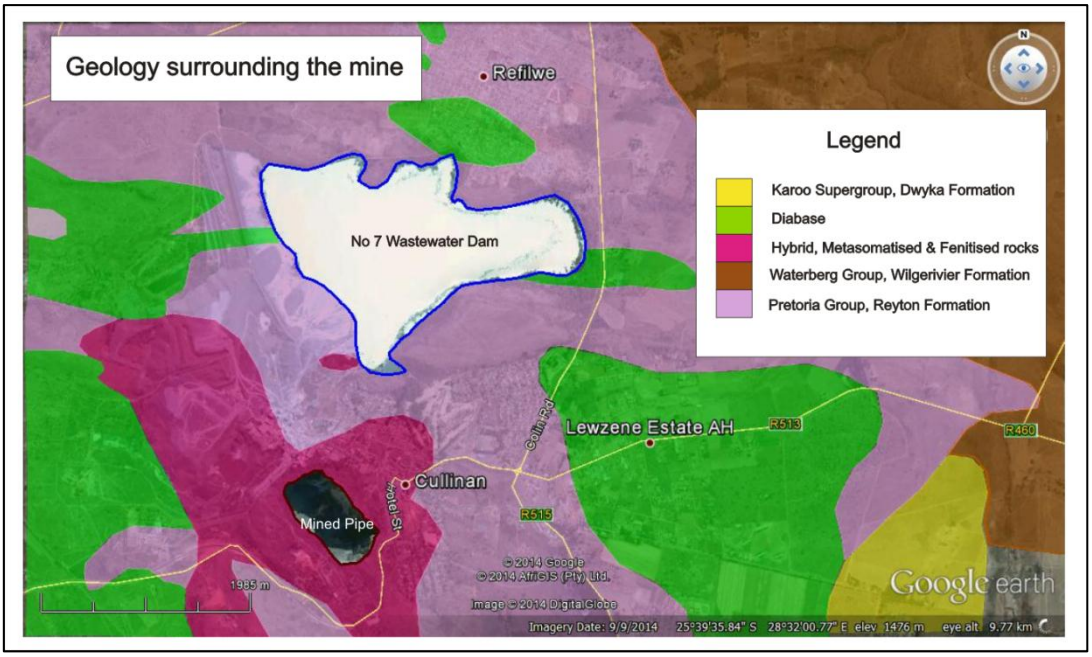

Figure 6: An aerial Google earth image, with superimposed geology, showing the location of the No 7 Dam in relation to the pit (bottom left) (Compiled with the assistance of Melissa Allert, 2014).

The No 7 Dam, as it can be seen today, resulted from a number of smaller tailings facilities merging from approximately 100 years of deposition. The 85 m high dam wall stretches for nearly 1200 m across the upper Premiermynloop valley adjacent to the Elands Rivier catchment area. The slurry of fine residue is pumped to the dam via a single pump station, while interval spray barring from spigot pipes builds along the length of the dam wall (Van Deventer, 2014, personal communication). A geophysical survey (see Figure 7) conducted in October 2008 by Marine Geosolutions (Miller *et al.,* 2008) estimated the total volume of the dam as 79,754,081 m^3. The valley floor was shown to be deepest, and closest to the current operational wall and pump station. The survey showed an isolated hill and V-shaped paleo-river channel. Five distinctive layers (horizontal stratifications) were observed in which density (as total suspended solids) increased with depth. In the top 5 m of the dam, one litre of sampled liquid contained12 g of solids. This increased dramatically to 200 to 300 g/L at depths from 10 to 28 m deep. The thickest accumulation of slimes layers can be seen closest to the point of deposition, suggesting larger particles settling out first. Various degrees of consolidation are observed, which make up an estimated 34 % of the volume of No 7 Dam.

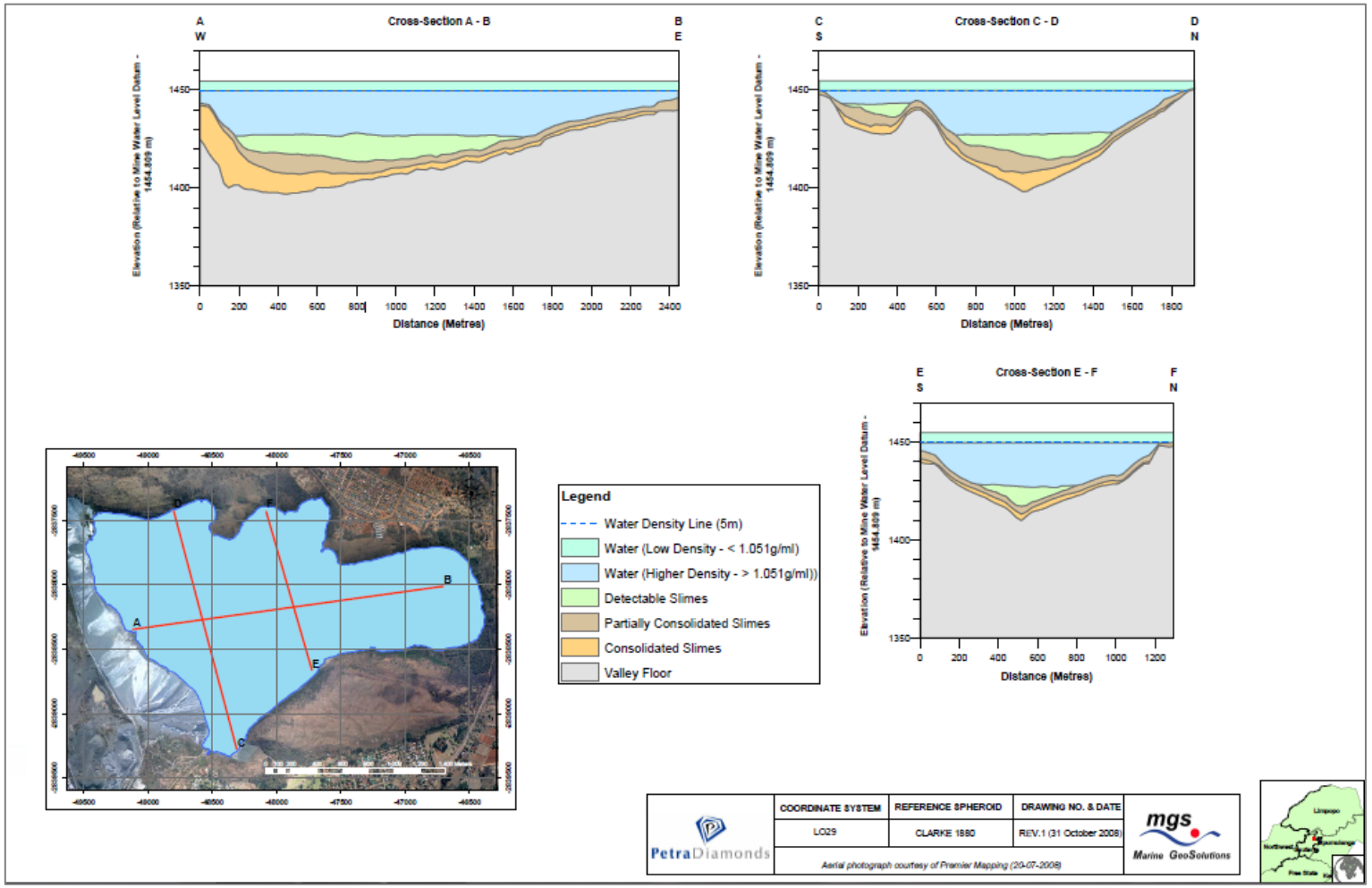

Figure 7: The depth profiles A-B, C-D, and E-F of the dam as geo-physically determined by Marine GeoSolutions in showing clear horizontal differentiation and consolidation in the deeper layers of the dam (Miller *et al.*, 2008). See text for discussion of the different profiles.

CHAPTER 3

THE INTERACTION OF KIMBERLITE WITH THE SURROUNDING AQUEOUS ENVIRONMENT

In this chapter some consequences of the interaction between the hydrosphere and lithosphere are considered. This interface is a dynamic and reactive environment sensitive to change. The chapter starts off by pointing out the influence of the lithosphere on the quality of water bodies, and progresses to ultimate end-products of these interactions, namely clay minerals. These minerals are of great value to Earth system processes due to their excessively large, charged, reactive surfaces. This chapter explores a number of the surface interactions of clay minerals, amongst which, the dynamics of dispersion.

3.1 WATER QUALITY AS A RESULT OF NATURAL WEATHERING

Chemical weathering, mainly driven by water, is the pre-dominant factor in the breakdown of rocks exposed at the Earth's surface. Brown & Calas (2011) stated that: *"The interfaces between mineral surfaces and aqueous solutions are the locations of most chemical reactions that control the composition of the natural environment, including the composition of natural waters."* Climatic conditions, environmental interactions (for example micro-organisms) and the parent material all control the rate of breakdown occurring at mineral surface contacts. When temperatures and annual rainfall are higher, weathering will be more intense.

The susceptibility of a mineral to dissolution is a function of both the solubility products (K_{sp}) of its ionic constituents (aqueous phase) at equilibrium with the mineral (solid), and its specific saturation index (SI). This means a mineral will continue dissolution until saturation (equilibrium between ions and mineral) is reached. The solubility product of a mineral is therefore an indication of the ease (larger value, closer to 0) or difficulty (smaller value, further from 0) to reach this equilibrium. On the other hand the saturation index (SI) indicates whether a mineral will dissolve (value < 0) or precipitate (> 0) by relating the ion activity product (often simplified to concentration) to the solubility product of the mineral in question. For example the SI of calcite will be calculated as follows:

$$SI_{calcite} = log\left(\frac{[Ca^{2+}][CO_3^{2-}]}{Ksp_{calcite}}\right)$$

Equation 1

Figure 8 shows the mineral groups considered by Brener & Brener (1996) as major contributors to the dissolved load (Ca^{2+}, Na^{+}, K^{+}, Mg^{2+}, HCO_3^{-}, SO_4^{2-}, H_4SiO_4) of surface water compositions. In open systems, such as the No 7 Dam, atmospheric gasses and rainfall are also minor contributors to the chemical composition of water bodies.

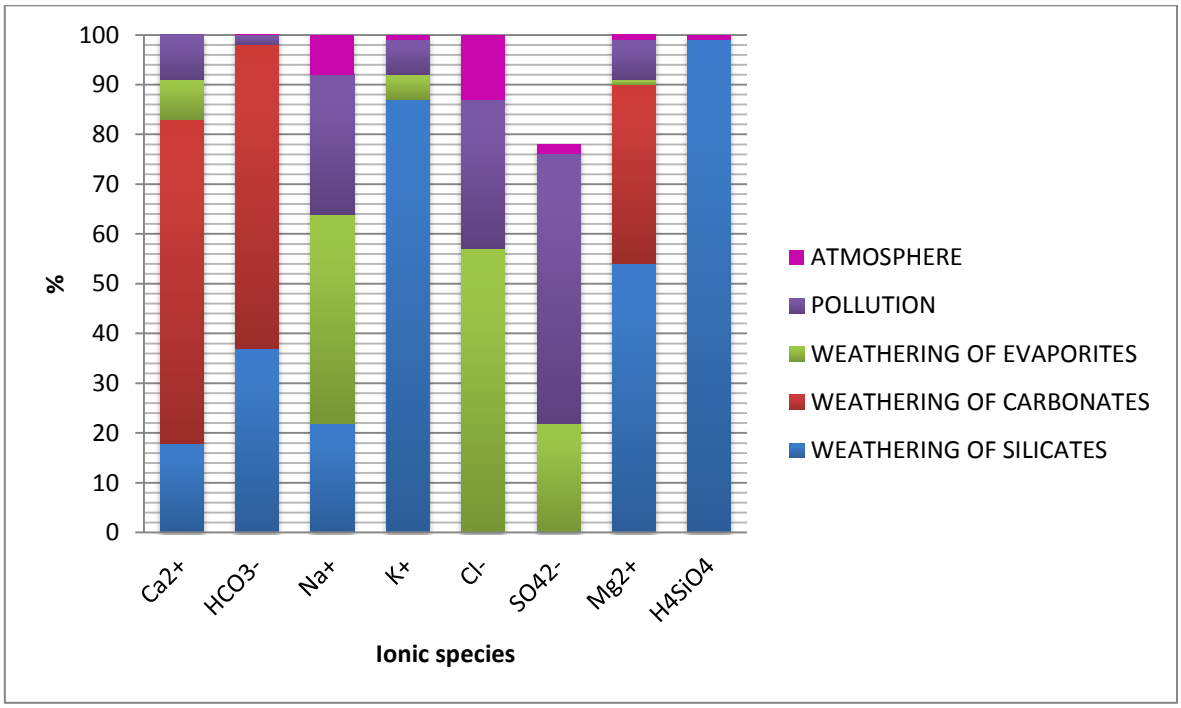

Figure 8: A representation of the relative percentages of dissolved components contributed to surface waters by mineral weathering.

Contamination or pollution of water resources can therefore appropriately be described as a result of the unnatural/artificial accumulation of constituents in the water body disregarding expected natural weathering. The 2007 South African state of the environment report (DEAT, 2007) lists salinity, water-borne diseases, low oxygen levels, eutrophication, suspended solids, hydrocarbons, acidification, solid litter, bioactive materials, herbicides, pesticides and radioactive contamination as the most pressing problems regarding the quality of water in the country. The main effects of the mining industry on local water quality was determined to be changes in pH, increased salinity and dissolved metals content, concentration of hazardous chemicals and increased sedimentation.

Water quality guidelines are set out by various regulatory bodies to indicate if the water resource is suitable for its desired application and to avoid possible negative effects that might result from its repeated use. It is, however, no simple feat to declare it as “good” or “bad”. The quality of the water is assigned relative to its application. Therefore guidelines can vary per application (see Table 14 for more detail).

The response to the removal of ionic compounds from rock into solution is unique for each mineral and system. This interaction is driven, firstly by the composition of the rock, and secondly by concentrations of the ions already dissolved in the solution (Velde, 1985). It has however been observed that alteration in the early stages of weathering of the parent minerals are not always the same (predictable) even in the same weathering profile (Velde & Munier, 2008).

Weathering often initiates at preferential pathways for solutions, including micro cracks, cleavages, inter-granular joints, crystal defect sites or crystal edges. Dissolution of primary rock-forming minerals increases porosity and preferential permeability of the rock, transforming it into a porous heterogeneous microcrystalline saprolite. Ultimate “collapse” of the saprolite exposes new mineral surfaces to the environment which once again changes the mineral-solution interaction equilibrium. Dissolved constituents will continuously diffuse or be transported away, promoting disequilibrium at the alteration interfaces. Weathering of primary minerals leads to the formation of secondary minerals resulting from either alteration or diagenesis i.e. direct precipitation from solution according to local physiochemical conditions.

These secondary weathering products are therefore also a function of both the parent rock and weathering solution as components are lost from or added to the system of concern. This is supported by the findings of Decarreau (1982) that, in laboratory conditions, saponites rapidly respond to their environment to closely approach chemical equilibrium within 20-60 days, retaining elements of the solution they were exposed to at the time of formation as opposed to timeous changes from one type of clay mineral to another.

Oxidation reactions as well as the congruent and incongruent dissolution of mineral compounds, by means of hydration or hydrolysis, are all mechanisms contributing to the chemical weathering of primary and secondary minerals.

- In oxidation reactions the oxygen readily accepts an electron from an element in reduced form, usually Fe or S.
- Incongruent solution leaves a solid/mineral with a different chemical composition as weathering product in that only some constituents will go into solution.
- When congruent solution occurs there will be no solid left over as weathering product as all ionic compounds go into solution.
- Complexation concerns reactions with organic components

In general the resistance to weathering increases from carbonates > primary silicates > clay minerals > oxides and hydroxides. Table 3 lists how some of these mechanisms affect a few selected common minerals.

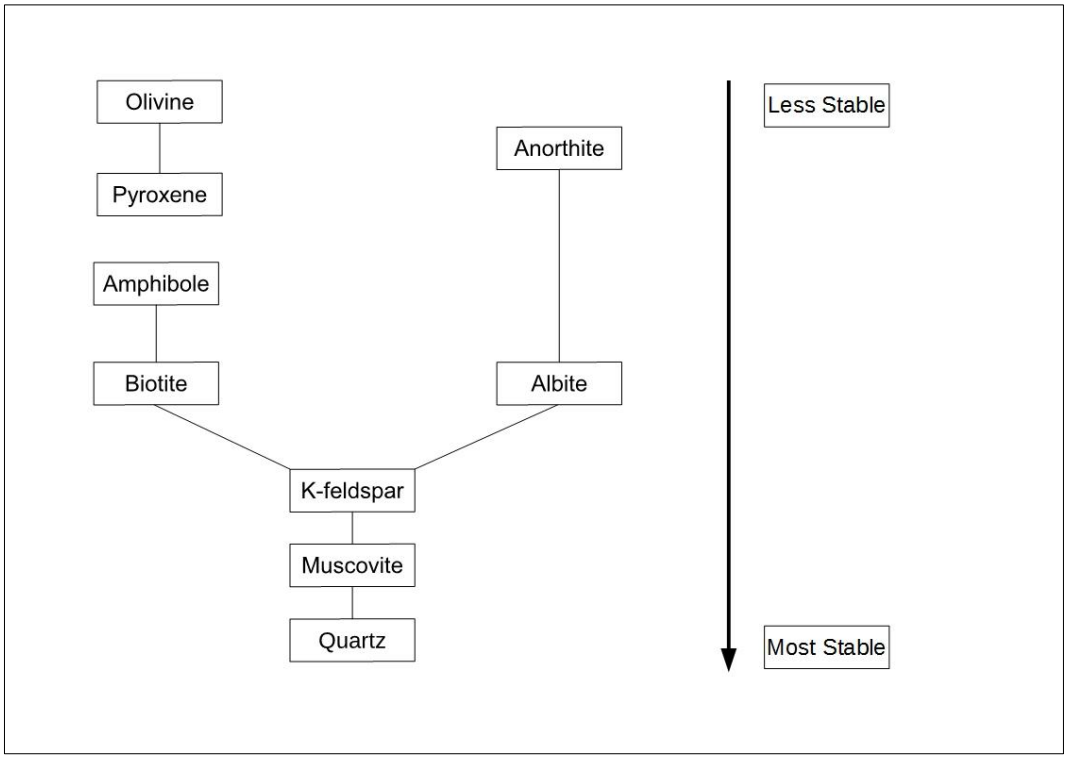

Figure 9: The well-known stability sequence for igneous minerals developed by Goldich in 1938.

According to Appelo & Postma (2005) the partial dissolution of silicate minerals ultimately results in (a) the release of common cations into solution, (b) insoluble Fe an Al phases and (c) an increase in pH level (to 8 - 8.5) because of HCO_3^- being released.

$$Silicate\ mineral + H_2O + CO_2 \rightarrow Al/Fe - residue + (HCO_3)^- + ions \pm H_4SiO_4$$

Equation 2

The weathering of carbonates mainly contribute Ca^{2+} and Mg^{2+} as well as HCO_3^- to the weathering solution.

$$CaCO_3 + CO_2 + H_2O \rightarrow Ca^{2+} + 2(HCO_3)^-$$

Equation 3

The HCO_3^- and CO_3^{2-} concentrations of a solution is collectively referred to as the alkalinity of a solution. The higher the pH of the system, the higher the CO_3^{2-} species will become, as the HCO_3^- dissociates further. The dissolved alkalinity also has the ability to consume H^+ (acid cations) as it recombines with the dissolved HCO_3^- and CO_3^{2-} and in doing so, resist a change in pH of the solution. Eby (2004) however reminds us that not only dissolved species but also interactions between the solution and adjacent minerals can control the pH of a solution.

Table 3: Common minerals in order of increasing resistance to weathering with the type of decomposition reaction(s) relevant to each (compiled from Eby, 2004 and Brener & Brener, 1996).

MINERALS	*DECOMPOSITION REACTIONS*	*MAJOR AQUEOUS SPECIES RELEASED INTO SOLUTION*
Pyrite	Oxidation of Fe and S	SO_4^{2-}
Calcite	Congruent dissolution	Ca^{2+}
Olivine	Oxidation of Fe Congruent dissolution	Mg^{2+}
Ca plagioclase	Incongruent dissolution	Ca^{2+}
Pyroxenes	Oxidation of Fe Congruent dissolution	Mg^{2+}
Ca – Na plagioclase	Incongruent dissolution	Na^{+}, Ca^{2+}
Amphiboles	Oxidation of Fe Congruent dissolution	Mg^{2+}
Na-plagioclase	Incongruent dissolution	Na^{+}
Biotite	Incongruent dissolution Oxidation of Fe	Mg^{2+}, K^{+}
K-feldspar	Incongruent dissolution	K^{+}
Muscovite	Incongruent dissolution	K^{+}
Vermiculite, smectite	Incongruent dissolution	Mg^{2+}
Quartz	Resistant to dissolution	*HCO_3^-, $H_4SiO_{4(aq)}$
Kaolinite	Resistant to dissolution	
Gibbsite, hematite, goethite	Resistant to dissolution	

*All silicate weathering produces HCO_3^-, $H_4SiO_{4(aq)}$

3.2 THE FORMATION OF ASSOCIATED CLAY MINERALS

Stable clay minerals form as eventual secondary products of silicate weathering reactions. The term ‘clay’ can refer to any particle smaller than 2 micron while ‘clay mineral’ indicates a specific group of minerals with distinct physical and chemical properties. Clay minerals are stable because they are adapted to the conditions and composition of the interface between rock and water but also because their formation is governed by the thermodynamics of the system of concern. The mineral that forms will possess the lowest possible amount of free energy at that time in those particular conditions. This explains the homogenisation that is observed in weathering environments.

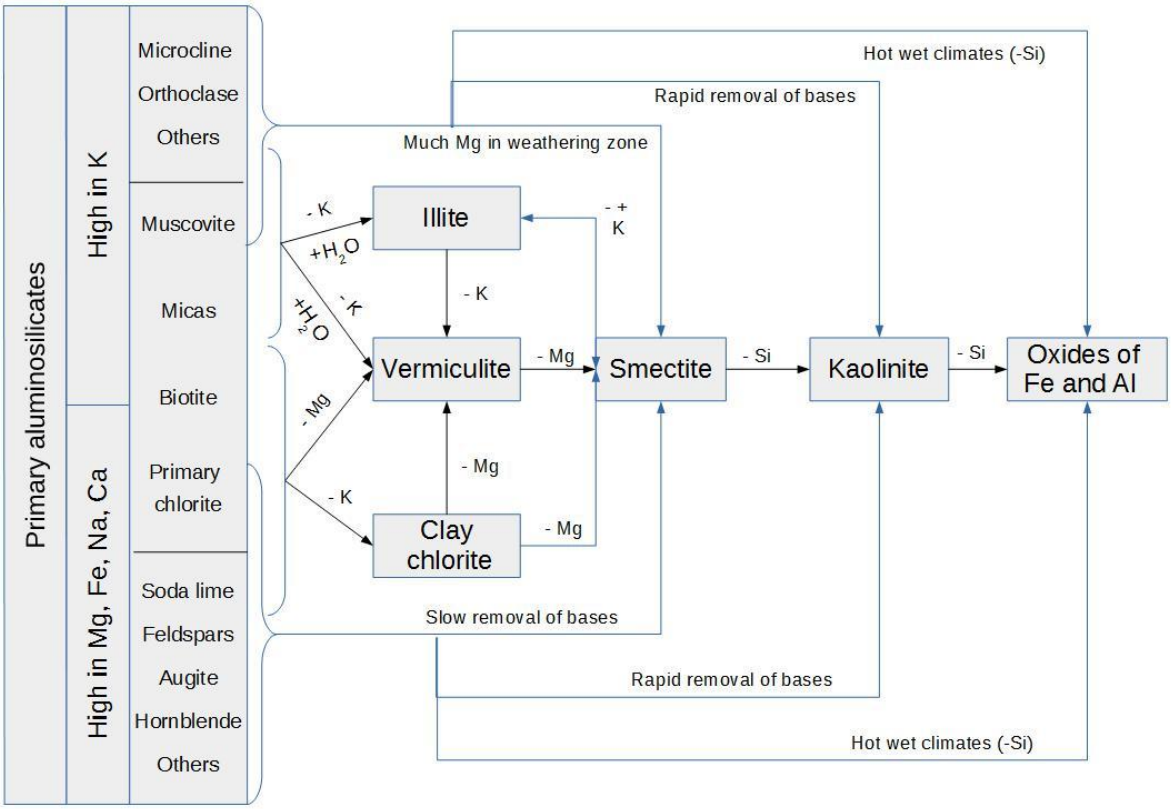

Figure 10: A flow diagram illustrating the influence of climatic conditions on progression of weathering of primary minerals from Brady & Weil (2008).

The physical and/or chemical breakdown of kimberlite is known to be comparatively quick, ultimately resulting in especially smectitic clay (Fairbairn & Robertson, 1966; Morkel, 2006). A simplified representation of this process was compiled by Brady & Weil (2008) and is shown in Figure 10. Crushing of the kimberlite during processing and prior to disposal on the waste dump disintegrates the larger fragments of rock in order for chemical weathering to occur readily at the increased water-rock interface surface areas.

Clay minerals are classified according to their structure, i.e. silicate sheet composition and stacking as well as its interlayer spaces and interlayer constituents (Wenk & Bulakh, 2004). There are two basic clay mineral sheets structures, the one composed of coordinated tetrahedrons (Figure 11 A) and the other of coordinated octahedrons (Figure 11 B). In the tetrahedral sheet Si^{4+} (or Al^{3+}) coordinates with four O^{2-} ions. Three of these occur in a basal position and the other in an apical position. Each of the basal O^{2-} ions binds to another cation to form a lattice with hexagonal cavities with all apical O^{2-} toward the same side. The unit cell dimensions are 9.15 Å and 2.12 Å (Velde & Munier, 2008). Sparks (2003) reported the Si-O bond distance as 1.62 Å and the O-O distance as 2.64 Å.

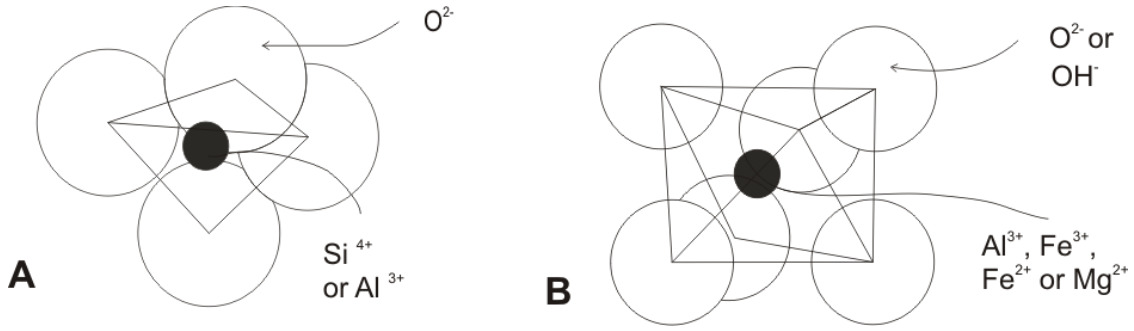

Figure 11: The coordination polyhedra: A illustrates the tetrahedrons and B illustrates an octahedrons (From Hillel, 2004).

In the octahedral sheet the central cation, ideally Mg^{2+} or Al^{3+}, coordinates with six O^{2-} (or OH^{-}) ions, four on the same plane and the remaining two as opposite apexes (Figure 11 B). Each of the six sides can be shared with another octahedron to laterally extend the sheet so that two planes of closest-packed oxygen (or hydroxyls) make up the top and bottom of the octahedral sheet. Such a structural composition allows for each anion to be bonded to three cations. The unit cell can therefore be dioctahedral (or gibsite-like) when Al^{3+} fills two thirds of the available cation positions, or trioctahedral (or brucite-like) if Mg^{2+} fills three cation positions. The unit cell dimensions differs accordingly with 8.64 Å to 2.74 Å for dioctrahedral sheets and 9.43 Å to 2.45 Å for trioctahedral sheets (Velde & Munier, 2008). The O-O distance for the octahedral sheet is given by Sparks (2003) as 2.67 Å and 2.94 Å for OH-OH bonds. Therefore in each dioctahedral sheet there are two anions to satisfy the charge for each cation but in the trioctahedral sheet each cation is coordinated with three anions of a smaller charge.

These individual sheets combine into layers with a ratio of tetrahedral sheet(s) to octahedral sheet of 1:1 (two layer structure) or 2:1 (three layer structure). This occurs when the apical oxygen of the tetrahedral sheet is shared with surface oxygen of the octahedral sheet. Necessary deformations occur due to differences in the size of the basic tetrahedral and octahedral sheets as well as differences induced by cation substitution resulting in ditrigonal symmetry. Cation substitution is a process wherein Si^{4+} in tetrahedrons are often exchanged by Al^{3+} while in octahedrons Mg^{2+} will often be substituted by Al^{3+} in dioctahedral sheets or vacant sites creating a net negative charge for the layer. According to Newman (1987) it can be expected that all Si will first be allocated to tetrahedral sites where after Al and Fe^{3+} will fill the remaining tetrahedral sites. Al^{3+} and Fe^{3+} will then fill the octahedral cation sites. Cr^{3+}, Mg^{2+}, Fe^{2+}, Mn^{2+}, Ni^{2+}, Li^{+} and Ti^{2+} will follow in the octahedral cation sites. The layer charge can be neutralised either by ions, as in micas (K^{+}, Na^{+} or Ca^{2+}), or sheets, as for chlorite and vermiculite (Fe^{2+}, Mg^{2+}, Al^{3+} or Fe^{3+}; hydroxides (OH)), in the interlayer space. Larger cations such as Na^{+}, K^{+} and Ca^{2+} are often also adsorbed on the external surface to satisfy the charges.

The main clay mineral groups classified according to their structural composition are introduced below. Within a clay mineral group polymorphs and polytypes are distinguished. The difference in crystal structure (short range atomic arrangement) between polymorphs justifies a different mineral name. The structural variations in polytypes are limited to the stacking arrangements (Wenk & Bulakh, 2004).

3.2.1 The Kaolin - Serpentine Group

Kaolinite: $Al_2Si_2O_5(OH)_4$
Serpentine: $(Mg,Fe^{2+})_3Si_2O_5(OH)_4$

These 1:1 layer type minerals are stable at surficial conditions and often dominate in the weathering environment (Appello & Postma, 2005). It is also a common authigenic mineral during early sedimentary diagenesis (Velde 1985). The dioctahedral kaolin subgroup includes kaolinite, dickite, nacrite and halloyisite while the trioctahedral serpentines include species like chrysotile, antigorite, lizardite, berthierine and odinite. Note the HCO_3^- produced in the various recations.

The kaolinitisation of K-feldspar progressively produces firstly muscovite and secondly kaolinite, according to the following reactions:

$$3KAlSi_3O_8(K-feldspar) + 2H_2O + CO_2 \rightarrow KAl_2Si_3AlO_{10}(OH)_2(Muscovite) + 6SiO_2 + 2K^+ + 2(HCO_3)^-$$

Equation 4

$$2KAl_2Si_3AlO_{10}(OH)_2(Muscovite) + 5H_2O + 2CO_2 \rightarrow 3Al_2Si_2O_5(OH)_4(Kaolinite) + 2K^+ + 2(HCO_3)^-$$

Equation 5

The continued breakdown of kaolinite will result in the formation of gibbsite (see Figure 10)

$$3Al_2Si_2O_5(OH)_4(Kaolinite) + 5H_2O \rightarrow 2Al(OH)_3(Gibbsite) + 2H_4SiO_4$$

Equation 6

Kaolinites have been extensively studied because it occurs so commonly. These minerals are sensitive to environmental conditions during formation. Balan *et al*. (2014) report that larger, more crystalline flakes form at warmer supersaturated conditions as would be the case in deeper parts of weathering profiles. Surface weathering results in smaller clay particles with a

greater degree of disorder in their stacking. Earlier research by Velde (1985) established the sensitivity to weathering environment in that due to its basic composition (only Si, Al, O and H ions present) kaolinite is readily incorporated into other phases such as illite/chlorite when the concentrations of cations with 2+ valence increased in the environment. It was found that in certain alkali lakes high alkali concentrations produced mica at the expense of kaolinite (Velde, 1985).

The serpentine subgroup of minerals forms as a product of hydrothermal alteration of olivine. Fe^{2+} often replaces limited amounts of the structural Mg^{2+}. They are generally larger in size than the kaolinite minerals and fibrous in nature because of continuous bending of the sheets to compensate for shorter/smaller tetrahedra.

3.2.2 Talc-pyrophyllite

Talc: $Mg_3Si_4O_{10}(OH)_2$
Pyrophyllite: $Al_2Si_4O_{10}(OH)_2$

This group has the typical 2:1 structure. Talc exists as the trioctahedral variant and pyrophyllite as the dioctahedral one. Similar to serpentine talc forms from the alteration of mafic minerals olivine and pyroxene. Pyrophyllite forms from the hydrolysis of aluminium rich primary silicates.

Both these minerals have virtually no layer charge (no tetrahedral substitution occurs), can contain some octahedral Fe, Fe^{2+} in the case of talc and Fe^{3+} in the case of pyrophyllite, and show excellent cleavage. Contrary to other clays they are most common in hydrothermal and metamorphic rocks and limited in the hydrosphere (weathering) environment.

3.2.3 Mica

Phlogopite: $KMg_3AlSi_3O_{10}(OH,F)_2$
Biotite: $K(Fe^{2+}{}_2Mg)_3AlSi_3O_{10}(OH)_2$
Muscovite: $KAl_2(AlSi_3)O_{10}(OH,F)_2$

Although micas occur as primary rock-forming phylosilicates they are also common secondary products in the weathering environment from chemical weathering of olivines, pyroxenes and hornblende. A layer charge originates in micas as one tetrahedral Si^{4+} is substituted by an Al^{3+} in the typical 2:1 structure. This is then satisfied by a cation positioned in the interlayer space.

The most common trioctahedral species are biotite (octahedral Mg), phlogopite (octahedral Fe, Mg) and annite (octahedral Fe) while muscovite (interlayer K) and paragonite (interlayer Na) are dioctahedral.

3.2.4 Illite

Illite: $(K,Na)(Fe^{3+},Al,Mg)_2(Si,Al)_4O_{10}(OH)_2.nH_2O$
Glauconite: $K_{0.6}(H_3O)_{0.4}Al_{1.3}Mg_{0.3}Fe^{2+}_{0.1}Si_{3.5}O_{10}(OH)_2.H_2O$

Structurally illite, glauconite, smectite, vermiculite and chlorite are all similar 2:1 clays. They are regarded as transitional to each other and often occur inter-stratified (Moore & Reynolds, 1997).

Micaceous hydrous illite and its ferriferous counterpart glauconite are both dioctrohedral species with interlayer K^+ (preferred to Na^+) or NH_4. It is therefore also the no 1 source of potassium. Interstratified with smectite, illite is of the most common clay minerals forming as weathering products or diagenically, each distinctively recognisable. Illite is the weathering product of mica and if weathering continues, it is changed into swelling smectite.

Glauconite on the other hand is restricted to timeous formation in marine sedimentary environments transitional from the continental shelf to the slope. Microenvironments of reduction (Moore & Reynolds, 1997) where rivers enter the ocean (Velde, 1985) and organic matter interaction (Fanning, Keramidas, & El-Desoky, 1989) have also been motivated as crucial to its formation.

3.2.5 Smectite

Saponite: $Ca_{0.25}(Mg,Fe)_3((Si,Al)_4O_{10})(OH)_2.nH_2O$
Hectorite: $Na_{0.3}(Mg,Li)_3Si_4O_{10}(OH)_2.nH_2O$
Montmorillonite: $(Na,Ca)_{0.3}(Al,Mg)_2Si_4O_{10}(OH)_2.nH_2O$
Beidellite: $Na_{0.5}Al_2(Si_{3.5}Al_{0.5})O_{10}(OH)_2.nH_2O$
Nontronite: $Na_{0.3}Fe^{3+}_2(Si,Al)_4O_{10}(OH)_2.nH_2O$

2:1 Trioctahedral smectites include saponite and hectorite. The commonly found montmorillonite, beidellite and nontronite are dioctahedral species of this group. In the dioctrahedral species the relatively small layer charges originate from tetrahedral substitution and from octahedral substitution for the trioctahedral species. The most remarkable feature of this mineral group is their ability to expand significantly when in contact with water as water molecules is pulled into the interlayer space by the interlayer cation. The clay minerals have

high cation exchange capacities (a function of the layer charges) pertaining to the interlayer as well as adsorbed surface cations.

Smectites are said to form as weathering products of various parent materials but also diagenically. The chemical composition of the parent rock will be reflected in the composition of the secondary smectite (Bandfield et al, 1991).

3.2.6 Vermiculite

$[(Mg,Fe^{3+})_3(Si,Al)_4O_{10}(OH)_2]\cdot 4H_2O$

According to Moore & Reynolds (1997) vermiculite is found as a transitional part of three different compositional series:

(1) Biotite - vermiculite – smectite
(2) Muscovite – vermiculite –smectite
(3) Chlorite ↔ vermiculite

A reduced layer charge results from the oxidation if Fe^{2+} in the octahedral sheet to Fe^{3+} and subsequent stripping of K^+. Hydrated Mg^{2+} in the interlayer space balances the remainder of the charge. These often occur interstratified or as mixed layers especially in soils of humid regions with primary mica in the parent material. Vermiculite is less common in sedimentary environments.

3.2.7 Chlorite

$(Fe,Mg,Al)_6(Si,Al)_4O_{10}(OH)_8$

Chlorite minerals differ from vermiculite in that the negative charge of the 2:1 layer is partially balanced by positively charged interlayer hydroxyl sheet (not hydrated cations). Octahedral sheets (both) are rarely not trioctahedral with common varieties classified according to the dominant octahedral cation as clinochlore (Mg^{2+}) chamosite (Fe^{2+}), nimite (Ni) and pennantite (Mn). Di-trioctahedral chlorites are referred to as sudoites.

Chlorites are primarily associated with intermediate grade metamorphism but do occur in soil and sedimentary environments.

3.2.8 Sepiolite – Palygorskite

Sepiolite: $Mg_8Si_{12}O_{30}(OH)_4.6H_2O$
Palygorskite: $Mg_5Si_8O_{20}(OH_2)_4.4H_2O$

The fibrous nature of these distinct 2:1 minerals originate from the inversion of every two (sepiolite) or three (palygorskite) tetrahedra. This creates strips with channels in between. These channels are either filled with water or exchangeable cations. Moore & Reynolds (1997) suggest they form during transition stages to and from smectite. Although they occur in restricted environments they are of significant commercial value.

3.3 DISPERSION, COAGULATION AND FLOCCULATION

Water interacting with the surface of clay particles causes it to swell and ultimately, clays with much adsorbed monovalent cations, detach from aggregates and become dispersed or scattered throughout the solution. The mostly negatively charged surface of each particle attracts dissolved ions of opposite charge that result in a cloud of hydrated ions weakly bound by van der Waals forces, to the dispersed clay particles. This interaction between colloidal surface particles and its surrounding solution is explained by the widely accepted Gouy-Chapman-Stern model (Brown & Calas, 2011), which assumes that the collective charge on a particle surface is balanced by charge from counter- and co-ions in solution distributed between the Stern layer (immobile hydrated ions immediately adjacent to the particle surface) and the less tightly bound diffuse double layer (DDL). Together these layers comprise the electric double layer as illustrated in Figure 12 The concentration of counter-ions decreases with distance from the particle surface until there will be no distinction between the DDL and the bulk aqueous solution (at 10 to 20 Å).

The potential of a clay to disperse, depend as much on the clay mineralogy as on the dissolved salts in solution. Gerber & Harmse (1987) hold that: *"dispersion is a physical manifestation of mineral dependent physio-chemical properties that results from the interaction of the clay mineral colloids and its surrounding solution"*. There are mainly two causes of dispersion. The first is when monovalent cations dominate the available exchange sites on the clay particle surfaces. Monovalent cations only weakly bond to the particle surfaces as outer sphere complexes. Because they have larger hydrated sizes and a smaller charge (i.e. twice as many ions are needed to satisfy the negative charge), the ionic sphere of weakly attracted ions would be thicker.

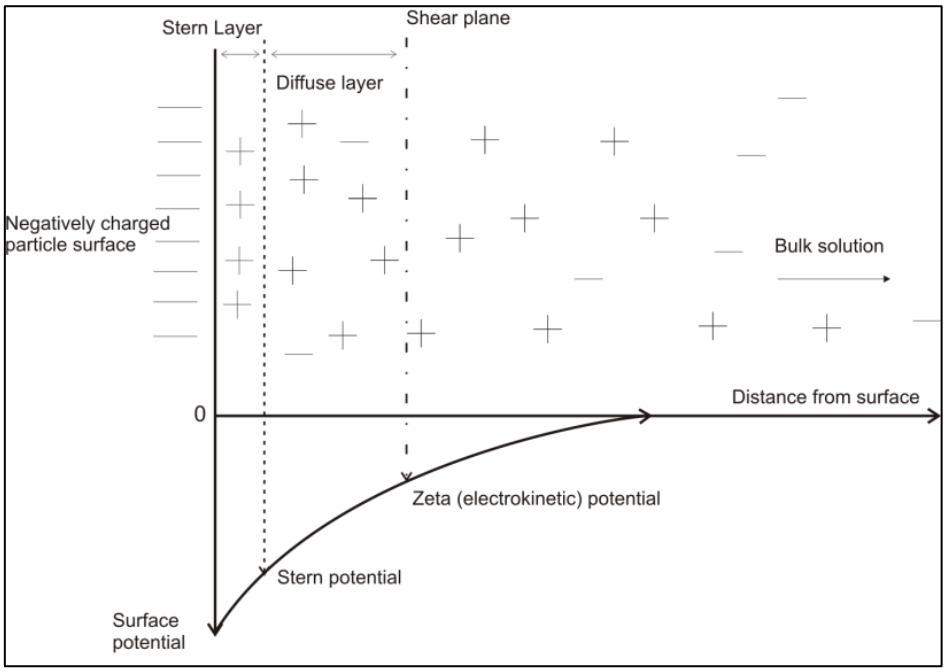

Figure 12: Zeta potential is measured at the shear plane or edge of the electric (or diffuse) double layer which comprises the Stern layer adjacent to the particle surface and the diffuse layer adjacent to the Stern layer.(after Maggi (2005)).

This relates to the measured Zeta-potential (ζ) of particles in solution as it measures the potential energy difference between the edge of the diffuse layer (called the shear plane) and the bulk liquid (ions not moving with the particle) based on the electrophoretic mobility of the particles (Malvern Instruments Ltd, 2004). A thicker double layer will give the measurement of a more stable suspension whereas the zeta potential (positive or negative) will decrease as the suspension approaches its most unstable state known as the isoelectric point or point of zero charge (pzc) (see Figure 13). Inter-particular attraction would be strongest at this point, *i.e.* pzc.

Marchuck & Rengasamy (2011) take it one step further and motivate that it is not only the valence state of the counter-ions, but also the nature of the bond between clay particle and cation, that is paramount to the dispersive nature of solutions. They define and calculate an iconicity or covalancy index that incorporates the charge, ionic radius and polarizability of the cation. In all cases (various clay minerals were used) they found suspensions *saturated* by cations with a higher ionicity index (0.89 for Na^{+} vs. 0.67 for Ca^{2+}) to show a more negative ζ and higher turbidity. As expected their findings confirmed that multivalent cations bind much more strongly to negative particle surfaces and therefore do not have the same dispersive effect.

The second main contributor to highly dispersive solutions is low ionic strength. In the case of a solution with low concentration of dissolved constituents the distances between particles can be too great to be overcome by the van der Waal's attraction forces that should bring the particles

together. Sparks (2003) states that: "*the addition of electrolyte results in not only a compression of the diffuse part of the double layer but also in a shift of the counter ions from the diffuse layer to the Stern layer and hence a decrease in electrical potential at the boundary between the Stern layer and the diffuse layer (Stern potential)".*

In other words increasing the ionic strength of a solution will crowd ions together decreasing the thickness of the electric double layer for effective inter-particular attraction. As individual particles approach each other closely, the suspension will become more viscous when coagulation initiates. Possible flocculation follows due to aggregate size increase leading to gravitational settling (or precipitation of dissolved constituents).

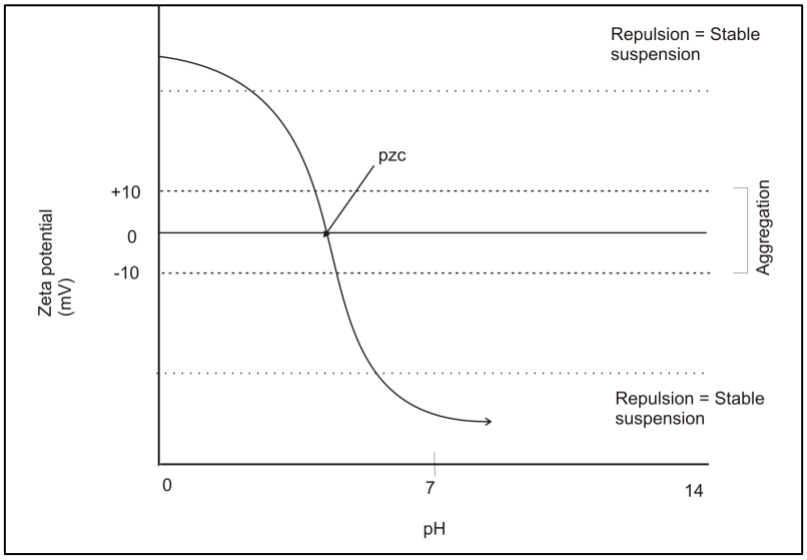

Figure 13: Dispersions are usually stable at high or low zeta-potentials. As the pH of a solution changes, the zeta-potential of the solution will change from positive to negative or from negative to positive, depending on the type of particles in suspension. (pzc = point of zero charge).

A combination of the above-mentioned characteristics of a system have been used by Gerber & Harmse, 1987 to indicate its potential to disperse (refer to Figure 14). Calculation of the exchangeable sodium percentage (ESP) for a soil/clay relates the exchangeable sodium content to the total exchangeable cations, while the sodium adsorption ratio (SAR) calculated for the (soil) solution provides for the stabilizing effect that the Ca:Mg ratio can have on depressiveness (Brady & Weil, 2008). SAR is generally the recommended measurement because the chance for analytical error is less than for determining CEC.

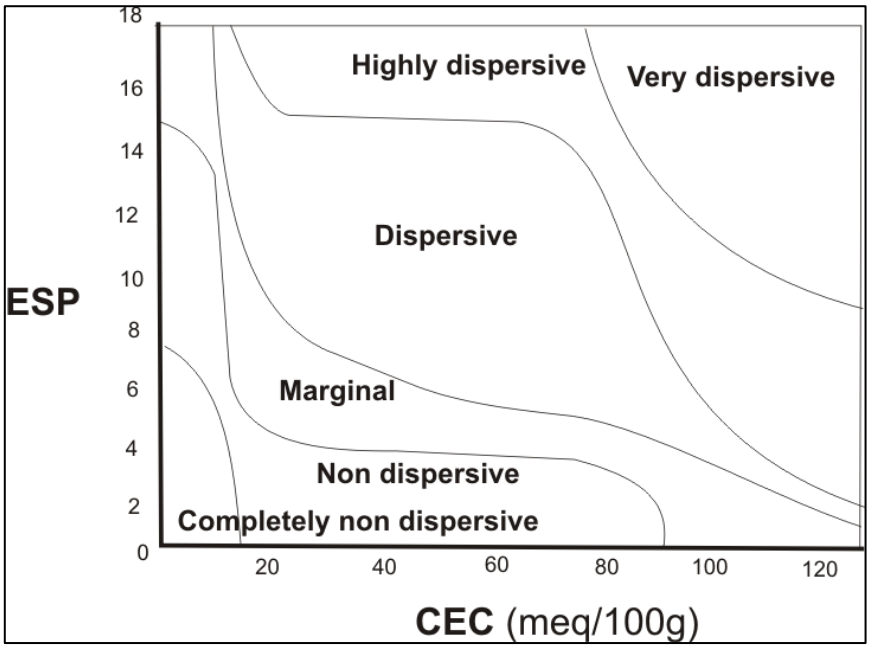

Figure 14: Gerber and Harmse motivated that soils are most dispersive when both ESP and CEC are high (Gerber & Harmse, 1987; Bell, 2007;Sparks, 2003).

Up to values of 25, ESP and SAR are approximately equal (Sparks 2003). An ESP value of 15 (or SAR value of 13) is generally regarded as the threshold for dispersivity. Bell (2007) concludes that smectitic, illitic or other 2:1 clay minerals are most susceptible to high ESP and dispersion whereas soil/material in which kaolinite dominate the clay fraction, high ESP and dispersion is unlikely. However, Crescimanno, Iovino & Provenzano (1995) argued rather convincingly that this recommended threshold value for ESP is not set in stone, so to speak. Even at low ESP values in combination with low salt content they observed strong correlation between the ESP and typical decrease in infiltration, hydraulic conductivity, and structural integrity associated with dispersive soils.

In commercial wastewater treatment coagulants and flocculants are commonly used to destabilize the negatively charged inter-particular repulsion through charge. Coagulants are usually Al- or Fe based compounds that rapidly hydrolyse to form highly adsorptive metal complexes. For each clay–electrolyte system a unique critical coagulation concentration (c_K) exists. This is the minimum salt concentration needed to initiate coagulation. Although smectitic clay is more prone to dispersion, illitic clay requires a much higher salt concentration to induce flocculation (Brady & Weil, 2008).

Penner & Legaly (2001) determined c_K values for laboratory prepared sodium montmorillonite and kaolinite suspensions of 2 % weight per volume and 0.025 % weight per volume after treatment with various neutral and acidic salts. The difference in their flow behaviour highlights the difference in the surface properties of these two clay mineral types. The montmorillonite suspensions are of particular interest to this study. It was found that, for the 2 % suspension, c_K

values resulting from treatment with acidic salts, in general were lowest, although some anions did have a negative effect on coagulation. The liquefying effect of the SO_4^{2-} ions, for example, were overpowered by the strong coagulating power of the H^+ for salts like H_2SO_4 and $NaHSO_4$ (8 and 4 millimole/L respectively compared to 35 millimole/L for $NaSO_4$ were required for coagulation). $NaSO_4$ is the leachable salt that forms when gypsum is applied as ameliorant to dispersive soils. Legaly & Zeismer (2003) concluded that the anisometric shape and charge distributions of montmorillonite particles provide for very low c_K values for inorganic salts.

Flocculation follows coagulation when the microflocs come together into macroflocs, that have enough weight for gravitational settling. Commercial flocculants are mostly synthetic polyacrylamide polymers that act as a bridge between dispersed particles. It can be given a cationic or anionic nature and the effectiveness of the flocculant often increases with molecular weight. It is customary to use inorganic anionic flocculants for destabilizing clay suspensions even though they are electronegative (negative ζ) (Van Duuren, 2007).

3.4 OTHER IMPORTANT CHARACTERISTICS OF CLAY PARTICLE SURFACES

Clay minerals are as reactive (and essential for environmental well-being) because of the associated surface charges that are a function of the structure of the clay mineral. Charges that originate from isomorphic cation substitution in the tetrahedral or octahedral layers (discussed in section 2.2.2) are termed *permanent charges*. *pH dependent charges* are known to arise mainly from protonation (adsorption to) and deprotonation (dissolution) of surface functional groups (such as hydroxyl). The equations below illustrate how the net negative charge will increase as the pH of the solution increases and vice versa.

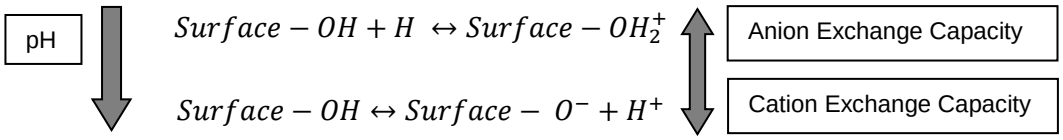

Schofield (1949) showed that below a pH level of 6 only permanent charge sites were available for montmorillonite. The pH dependent sites influenced the net negative charge (CEC) at pH levels 6-9. For clay minerals with small or no layer charge (permanent charge) the pH dependent charge becomes more important to their functionality, *i.e.* chemical interaction, exchanges and adsorption.

pH is, per definition, a measurement of the activity or concentration of H^+ in a particular (soil) solution. A high concentration H^+ gives a low pH and vice versa. The negative charge sites will preferentially be satisfied by H^+ - ions because of its greater iconicity in bonding with clay mineral surfaces (Marchuck & Rengasamy, 2011). As the pH of a solution change, the pzc or

isoelectric point (sometimes also zero net proton charge) will be approached. This is the critical pH level where the particle surfaces display no charge (i.e. all surface charges are satisfied). In a colloidal suspension, this is the point where coagulation or flocculation should initiate (Sparks, 2003). Legaly & Zeismer (2003) gave the pzc for montmorillonite at a pH of around 5.

As illustrated in Figure 15, negative charges are distributed along flat faces of clay particles while the edges usually host positive charge sites (Legaly, 1989). Particles therefore combine in edge to face, face to face or edge to edge structures depending on the thickness of the edges relative to its length at the c_K. as studied by Legaly & Zeismer (2003). They found that edge to face attractions dominated in montmorillonite suspensions at near neutral pH levels as the electrostatic repulsion was distinctly smaller than for face to face combinations. When face to face attractions did occur it was because of lower charge density on the faces of particles. Particle aggregates mostly occur as an irregular porous cluster.

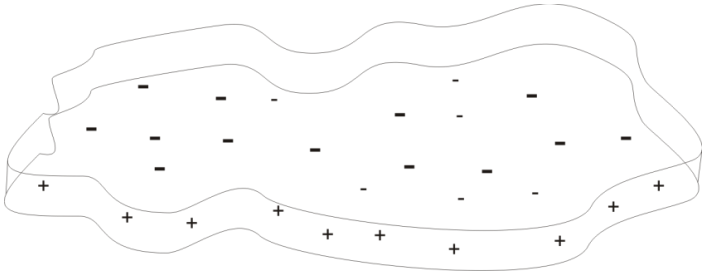

Figure 15: Negative charges are located on the larger flat faces of particles and positive charges on the thin edges of clay particles.

Cation exchange capacity (CEC) is a measurement of the maximum adsorption of readily exchangeable cations on a clay particle. This together with the anion exchange capacity (AEC) is an important parameter to indicate the ability of the clay minerals to retain ions on/around the charged particle surface (keep it from dissolving in solution and leaching away) for later exchange by another ion. Some degree of selectivity does occur as the electrostatic forces involved invoke Coulomb's law. One can generalize by saying for cations higher valence is preferred and for a given periodic group of elements (same valence) the smallest hydrated ionic radius would be preferentially adsorbed. For anions the ones with the greatest polarization potential is usually preferred implying the larger ions. The adsorbed ions are also governed by the composition of the dissolved components in the solution surrounding the particle (Brady & Weil, 2008). Boshoff *et al*. (2007) proved that dissolved cations interacting with kimberlite mineral interfaces, significantly influenced the extent for weathering observed, with Al^{3+} and Cu^{2+} inducing fastest weathering rates.

The ionic composition of the bulk solution is in turn also a function of the solution pH as it influences the rate of mineral dissolution and mobility of elements. In combination with pH, the redox potential (E_H) of the weathering environment will determine the prominent species.

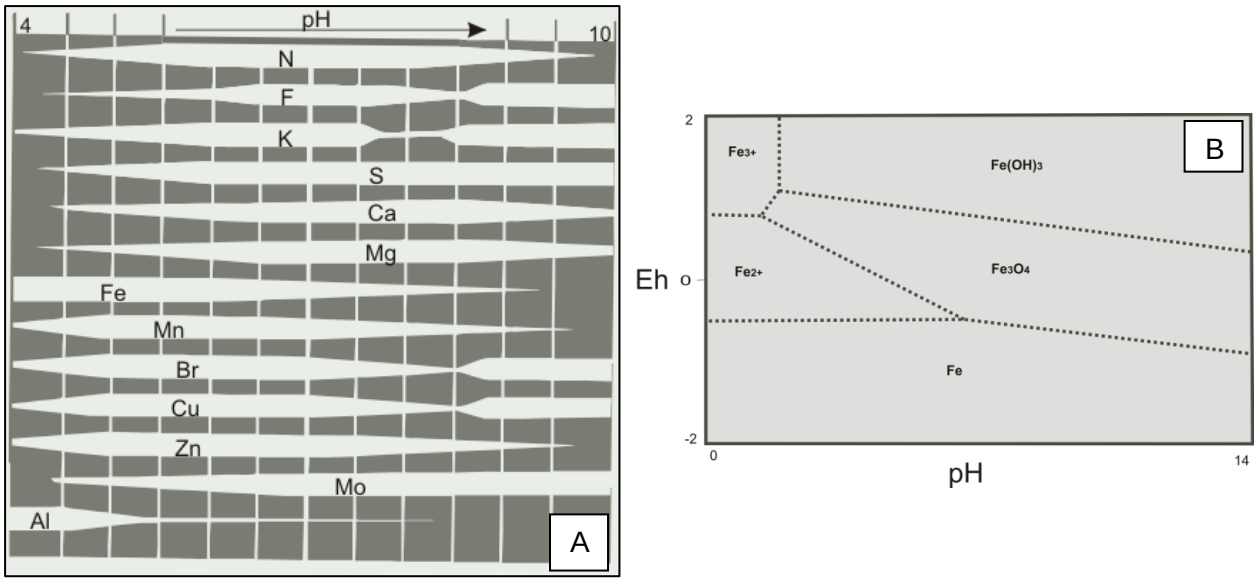

Figure 16: The dependence of the plant-availability of certain elements on pH levels of the environment is illustrated in the diagram A from Thuogh *et al,* (1964). The species of a specific element is then in turn a function of the Redox potential of that environment B (Pourbaix, 1974) is illustrated in diagram B.

As the size of these minerals decrease, their relative reactive surface areas (and therefore available charge sites) increase. Smaller particles move around (Brownian motion) more easily (Malvern Instruments Ltd, 2004) but is influenced by gravity a lot slower (Stoke's Law). Drever (1969) however, motivated that the influence of size is actually negligible in clay fraction particles and that their movement in solution is regulated by their charge.

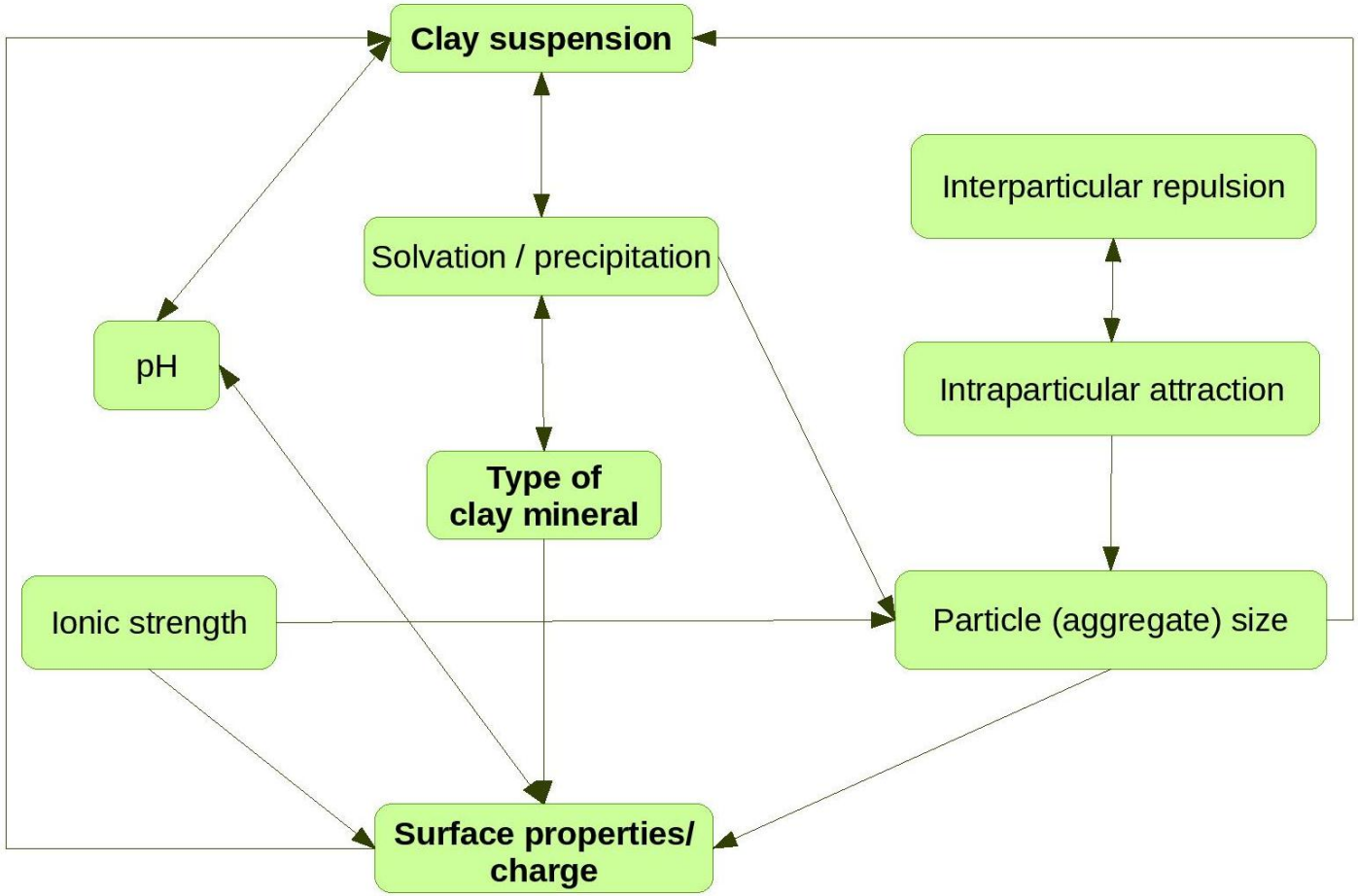

Figure 17: The many interactions and relationships between components of the No. 7 Dam system highlight its complexity and the need for thorough characterization. Of these, perhaps the surface charge are centre, as Leong *et al*., (2012) state that the nature and strength of inter particular forces govern slurry behaviour in flow, mixing, thickening and sedimentation".

CHAPTER 4

METHODS AND MATERIALS

4.1 RESEARCH DESIGN

Refer back to Figure 3 that illustrates the rationale followed in undertaking the research. The characterization of each of the components was approached systematically, from parent material to final weathering product following through to accumulation inside the wastewater dam and then the treatments. This should reflect when and what changes occur during the weathering process. This approach was decided upon to allow for easy comparisons and correlation between inter-dependent physical and chemical characteristics of both the material and surrounding aqueous environment, the importance of which was explained in the previous chapter. To ensure quality data, most analyses were performed by specialized laboratories.

4.2 SAMPLING

Kimberlite boulders were collected from the underground mining operations at the 717 m, 732 m, 747 m levels. The tailings materials were sampled at surface to 30 cm deep at random locations on various tailings dumps on the facility as indicated on Figure 18. At JST08 fine tailings could be sampled from the side of the beach and coarse tailings from the top. In the proximity of each tailings sample site (JST) five samples of about 1 kg were collected separately. For most analyses the material were made up into a composite mixture as described in each subsequent section.

The water samples were collected in the late summer months at sites JSW as indicated on Figure 18. At each site a deeper sample were taken at 11 – 15 m and a sample closer to the surface between 4 – 5 m deep. This was done using a fabricated Kenmerer -type water sampler. Site JSW 04 was specifically chosen for its proximity to a well-established reed population. Water analyses for the No 7 Dam water were done by multiple laboratories for comparison and quality control.

The required particular preparations for the various analyses chosen to characterize the kimberlite, tailings and No 7 Dam water, are discussed in each subsequent section.

Figure 18: The distribution of tailings and water sampling locations.

Figure 19: Note the turbidity of the No 7 Dam water, while sampling, as it splashes up from the oar. (Courtesy of Anja van Deventer: 2013)

4.3 METHODS USED FOR PHYSICAL CHARACTERIZATION

4.3.1 Particle size distribution analyses (PSD)

A composite sample of the tailings material was compiled from the 20 samples taken. Equal amounts of each of the coarse and fine tailings were thoroughly mixed before riffling it down into an 800g sample that was used for a PSD analysis, according to the American Standard Test Method for Particle Size Analysis of Soils (ASTM D422, 1998). This entails using a range set of sieves of different apertures stacked from largest (7000 µm) at the top to smallest (75 µm) at the bottom. Mechanically shaking the stack for 10 minutes separated the tailings sample into corresponding fractions as retained by each of the sieves.

After the accelerated weathering experiment (see section 4.7) was completed, both the tailings and kimberlite material were re-evaluated to observe the change in PSD.

4.3.2 Electron Microscopy

According to (Moore & Reynolds, 1997) the most effective ways to study and characterize clay minerals are (1) microscopy, (2) spectroscopy, (3) diffraction and imaging. At the NWU Laboratory for Electron Microscopy, the external morphology of the clay suspended in the No 7 Dam water was imaged by Scanning Electron Microscopy (SEM) while Transmission Electron Microscopy (TEM) aimed at investigating internal- and micro structure of the smallest dispersed particles. In electron microscopy a finely focused electron beam impacts and interacts with the sample surface, to produce, amongst other, backscattered and secondary electrons (SEM) or transmitted electrons (TEM). The sample surface is scanned by means of two sets of electromagnetic coils in the focussing objective lens deflecting the beam in *x* and *y* directions. The signals are detected above the sample (*z* direction) and interpreted to a 3-D digital computer image for SEM and 2-D for TEM (Skoog, Holler & Crouch, 2007).

For investigation by SEM, a single drop of water was air dried to form a clay cake which was coated with a 21 nm layer of gold-palladium for better conduction and imaging. The mounting was then imaged with a FEI Quanta 200 ESEM with the assistance of Dr Louwrens Tiedt.

To prepare the sample for TEM investigation, a drop of the No 7 Dam water was diluted and the particles separated in a sonic bath, before being mounted and dried. Dr Anine Jordaan conducted the investigation and imaging with a FEI Tecnai G2 high resolution TEM.

4.3.3 Coefficient of Linear Extensibility

Calculating the coefficient of linear extensibility (COLE) is a simple yet effective indication of the amount of shrinkage, i.e. volume change, which occurs upon drying of a soil. Despite numerous modern methods, this Atterberg limit method is still widely used. Traditionally, the COLE is calculated by means of measuring the reduction in length of a clay bar, from its plastic limit (PL) to air-dried state. The PL refers to the water content of a soil, when it is between a plastic state and a solid state. The volume reduction in the bar (COLE) is quantified according to the formula below. L_M denotes the initial length of the bar and L_D the length of the bar when air dried.

$$COLE = \frac{L_M - L_D}{L_M} \times 100$$

Equation 7

Because the PL is a rather subjective attribute, the COLE was translated to the mass of saturated clay (L_M) minus the mass of dried clay (L_D). This is conventional since the mass of water lost from a saturated column of soil (no air), reflects the volume lost, as the density of water is 1g/cm^3. What remains, is the volume of soil.

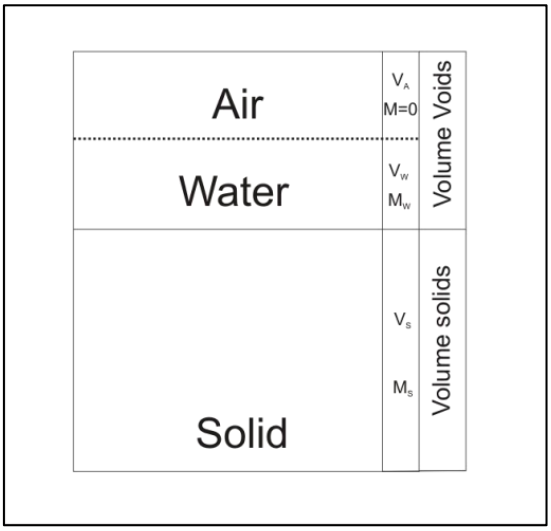

Figure 20: The mass to volume ratio of a column of soil (Adapted from Hillel, 2004).

Water from the No 7 Dam was centrifuged to extract the clay. At its plastic limit a 15 cm metal bar was filled, weighted, air dried and re-weighted. Five repetitions were done to obtain an average. The same procedure was repeated with the sedimented clay retrieved after the No 7 Dam suspension was subjected to the mineral acid treatment (see section 4.9).

4.4 METHODS USED FOR MINERALOGICAL CHARACTERIZATION

4.4.1 Microscopy

For petrographic microscopy, two thin section mountings of the kimberlite from each of the three underground levels sampled, were prepared at the North-West University Geology Museum with the assistance of Mr Kosie Oosthuizen. Struers water free cutting fluid was used as substitute in the cutting process. The slides were mounted on glass, ground and polished down to a thickness of 30 µm. It was investigated with a Nikon Eclipse 50*i*POL petrographic microscope. Selected macroscopic features of various kimberlite boulders were also investigated with a stereo microscope.

4.4.2 X-Ray Diffraction

X ray diffraction spectrometry (XRD) is commonly used as an effective method for determining clay minerals. The preparations of clay-containing samples are somewhat different due to the specific platy nature of phylosilicates. It is ideal to prepare mounts that show either no orientation of the particles at all wherein all the reflections *(hkl)* of the minerals are represented, or to have perfect orientation of all particles (Moore & Reynolds, 1997). Strong orientation in mineralogically homogeneous mountings boosts the most diagnostic, basal *(00l)* reflections (Moore & Reynolds, 1997; Morkel, Kruger & Vermaak, 2006). For this reason, random powder mounts were prepared for the kimberlite and tailings material (before and after accelerated weathering) and oriented mounts were prepared for the No 7 Dam clay (before and after chemical treatment).

In a pipe crusher, the respective kimberlite and tailings samples were manually crushed to gravel size, riffled down to 50 g samples and powdered using a tungsten carbide ring mill. The particle size was reduced to < 5 µm to minimize deviation in peak intensities and preferential orientation as discussed by Klug & Alexander (1974).

When identifying clay minerals within a rock, obtaining this random orientation is often a major problem as the platy nature of clay minerals cause them to orient associated to the preferential brakeage faces of crystalline minerals. Morkel *et al.* (2006) suggests a side-mounting technique to mitigate this preferential orientation in clay-bearing kimberlite. To obtain the least amount of orientation with the available resources, the powdered rock was back loaded into the sample holder and only slightly packed for minimum induced orientation.

The No 7 Dam clay mounts for XRD were prepared according to the filter transfer method described by Moore & Reynolds (1997). For quantitative analysis it is essential that the sample on the slide must be mineralogically homogeneous throughout, with minimum size segregation. The clay suspension was centrifuged at 1000 rpm for 5 minutes to obtain a more viscous concentrated sludge. A few ml of the concentrate were suction-filtered through 0.45 micron filter paper to induce best possible orientation of the clay particles on the filter paper. The filter paper was removed from the device and carefully rolled, upside down, onto a glass disk. Air drying the disk for a couple of minutes was sufficient for successful removal of the filter paper. In the case of trapped air bubbles or surface irregularities the mounting was discarded and another was prepared.

As suggested by Morkel, (2006) and Morkel *et al.* (2006) three repetitions for each of the samples were run. First, the samples were only air dried. Secondly, the mountings were subjected to ethylene glycol vapours in a desiccator for eight hours to open up the interlayer spaces of any swelling clay minerals present. A third run followed after the prepared mountings were heated to 550˚C for two hours. Table4 list the instrument specifications and settings for the various analyses. The mineral content for each run was determined by means of Rietveld semi-quantification (Rietveld refinement technique) at the NWU XRD & XRF Laboratory with the assistance of Mrs Belinda Venter.

Table 4: Specifications to consider for XRD analyses.

MAKE	PANalytical X'Pert Pro
RADIATION	Cu
POWER SETTING	45kV, 40mA
RANGE OF °2Θ	4° – 100°
STEP WIDTH	20.955˚
TIME PER STEP	17 s

4.5 METHODS USED FOR CHEMICAL CHARACTERIZATION

4.5.1 Contamination Index

The contamination index (C.I.) for kimberlite, devised by Clement (1982) relates the Si/Mg ratio of the kimberlite on the basis that for kimberlite melts uncontaminated by the incorporation of crustal species, the matrix should comprise essentially olivine and phlogopite. The C.I is calculated according to the equation below. A C.I. > 1.2 denotes significant crustal contamination.

$$C.I. = \frac{(SiO_2 + Al_2O_3 + Na_2O)}{(MgO + 2K_2O)}$$

Equation 8

4.5.2 X-Ray Fluorescence

For X-Ray Fluorescence (XRF) analyses (alternatively known as X-ray emission spectroscopy), the difference in energy when an electron drops from an outer orbit to an inner orbit, yielded as emission spectra comparable to a standard reference, specifies the chemical elements present in a sample. The characteristic fluorescence indicates the chemical element present in a sample (qualitative), whereas the intensities of these energies indicate the amount of that element present (quantitative) (Brouwer, 2003). XRF studies are particularly handy in determination of major elements (Si, Ti, Al, Fe, Mn, Mg, Ca, Na, K, P) and trace elements (Ba, Ce, Co, Cr, Cu, Ga, La, Nb, Ni, Rb, Sc, Sr, Rh, U, V, Y, Zr, Zn) in excess of 1 ppm in a representative, homogeneous powder of rock material.

The chemical compositions were determined, once again, for the kimberlite (before and after accelerated weathering), the tailings (before and after accelerated weathering) and the No 7 Dam clay (before and after chemical treatment). The same crushing, riffling and milling procedures were followed as for XRD. The powder was prepared as fused glass beads by adding a small amount of flux and melting at 1000 to 1200 ˚C, for major element analyses and powder pellets pressed with 20 000 kg, for trace element determination at the NWU XRD & XRF Laboratory with a PANalytical Axios Max WDS. The elements that can be lost through excessive heat (H_2O, CO_2, S etc) were recorded as the respective loss on ignition values (LOI), obtained by heating 15 g of material to 1000°C for 2 hours.

4.5.3 Adsorbed Cations and Cation Exchange Capacity (CEC)

For the No 7 Dam clay (removed from suspension by centrifugation) the cations filling the surface exchange sites were determined by the NWU affiliated soil and water laboratory, Eco Analitica. Principally this is done by replacing the cations adsorbed on the clay particle surfaces with a specific alternative cation not commonly found in natural soils by means of saturating the clay/soil with a salt solution thereof. The standard ammonium acetate extraction method was used at pH of 7 (Brady & Weil, 2008) to determine the nature and quantities of replaced cations.

The CEC is, per definition, the amount of available adsorption sites per unit volume of the fine-grained clay, (1) calculated from the exchangeable cations or (2) measured as the above mentioned NH_4^+ is again replaced by another salt solution, usually K^+.

4.5.4 Exchangeable Sodium Percentage and Sodium Adsorption Ratio

Parameters for expressing sodium content is either exchangeable sodium percentage (ESP) or as sodium adsorption ratio (SAR). The latter takes into account the influence that the presence of calcium and magnesium has on the adverse effects of sodium. It is also more accurately measured than ESP (Sparks, 2003). To calculate SAR concentrations should be in mmol per liter of solution.

$$ESP = \frac{Exchangeable\ sodium, cmol_c/kg}{Cation\ exchange\ capacity, cmol_c/kg} \times 100$$

Equation 9

$$SAR = \frac{[Na^+]}{\sqrt{[Ca^{2+}] + Mg^{2+}]}}$$

Equation 10

4.6 HIGH HUMIDITY ACCELERATED WEATHERING KINETIC (HHAWK) TESTS

Sapsford *et al.* (2009) defines accelerated weathering - or kinetic tests as: “weathering tests conducted to aid prediction of drainage quality from mine wastes”. Humidity cells and leaching columns are included amongst the most common of these methods used (especially for determining weathering rates). They are designed to simulate natural weathering conditions and reveal something about the dissolvable agents present. Usually it is purposed for determining the acid drainage potential of a specific material, be it tailings or waste rock. Many variations to the accepted ASTM D 5744 (ASTM, 1996) standard procedure have been published, mainly due to high setup and operating costs of the ASTM D 5744 (ASTM, 1996) method. The basic concept requires subjecting the materials to a seven day cycle which comprises three days exposure to high humidity air followed by three days exposure to dry air and a leaching on the last day in a controlled/regulated environment. For extensive discussions on different kinetic

methods, protocols and variations to the protocols the reader is referred to Frostad, Klein & Lawrence, (2002); Sapsford *et al.,* (2009); Prince (1997); and Hornberger & Brady (1998).

Sapsford *et al.,* (2009) summarizes weathering rate as: “the rate (mass per unit time) at which a primary mineral is transformed into a secondary product”. Therefore to measure the rate the sample should, by definition, be free of secondary minerals initially. This is not the case in kimberlite, but a comparison can be made between initial amounts of secondary minerals to post-experimental amounts. One notice a concern that repeatedly arises regarding the discrepancies occurring between the rate of weathering observed in laboratory conditions verses in situ in the field. The sole application of kinetic testing in this study however, is observing the quality of drainage generated by kimberlite weathering - not necessarily determining the weathering rate.

Ten kg tailings material (a composite from all sample sites - mixed coarse- and fine-grained material) was continuously passed through a cone-riffler into three homogeneous aliquots of one kg each (labelled T1, T2 and T3). The particle sizes of the tailings material was not altered. Ten kg kimberlite was crushed by means of a pipe crusher to resemble the particle size distribution of the tailings material. This was achieved when 100 % of the material passed 7 mm and D_{50} was ~ 1.7mm. After crushing, the kimberlite was also continuously riffled to obtain three homogenous one kg aliquots (labelled R1, R2 and R3).

The setup approximately followed the method suggested by Kargbo & He (2004). Six leaching columns were suspended in a metal frame and isolated inside a fabricated humidity chamber (dimensions 1m x 0.5m x 0.5m). Temperatures inside the chamber fluctuated between an average minimum of 12 and average maximum of 25. An Elektra (model 8076, 230 – 50 Hz, 700W) humidifier and extractor fan was positioned to direct humid airflow across the surfaces of the samples as suggested by Prince (1997) (not necessarily from below). It was decided to follow this deviation because of the hydrophillic nature of kimberlite. The fan was coupled with an Xpelair XRH humidistat (model 21856A) humidity sensor in order for the fan to switch off when humidity lowered below 70 %. Work done by Bouzahzah, Benzaazoua, & Bussière (2010) highlights the benefits of this modification.

The diameter of the leaching columns were 15 cm and the height 30 cm. Inside each column the material was suspended on a perforated plate covered with durable filter paper. To initiate the 20 week experiment, each column was flushed with 750 ml of de-ionized (DI) water and drained after one hour.

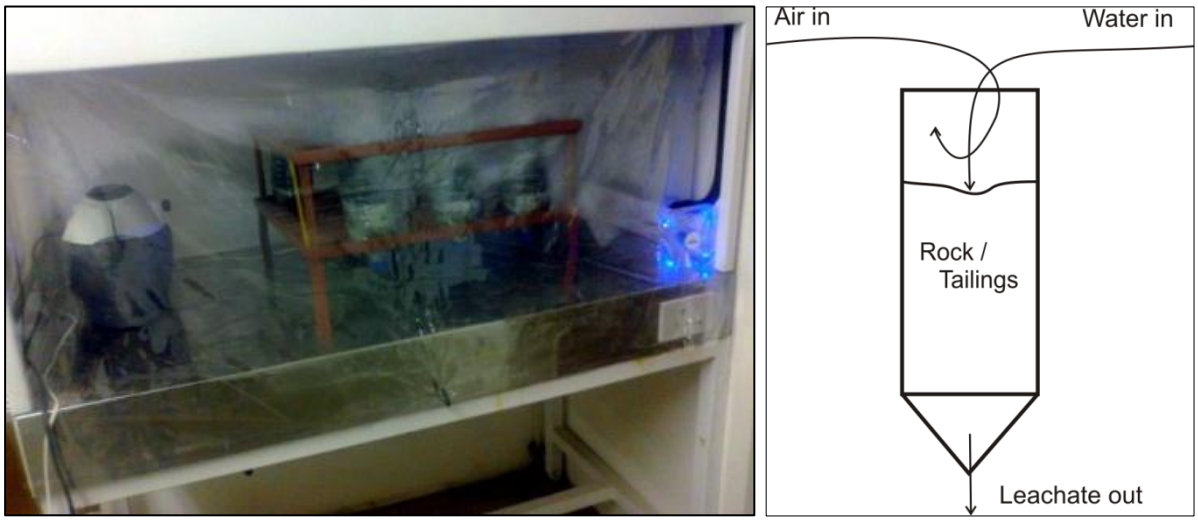

Figure 21: Setup of the leaching columns inside the humidity cell.

The leachate collected was weighed and the pH and conductivity determined. The relative humidity was maintained at 70 % or above for seven days continuously with the leaching concluding the seventh day. During the weekly leaching the cells were flushed with 500 ml DI water, allowing two hours for equilibration before they were drained. The pH and EC were measured with a Hannah (HI9828) multi-parameter meter. The amount of water leached out was recorded and the leachate refrigerated for one week. After every second cycle a composite sample (e.g.T1-1 & T1-2) was sent to Eco Analitica laboratory for water quality analyses. Before and after each leaching the weight of the column was recorded (dry and wet weight). Upon completion of the 20 weeks, each aliquot was weighed and characterized as before the commencement of the kinetic tests (PSD, XRD, XRF).

4.7 WATER QUALITY ANALYSES

Water quality analyses were done on the No 7 Dam water as well as the leachate from both kimberlite and tailings material. After chemical treatment of the No 7 Dam water it was analysed again for the same parameters. The water was sent to 2 different laboratories for initial analysis of the parameters set out in Table 5: The various parameters analysed for by the laboratories mentioned below, to evaluate the quality of the No 7 Dam water.. The leachates from the accelerated weathering experiment were only sent to Eco Analitica because of budget considerations.

Water was sampled and submitted in May 2012, January 2013 and May 2014. The various analyses were processed to obtain a statistical average composition that was to be used in the chemical modelling. See Annexure G for the individual laboratory reports.

Table 5: The various parameters analysed for by the laboratories mentioned below, to evaluate the quality of the No 7 Dam water.

	NWU Eco Analitica	Midvaal Water (SANAS Accredited)	Waterlab (SANAS Accredited)
Bicarbonate		X	
Carbonate		X	
Electrical conductivity	X	X	X
pH	X	X	X
Sodium Adsorption Ratio	X	X	X
Suspended solids		X	X
Total dissolved solids		X	X
Turbidity		X	X
Alkalinity	X	X	X
Dissolved Major elements **(Cations: Ca, Mg, K, Ca)** **(Anions: Cl, F, PO, SO_4, NO_3)**	X	X	X
Dissolved Minor/Trace elements **(Al, Sb, As, Ba, Be, B, Cd, Cr, Co, Cu, CN, Au, Fe, Pb, Li, Mn, Hg, Mo, Ni, Se, Ag, Sr, Sn, Ti, U, V)**	X	X	X

For all samples pH, EC, dissolved oxygen and redox potential were measured on site immediately after sampling. A three point calibrated HI 9828 multi-parameter meter from Hannah Instruments was used to make the measurements before sealing the water containers.

4.8 ZETA POTENTIAL (ζ)

A sample from No 7 Dam was sent to Micron Scientific PTY Ltd. for analysis. Zeta potential (ζ) auto-titrations are necessary to determine the exact pH level where flocculation will initialize for a particular clay – electrolyte system. If pH passes this isoelectric point towards a net positive charge, the same inter-particular repulsion can re-stabilize the dispersion (Maggi, 2005).

The major phases (solid and dissolved) present in a suspension, will influence the coagulation behaviour of the suspension due to unique surface characteristics, charge distribution and salt content (Malvern Instruments Ltd, 2004). After characterization of the No 7 Dam clay the ζ experimental setup was modelled after the behaviour of sodium montmorillonite suspensions.

Coagulation by acids has been well motivated because of the particularly strong coagulating power of protons (H^+) compared to other cations (Therialut, 1923; Peckham, 1962; Kim, Ludwig & Bishop., 1965; Penner & Legally, 2001). The H^+ has been found to overcome some of the usual liquefying effects of certain anions, especially SO_4^{-2} or PO_4^- (Penner & Legally, 2001). In acidic suspension the c_K are much smaller than for the same suspension at a higher pH. Therefore acidic solutions become more sensitive to coagulation by inorganic salt concentration as well (Bartlow & Peterson, 1928; Lagaly & Zeismer, 2003). The influence of acid addition to the system will not only eliminate pH dependent negative charges, but also liberate alternative cations from the octahedral sheet into solution (Brady & Weil, 2008) effectively increasing the ionic strength of the solution at the same time, possibly approaching the c_K of many of the inorganic components (Na^+, Ca^{2+}, Al^{3+}). Van Duuren (1997) claims the duty of a coagulant to be the release of ions or electrolyte to promote coagulation (interparticular attraction).

The No 7 Dam sample was first diluted to an acceptable turbidity by adding supernatant cleared by centrifugation. This is essential as the instrument optically detects movement of particles by dynamic light scattering. Multiple scattering by various particles can occur if the suspension is too concentrated. It is recommended that no more than 1 % of the sample-mass constitute solids if the particles > 10 µm. The way particles move in a solution, called Brownian motion, reflects a scatter pattern that moves quicker if the particles are smaller and more slowly for larger particles. This movement is measured as electrophoretic mobility from which it is re-calculated to zeta-potential according to the Henry equation (given below). The given $f(ka)$ value indicates whether the Smoluchowski (1.5) or Huckle (1) approximation was used in calculating the ζ from:

$$U_E = \frac{2\varepsilon\zeta f(ka)}{3\eta}$$

Equation 11

Where U_E = Electrophoretic mobility
ε = Dielectric constant
η = Viscosity

The Smoluchowski approximation is applicable in suspensions with particles > 0.2 µm and 10^{-3} molar salt in solution. In systems with low dielectric concentration and small particles the Huckle approximation is applicable (Malvern Instruments Ltd, 2004).

An auto-titration with 0.1 M HCl was done by Dr A Truter with a Malvern Zetasizer Nano Series Zetasizer V 7.11, from the existing pH (~ 9) down to 2. Three readings of the particle electrophoresis were taken at each interval during the 2 hour procedure. Statistical interpretation is included in the Zetasizer Nano software application.

4.9 MINERAL ACID BATCH JAR TREATMENTS

The American Standard Test Method D2035-(ASTM, 2008) is a general three step systematic evaluation of variables (pH, temperature, mixing conditions and chemical additives) that one can expect to encounter during complex coagulation-flocculation interactions. It ultimately evaluates colour, turbidity and hardness of the water.

The procedure basically requires (1) rapid mixing of coagulant and (effluent) water for complete and effective distribution followed by (2) slow mixing to allow reaction at contact surfaces and to facilitate large flock formation before (3) mixing is terminated to observe settling velocity. The mixing intensity/velocity and mixing times are essential parameters to observe. Ideally square containers with at least 2 L capacity and various possibilities of mixing paddles driven by magnetic mixing are used, while simultaneously controlling temperature and coagulant (and/or flocculant) dosing. Square containers are recommended to overcome syphon mixing after stopping the mixer in time sensitive trials. An extraction tube should be fitted below the water level providing for easy sampling with minimum disruption/ mixing when samples are taken. The test is designed in such a way that it can easily be up-scaled by engineers for treatment of large volumes of water. Early work by Hudson & Wagner (1981) and Van Duuren (1997) highlights the many advantages and applications of using jar tests in coagulation studies while Leopold & Freese (2009) point out the necessity of a continued routine jar test at an operational plant.

Since the results from the zeta potential analysis were not as specific as anticipated, the jar tests were applied to test and validate the effectiveness of the acid addition, and identify concentrations (acid and salt) most effective in coagulation.

Error! Reference source not found. below sets out the conditions for each of the batches run. The volume of each repetition was reduced to 500 ml and the pH was monitored throughout with the HI 982 multi-meter. The following measurements were also recorded for each batch of three repetitions:

- time it took for visible flocculation to initiate (or fast mixing time)
- total settling time
- change in pH
- change in EC

After complete sedimentation, the cleared supernatant was decanted, pH and EC were measured with the three point calibrated HI 982 multi-meter. One half was sealed and sent to Waterlab for a complete quality analysis, while the other half was equilibrated with dolomitic lime overnight before being sent to Waterlab for the analyses mentioned in Table 5: The various

parameters analysed for by the laboratories mentioned below, to evaluate the quality of the No 7 Dam water. above. The coagulated clay was sent for XRD and XRF analyses.

4.10 DATA MODELLING, PROCESSING AND PRESENTATION

Results from the various datasets were processed with specialised software and presented in standard diagrams that warrant a brief introduction.

GEOCHEMICAL MODELLING WITH PHREEQC

The PHREEQC software is freeware distributed by the United States Geological Survey (USGS). It was developed to simulate reactions and processes in aqueous environments, be it surface water, wastewater or groundwater. The reaction conditions for a simulation are specified with certain keyword codes which defines the reaction conditions. The software has become a widely accepted, valuable and often necessary method to incorporate into the research method of geochemical studies. There are numerous works proving the success of modelled reactions in comparison with actual experimental results. Applicable studies are highlighted in the relevant discussions.

In this study, the program, PHREEQC Interactive, Version 3.1.2.8538, Released March, 2014, was utilized to (1) verify the viability of planned experimental outcomes and (2) to reduce experimental costs where possible, through identifying those options most suitable out of several possibilities.

The first instance was evaluating the water quality outcomes of the various plausible acid reactions suggested by Penner & Legally (2001), before conducting zeta potential auto-titrations with the No 7 Dam suspension to determine the pzc. This was focussed on identifying the most suitable concentration applicable to the No 7 Dam, as the concentrations of the various acids used were not sufficiently clear from the previously mentioned work. From this the expected supersaturated solid phases could also be seen and compared with the actual solids retrieved.

Amongst other, the program gives an indication of the SI of various minerals in solution as well as what species occur in a specific system, of which the user specifies the composition. Figure 22 and 23 below are examples of information specified for some batch reactions that were modelled with the dissolved load of the No 7 Dam solution.

Because geochemical interactions are complex, intricate and interdependent, the results of these modelled reactions should not go without scrutiny.

.

Table 6: Experimental setup for sets of four different batch jar tests to observe the rate of (chemical) flocculation in the No 7 Dam suspension.

BATCH NR.	***ADDITIVE(S)***			***RATIONALE***	***REFERENCE***
	HCl	No7 Dam Water	Solids		
1	6 ml 0.5 M	500 ml	-	To adjust pH to 5.5 - Geochemical modelling indicated 7ml 0.1 M HCl is needed.	See section 4.10 Lagaly & Zeismer, 2003
2		Inconclusive		Per Zeta-potential results	See section 4.8
3	23 ml 0.5 M 10.9 ml 1M	500 ml		Observable flocculation from acid addition	
4	3 ml 1 M 2 ml 1 M 1 ml 1 M 5 ml 0.5M 5 ml 0.5M 10 ml 0.5M 12 ml 0.5 M 30 ml 0.5 M	100 ml 100 ml 100 ml 150 ml 250 ml 300 ml 400 ml 1 L	5 g 3 g 2 g 5 g 5 g 10 g 20 g 50 g	The addition of a small amount of alternative clay (and tailings) material was suggested as pre-treatment to enhance flocculation mediated by pH alteration.	Kim *et al*., 1965 & van Duuren, 1997

```
SOLUTION 1 # Average No 7 Dam Dissolved
    temp      25
    pH        8.98
    pe        4
    redox     pe
    units     mg/l
    density   1
    Alkalinity 675
    Ca        11
    Cl        99
    F         5.9
    Mg        9.2
    N         2.5
    K         35
    Na        279 charge
    S(6)      409
    Al        1.2
    Ba        1.2
    B         0.73
    Fe        1.6
    Ni        0.05
    Sr        0.18
    -water    1 # kg
END
REACTION 1
    H2SO4     1
    0.001  0.005  0.01  0.05 0.1 moles
USE solution 1
END
```

```
SOLUTION 1 # No 7 Dam Average Dissolved
    temp      25
    pH        8.98
    pe        4
    redox     pe
    units     mg/l
    density   1
    Alkalinity 675
    Ca        11
    Cl        99
    F         5.9
    Mg        9.2
    N         2.5
    K         35
    Na        279 charge
    S(6)      409
    Al        1.2
    Ba        1.2
    B         0.73
    Fe        1.6
    Ni        0.05
    Sr        0.18
    -water    1 # kg
END
REACTION 1
    HNO3      1
    0.001  0.005  0.01  0.05 0.1 moles
USE solution 1
END
```

Figure 22: Input files for PHREEQC Interactive batch reactions with H_2SO_4 and HNO_3 mineral acids ranging from 0.001 M to 0.1 M.

```
SOLUTION 1 # No 7 Dam Average Dissolved
    temp      25
    pH        8.98
    pe        4
    redox     pe
    units     mg/l
    density   1
    Alkalinity 675
    Ca        11
    Cl        99
    F         5.9
    Mg        9.2
    N         2.5
    K         35
    Na        279 charge
    S(6)      409
    Al        1.2
    Ba        1.2
    B         0.73
    Fe        1.6
    Ni        0.05
    Sr        0.18
    -water    1 # kg
END
REACTION 1
    NaHSO4     1
    0.001 0.005 0.01 0.05 0.1  moles
USE solution 1
END
```

```
SOLUTION 1 # No 7 Dam Average Dissolved
    temp      25
    pH        8.98
    pe        4
    redox     pe
    units     mg/l
    density   1
    Alkalinity 675
    Ca        11
    Cl        99
    F         5.9
    Mg        9.2
    N         2.5
    K         35
    Na        279 charge
    S(6)      409
    Al        1.2
    Ba        1.2
    B         0.73
    Fe        1.6
    Ni        0.05
    Sr        0.18
    -water    1 # kg
END
REACTION 1
    HCl     1
    0.001 0.005 0.1  0.5  1  2  5 moles
USE solution 1
END
```

Figure 23: Input files for PHREEQC Interactive batch reactions with $NaHSO_4$ and HCl mineral acids ranging from 0.001 M to 5 M.

4.11 STANDARDDATA PROCESSING AND PRESENTATION

4.11.1 Weathering indices

As many as 30 different chemical indices have been proposed to evaluate to what degree weathering of a parent material extend. In calculating these indices the degree of weathering is evaluated against the loss of certain elements (Ca, Na, Mg, K and Si) and accumulation of others (Al, Fe, Ti, Mn) with respect to the composition of the parent material. Unfortunately most chemical weathering indices were developed with systems of felsic or intermediate composition. Duzgorin-Aydin *et al.* (2002) assessed the various indices by correlating the respective indices, calculated for samples along a weathering profile, with petrographic observations. Their assessment revealed Parkers index developed in 1970 and Colman's (1982) bases:alumina ratio to show good correlation for mafic or ultramafic systems. In 2007 Ohta & Arai proposed an alternative statistical weathering index independent of parent rock composition. Principal component analysis (PCA) is represented on a ternary diagram where the M and F vertices represent the character of the mafic (M) and felsic (F) parent material and the W-index the degree of chemical weathering.

However, the leaching factor developed by Jenny (1941) is a simple yet accurate indication of the removal of monovalent or divalent cations with respect to Al_2O_3. The leaching factor (β) was calculated as set out below to indicate the degree of weathering from the kimberlite (parent material) in relation to the tailings material, after 20 cycles of leaching for the kimberlite and the tailings, as well as the No 7 Dam clay.

$$\beta = \frac{b_a leached\ material}{b_a parent\ material}$$

Equation 12

Where $b_{a1} = \frac{(Na_2O+K_2O)}{Al_2O_3}$ or $b_{a2} = \frac{(CaO+MgO)}{Al_2O_3}$

Equation 13

4.11.2 Stiff diagrams

Named after the developer, Stiff (1951), these diagrams give a visual summary of the major cation and anion components and concentrations on opposite sides of a T-shaped graph. The mg/L concentrations are usually converted to meq/L. The Stiff diagrams presented were compiled with Rockworks 16, a software program used for processing and visualising earth-science datasets.

CHAPTER 5

PRESENTATION AND INTEGRATED DISCUSSION OF THE RESULTS

The results are ordered to follow the rationale of Chapter 3. This chapter is sub-divided into four sections. The first section regards the physical character of the materials, the second regards the mineralogy of the materials and the third regards the chemical character of the materials. Each of these sections progresses from the kimberlite rock, to the tailings and then, finally, to the No 7 Dam clay. The forth section of this chapter regards the water quality of the No 7 Dam. Where applicable, throughout the sections, a comparison will be made between the character of the material before and after any treatment as set out in the previous chapter.

5.1 PHYSICAL CHARACTERISTICS OF THE KIMBERLITE ROCK, TAILINGS AND SUSPENDED CLAY

5.1.1 Description of the Kimberlite

According to the classification scheme developed by Cas (2009) the physical appearance of the kimberlite can be described as coherent (Cas & Hayman, 2011) and inequigranular. Much of the groundmass shows alteration to serpentine and visible autholiths. Macrocrysts range from extremely large (16-32 mm) to medium (0.25 mm) crystals. In the case of rounded (often oblate) macrocrysts, alteration rims are prominent. Angular euhedral to anhedral macrocrysts are also occurring. The kimberlite is relatively crystal poor (<10%) and shows very poor vesicularity (0-20%).

5.1.2 Particle size distribution of the materials

A standard mechanical sieve analysis of the composite sample shows the bimodal PSD of the tailings materials as illustrated in Figure 25. It is clear that the fractions > 1 mm dominate. The sloping of the cumulative % passing curve shows the relatively even distribution of the smaller fraction particles. Only 3 % material sampled from the tailings dumps were smaller than 75 µm.

A remarkable change in PSD observed after just 20 cycles of leachings. The % of particles exceeding 7mm changed from 20% to below 5%. The larger particles are now dominated by fractions retained on the 4 mm and 1.7 mm sieves, somewhat more for kimberlite than tailings material. The 1.4mm fraction was also reduced from 10 % to less than 5 %.

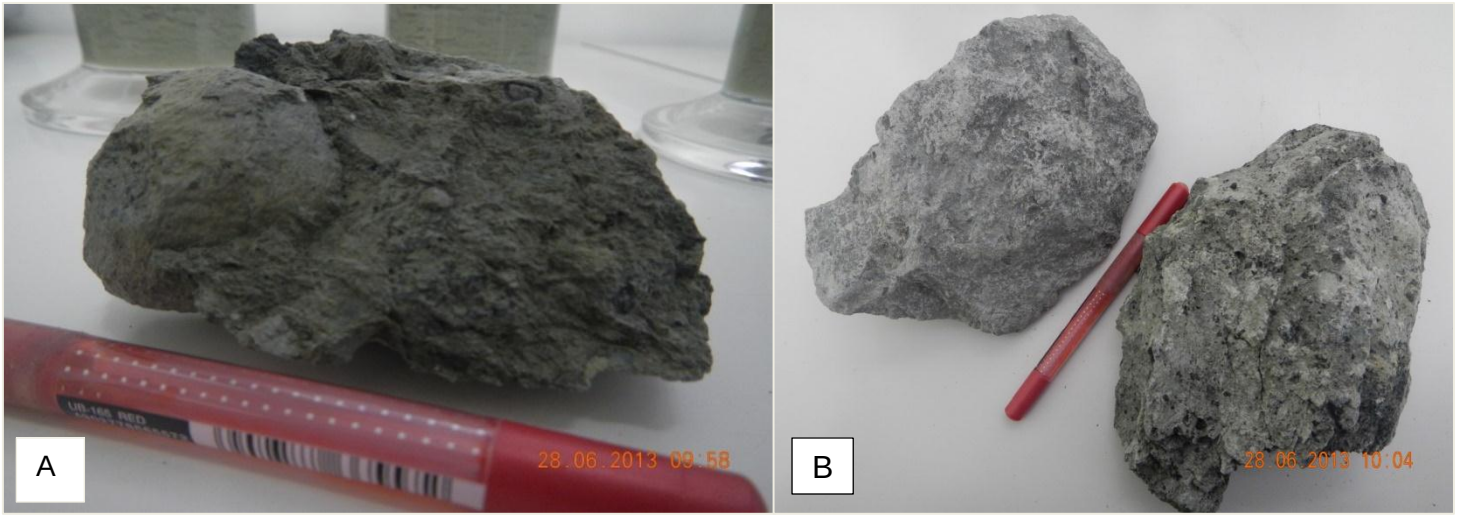

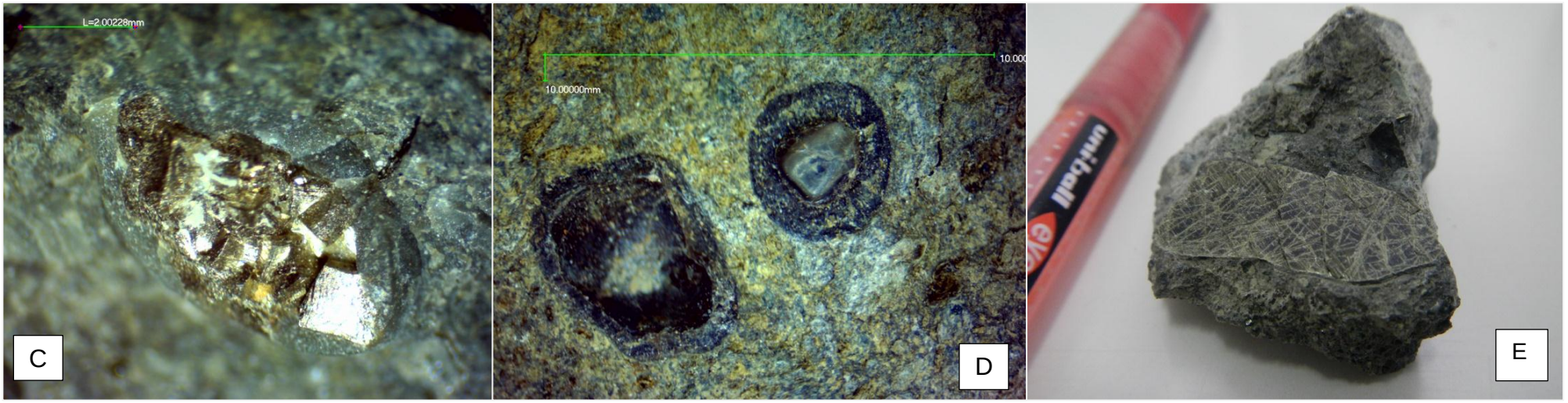

Figure 24: Kimberlite aggregates showing serpentinization in A and a range of macrocrist sizes in B. Vesicular cubic pyrite (C), alteration rims around garnet (D) and macrocrystic olivine (E) were amongst interesting observations.

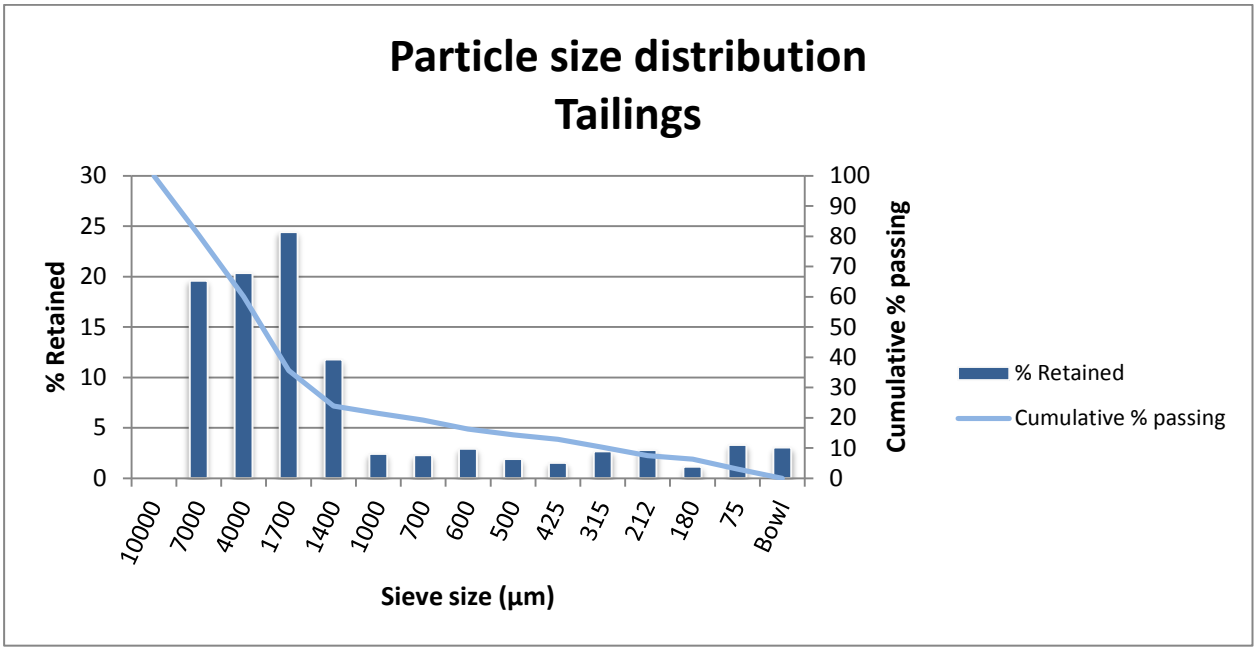

Figure 25: The distribution of particle sizes of the tailings material sampled from the storage sites at the Cullinan mine.

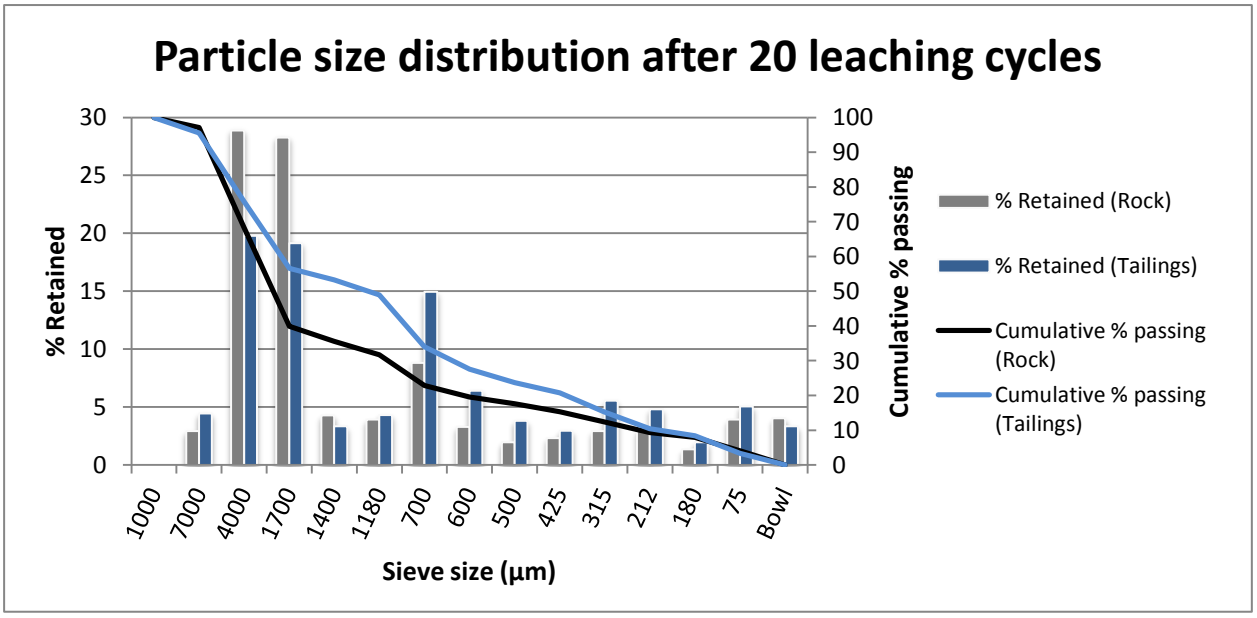

Figure 26: The distribution of kimberlite and tailings particle sizes after it has been subjected to 20 cycles of leaching.

There was a significant increase in the fraction of particles retained on the 0.7 mm sieve, from 2 % for the tailings before to 15 % after. The less steep decline in the cumulative % passing curve reflects a better distribution of particles across the measured size fractions. There was a slight increase in most of the fractions smaller than 0.6 mm but still only about 3 to 4 % of both fresh rock and tailings material were smaller than 0.075 mm.

5.1.3 No 7 Dam suspended clays:

Each litre of the No 7 Dam water contain 6 058 mg of solids in suspension (TSS). In the more dense, more turbid subsurface layer of the No 7 dam, the TSS exceeded 200 000 mg/L. Once removed the clay has a uniform green-grey colour matching 10Y-5GY 6/2 on the Munsell soil colour chart. The 15 cm clay bar showed linear shrinkage (length) of 7 % but the total volume reduction amounted to 65% as set out below.

$$COLE = \frac{L_M - L_D}{L_M} \times 100$$
$$= \frac{18.72\ g - 6.42\ g}{18.72\ g} \times 100 = 65.7\ \% (\pm\ 2.14)$$

Equation 14

After treatment the clay collected at the bottom of the sedimentation column displayed a volume reduction of 73 % upon air-drying.

$$COLE = \frac{L_M - L_D}{L_M} \times 100$$
$$= \frac{15g - 4.02\ g}{15\ g} \times 100 = 73.02\% (\pm 2.97)$$

Equation 15

The change in mass from saturated state to dry (Figure 27) shows that the clay has the capacity to retain about twice its mass in water at the PL. The decrease in weight (and increase in shrinkage capacity), post treatment, can be explained by the formation of disorganised, increasingly complex cohesive aggregates (flocks) of larger volume as found by Maggi (2005).

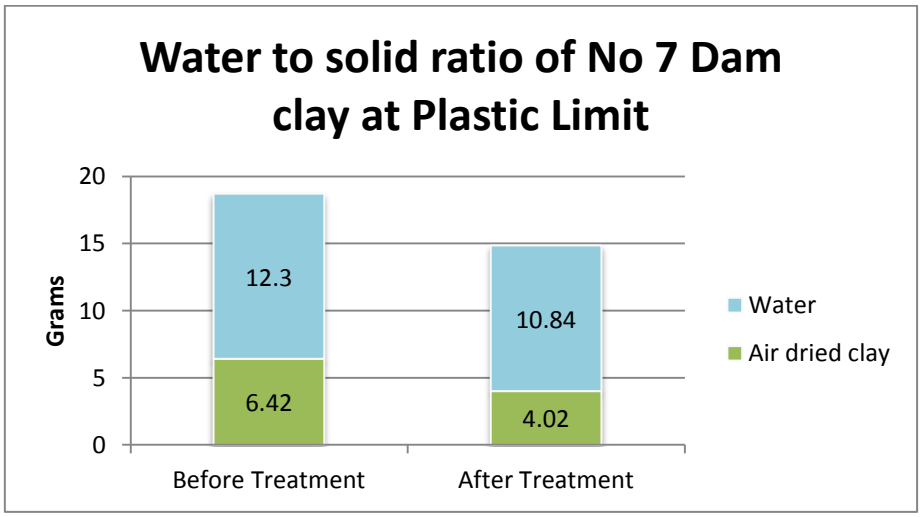

Figure 27: The amount of water contained by the No. 7 Dam clay is reflected here from the difference in weight when 15 cm^3 of saturated clay air dries.

The images following captured by SEM and TEM respectively, shows the typical platy structure of phylo-silicates, exhibited by the No 7 Dam clay. The separated flakes range from several microns to a few nanometres in length. They are mostly irregularly shaped but some hexagonal flakes have been identified. With respect to their thickness these flaky particles are excessively long along their *b* and *c* crystallographic axes. Brownian movement of small particles is at a relatively higher velocity (Malvern Instruments. 2004.) and could contribute to turbulence that keep these clay particles from settling. The physical character of the clay flakes (extremely thin and long in comparison) means it has virtually no mass because of its resistance to settling in water. The shape of the particles (large faces and small edges) also influence charge distribution. Less/ smaller anion exchange capacity compared to negative charge or cation exchange capacity is expected.

5.2 MINERALOGICAL CHARACTERISTICS OF THE KIMBERLITE ROCK, TAILINGS AND SUSPENDED CLAY MINERALS

5.2.1 Observations from Petrographic Microscopy

The six thin section slides produced from the 717 m, 732 m, 747 m levels are dominated by altered grains of olivine > diopside; mostly anhedral, rounded, often elongated and enclosed by sphene and perovskite. These minerals are completely pseudomorphed by chlorite, serpentine, talc and mixed layer smectite-chlorite. Olivine was probably the first to start weathering by breaking down into Fe-rich brucite + serpentine (Bach *et al*., 2006), from which magnetite was then deposited as the brucite dissociates in the low silica environment (Barnes & O'Neil, 1969; Frost & Beard, 2007) under reducing conditions (Shervais, Kolesar & Andreasen, 2005). As the alteration product of the primary olivine the serpentine, and associated magnetite precipitation, occur in the rims and extensive fracture systems that are seen throughout the kimberlite samples. This is clearly visible in both Figure 29 and Figure 30 below indicating progressed alteration to lizardite (Beard *et al.*, 2009), which is supported by the XRD results presented in the next section (see **Error! Reference source not found.** and Table).

Following serpentinization, the re-equilibration of the precipitated oxides, contribute to the development of complex interstratified mixed layers of serpentine and chlorite as the weathering process continues to break down serpentine. Golding & Bayliss (1968) explain how the alteration of spinels induces metasomatic exchanges in the micro-environment which then feed the transformation of lizardite to chlorite.

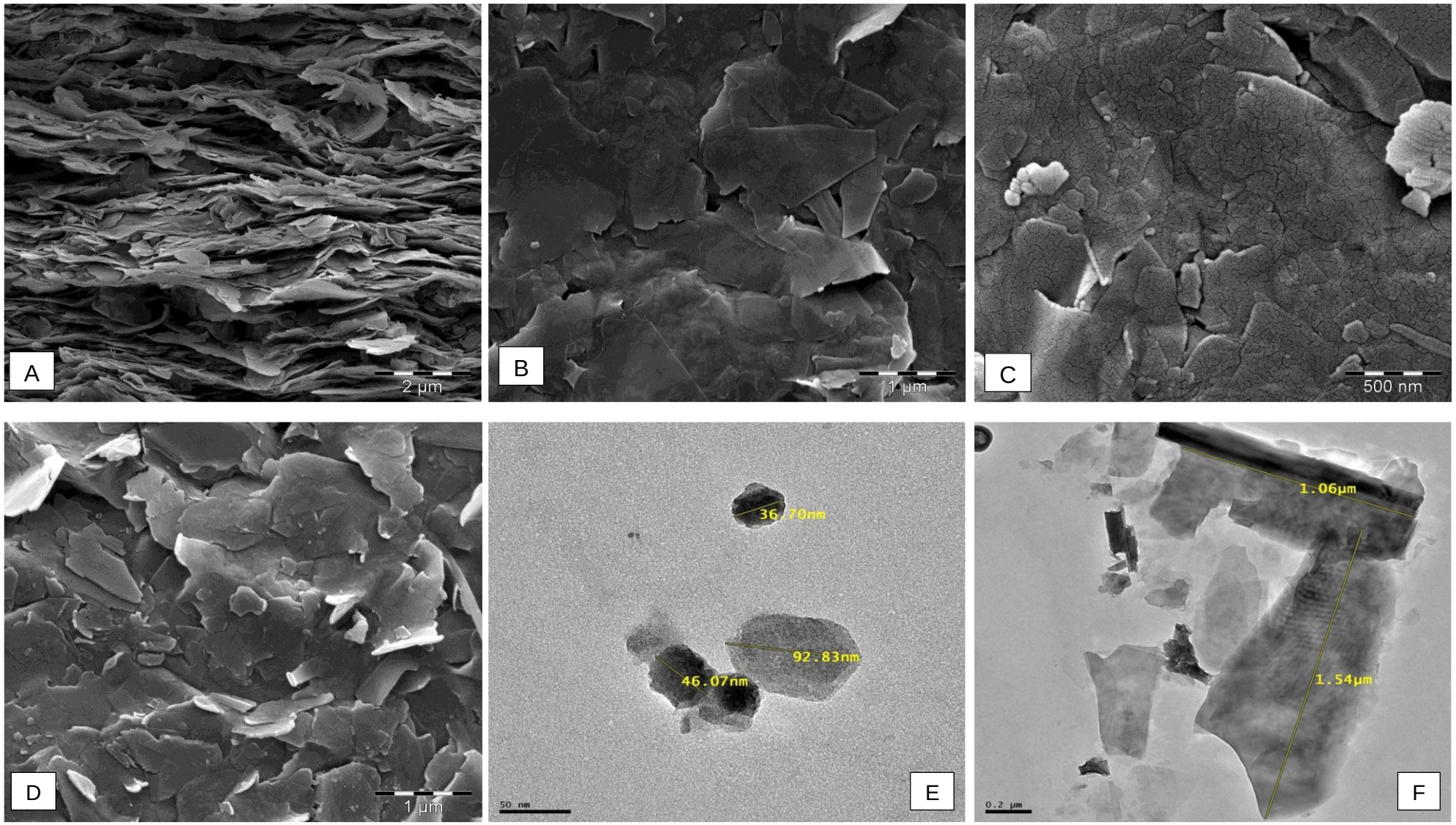

Figure 28: SEM (A, B, C & D) and TEM (E &F) imaging of the No 7 Dam clay. Image A is a cross-section through the clay cake. Image B and D emphasise how thin these particles are as some of the flakes appear transparent. Note the stacking of flakes pointed out in D. C illustrates micro-cracks as the clays dry out. E shows stacking of hexagonal shaped flakes. F displays some of the internal structuring.

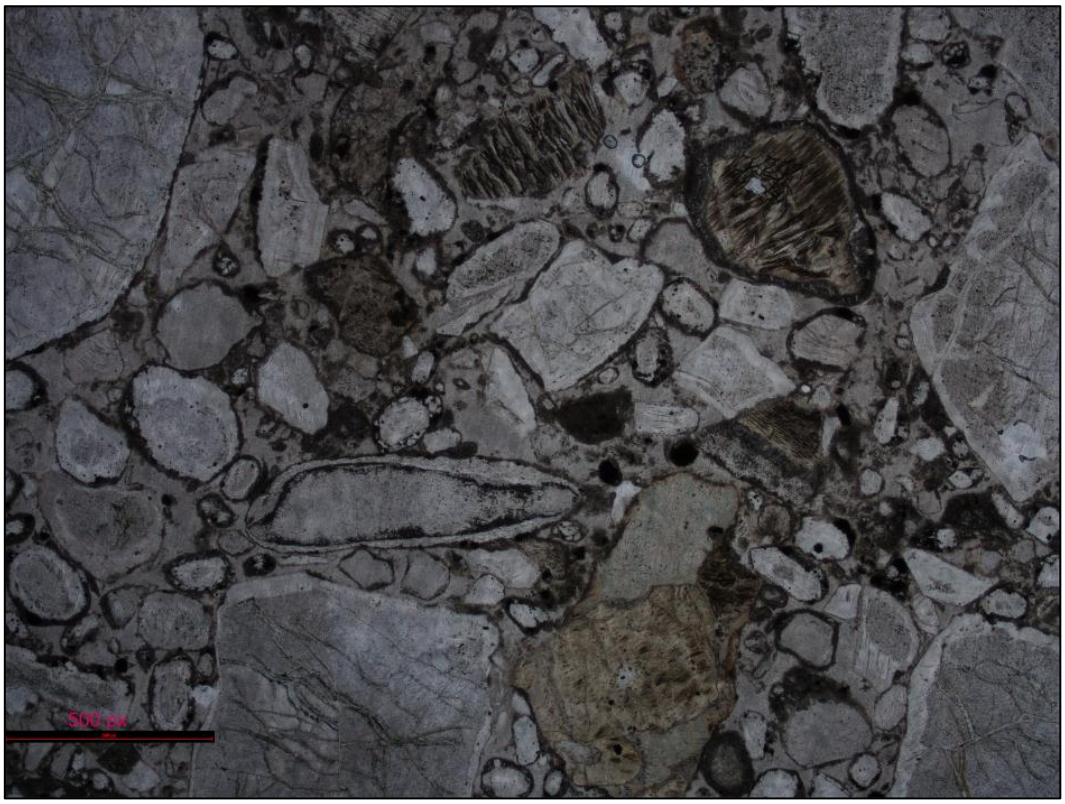

Figure 29: A photomicrograph of a 747 m level kimberlite sample, in plain polarised light with 50x magnification, depicting an overview of the Cullinan kimberlite texture, composition and extent of alteration. Note the presence of isotropic magnetite along the rims of altered olivine pseudomorphs.

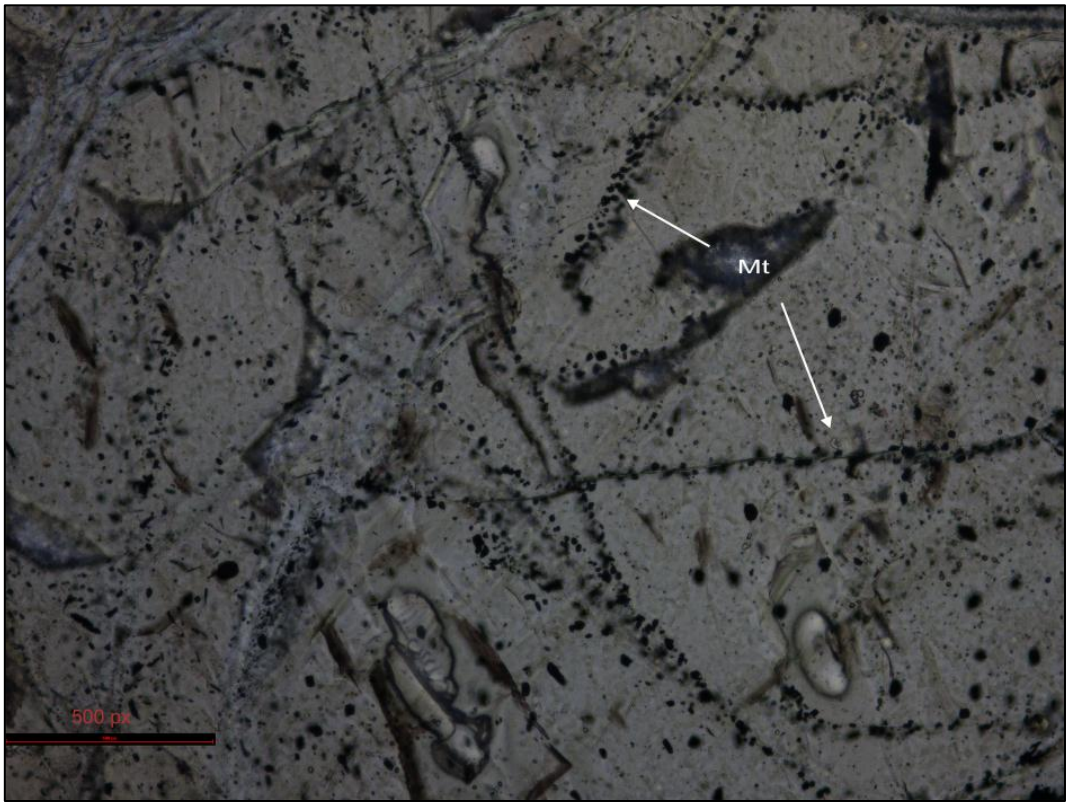

Figure 30: Magnetite grains are visible along fractures in an altered olivine grain of a 732 m level kimberlite sample, as a by-product of serpentinization. A 200 x magnification in plain polarised light was used.

Mellini, Rumori & Viti (2005) and Beard *et al.* (2009) reinforce this association in their respective studies with the description of chlorite aureoles overgrowing mesh serpentinization textures, and chlorite only occurring adjacent to magnetite-containing serpentine-filled factures in early stage transformation. Chlorite then transforms to vermiculite through structural adaptation as a response to loss of cations (Fe > Mg > Al) from the interlayer brucite-like sheet of the chlorite, by means of incongruent dissolution (Douglas, 1989; Banfield, & Murakami, 1998). In terrestrial weathering environments this step is associated with goethite crystallization which does not occur in the given environment (meaning the Cullinan kimberlite).

The groundmass of the kimberlite mostly comprises olivine, phlogopite, talc, calcite and some pyroxene and amphibole. Frick (1970) adds fluoritic apatite, which was not identified in the samples investigated for this study. Similar alteration processes can be expected to affect the groundmass olivine and pyroxenes. Groundmass phlogopite, however, is also being transformed simultaneously (Figure 31 and Figure 32) to chlorite, mixed layer chlorite-smectite (saponite) to smectite (Mitchell *et al.*, 2008) or alternatively to mixed layer mica-vermiculite or mica-smectite.

This interstratification develops as K^+ in the interlayers of the phlogopite is replaced with other hydrated exchangeable cations dictated by the weathering solution (Fanning, Keramidas & El-Desoky, 1989) because of it approximation to preferential weathering planes (Jackson *et al.,* 1952). Norish (1973) made the observation that, as K is lost from interlayer spaces, a slight shift in structural OH towards the open cation sites occurs, which leads to K in the adjacent interlayer space to be more tightly bound.

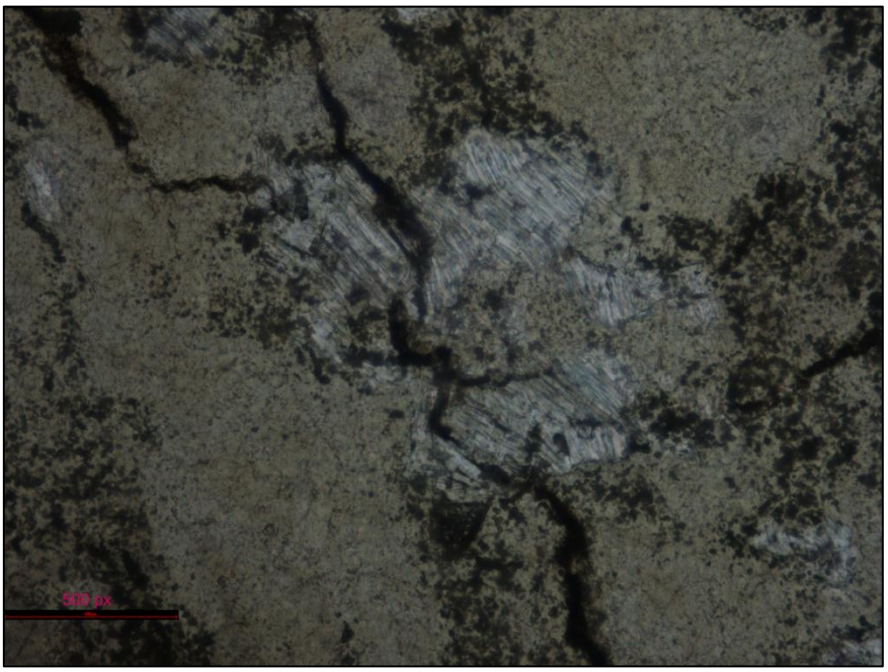

Figure 31: The alteration and interstratification in a groundmass phlogopite grain as seen in 200 x magnification of a sample of the 717 m level of the Cullinan kimberlite in plain polarised light.

This effect leads to the interstratification mica-vermiculite or mica smectite, even in progressively weathered samples.

It should be considered that the mineral transformations discussed here are subject not only to the influence of chemical potential gradients (ions in solution, Eh, pH) but also potentially to pressures and temperatures different from that of surface weathering environments.

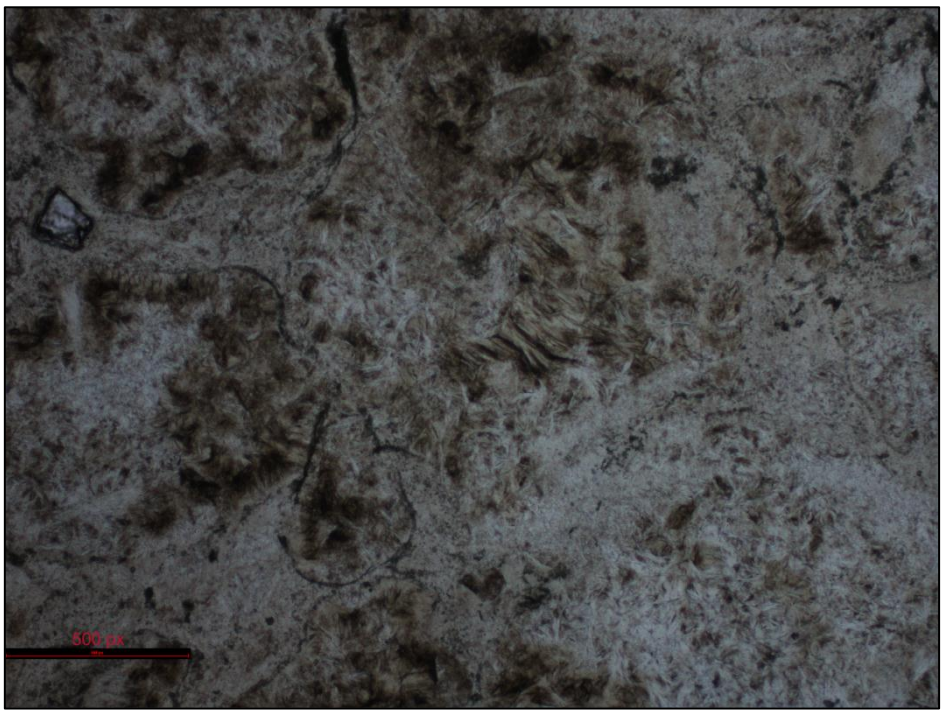

Figure 32: A 100x magnification of the 474 level Cullinan kimberlite, in plain polarised light, showing textures due to alteration of the groundmass to smectite clay similar to those described by Mitchell *et al.* (2008).

5.2.2 X-Ray Diffraction Analysis

The major minerals components, as identified with XRD, correspond with those identified by Morkel *et al.* (2006). Quantification is complicated by the changes induced by glycolation and heating of the samples. These changes are displayed in Figure 33 to Figure 38 below. Each corresponding table lists the peak positions and *d*-spacings for the various minerals identified for 4° to 20° 2Θ in the preceding diffractogram. The mineralogical compositional percentages are also given as for the minerals determined in untreated samples (see Table 14 to Table 21).

The chlorite peak at 6.1° 2Θ (14 Å) in the kimberlite rock and tailings material slightly intensifies and broadens significantly after exposure to ethylene glycol vapour. This peak diminishes again after the samples are heated at 550° C for two hours. Morkel *et al.* (2006) motivates this to be the appearance of a smectite peak. The broadening of the peak indicates an increase in thickness (Moore & Reynolds, 1997). Chlorite is a non-swelling clay and the broadening of this

peak can therefore be contributed to interlayer stratification with a swelling clay such as smectite.

The same peak intensification observed by Morkel *et al,* (2006), is seen for both phlogopite (8.8˚ 2Ɵ with *d*-spacing 10 Å) and talc (9˚ 2Ɵ with *d*-spacing 9.8 Å) after the rock samples are heated (see Figure 33). The peak at 12.3˚ 2Ɵ representing chlorite (7.3 Å) is also reduced in intensity after heating of the samples. This is consistent with the increase in relative intensity that Morkel *et al,* (2006), reported for the 14.1 Å chlorite peak at 6.3 ˚ 2Ɵ. There is no significant change in mineral composition after only 20 weeks of leaching. A longer observation period might be necessary.

Vermiculite appears in the post-leaching kimberlite sample, and becomes more prominent after glycolation. According to Moore & Reynolds (1997) approximately equal intensities for the peaks at 12.2˚ 2θ and 19.6˚ 2θ represent low Fe vermiculite. This is in order with the prediction of Velde & Meunier (2008) that trioctahedral magnesium-rich clays are formed at higher (above neutral) pH levels, which is the case for the No 7 Dam, while dioctraheral aluminium rich clays are formed under more acidic conditions. After heating, the vermiculite peaks disappear again. This confirms the presence of swelling clay. As stated in section 2.2.2, vermiculite commonly forms in transition to the smectite group of minerals from primary micas or chlorite with the loss of Mg or K. There is a slight decrease in Mg content after 20 weeks of leaching (21.9 to 21.5 % MgO; see annexure C) but a more evident loss of Mg content from the subsurface sample compared to the tailings (21.9 to 19 % MgO; see Annexure C).

In the tailings material vermiculite is present in the untreated sample as well as the glycolated sample. As expected, it is not detected after the samples have been heat treated. The presence of minor amounts of labradorite could be explained by plagioclase introduced by Bushveld norite/gabbro wall-rock contamination (see Figure 5).

The shift from 6˚ 2θ (15 Å) to a strong peak at 5.2˚ 2θ (16.9 Å) is a clear identification of the presence of smectite in the No 7 Dam as seen in both Figure 37 and Figure 38. The distinction between nontronite, montmorillonite and saponite are induced by variations in the Fe content. According to Moore & Reynolds (1997) significant changes in diffraction pattern after glycolation, along with general broad peaks, are a good indication that the smectite occurs interstratified with another clay mineral(s), most likely montmorillonite-chlorite indicated by the change occurring around 16 to 17.7˚ 2θ alltough illite/smectite is also likely.

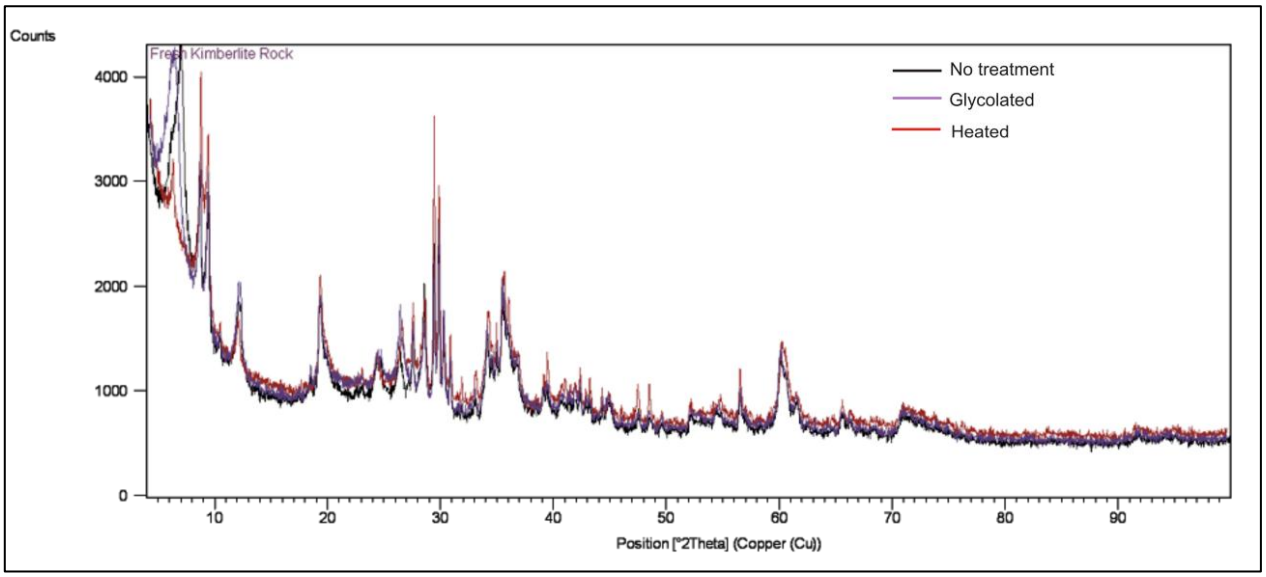

Figure 33: Mineralogical changes affected on the diffractogram of the Cullinan kimberlite, by glycolation and heating.

Table 7:Minerals present in the Cullinan kimberlite as represented by the 4° – 20˚ 2Θ section of the diffractogram (Figure 33) brought on by glycolation and heating (550 °C).

MINERAL	*PEAK POSITION °2Θ*			*d-SPACING*		
***Content* (weight %)**	***Untreated***	***Glycolated***	***Heated***	***Untreated***	***Glycolated***	***Heated***
Chlorite *12.6%*	6.4	6.4	6.1	13.9	13.6	14
	9.2		9.4	9.6		9.4
	12.3	12.9	12.3	7.2	6.8	7.2
	15.4		15.2	5.8		5.8
	18.5		18.5	4.8		4.8
Talc *6.5%*	8.9		9.2	9.9		9.7
	11.4			7.7		
	12		12.5	7.3		7.1
		14	13.8		6	6.4
	15.3	15.3		5.8	5.7	
	17	17	16.9	5.2	5.2	5.2
	18		18.3	5		4.9
Phlogopite *40%*	8.8	8.8	8.7	10.1	9.9	10.1
	17.5		17.5	5,		5
	19.3			4.6		
Lizardite *11%*	12.1	12.1	12.1	7.3	7.3	7.2
Pyroxene group *23.3%*	13.7	13.7	13.7	6.4	6.4	6.4
	18.9		8.9	4.7		4.7
Amphibole		9.8	9.8		8.9	9
		10.5	10.5		8.3	8
		17'3	17.3		5.1	5

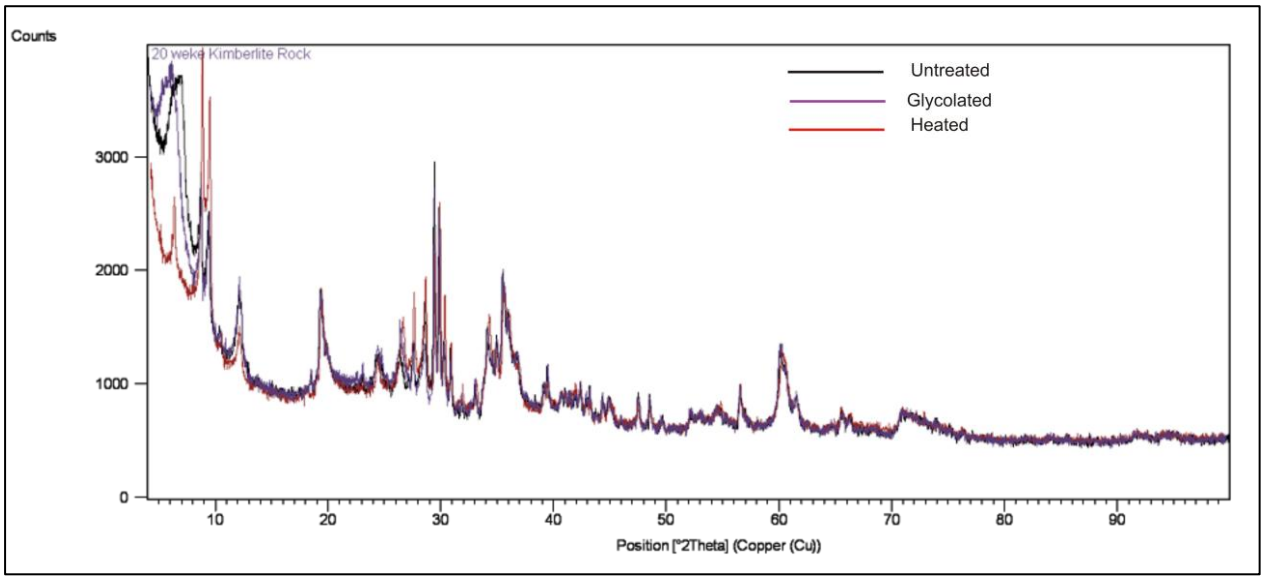

Figure 34: Mineralogical changes affected on the XRD diffractogram of the Cullinan kimberlite after 20 cycles of leaching, by glycolation and heating.

Table 8: Table 8: Minerals present in the Cullinan kimberlite as represented by 4°-20˚ 2Θ section of the diffractogram (Figure 34) after 20 cycles of leaching.

MINERAL	***PEAK POSITION 2Θ***			***d-SPACING***		
CONTENT (weight %)	***Untreated***	***Glycolated***	***Heated***	***Untreated***	***Glycolated***	***Heated***
Chlorite *20%*	6.1, 9.2, 12.3, 15.3, 18.5,	6.6, 13.2,	6.6, 9.4, 13.2, 15.2, 18.5,	14.4, 9.6, 7.2, 5.8, 4.8,	13.4, 6.7	13.4, 9.4, 6.9, 5.8, 4.8,
Vermiculite *17.4%*	6.4 12.8	6.1 12.2, 18.3, 18.7 19.6		13.9 6.9	14.5 7.3, 4.5, 4.7 4.5	
Talc *3%*	9.5, 11.4, 12, 13.4 15.3, 17	9.7, 11.9, 14,3 15.3, 16.5	9.2, 10 12 13.8, 15.2 17.2	9.3, 7.7, 7.3, 6.6 5.8, 5.2,	9.2 7.4, 6.2, 5.7, 5.4,	9.5, 8.8 7.4 6.4, 5.8 5.2
Phlogopite *25.2%*	8.8, 17.5, 19.3	8.8, 17.5	8.8, 17.7	10.1, 5 4.6	10.1, 5	10.1, 5
Lizardite *14.6%*		12.1	12.1 19.3		7.3	7.3 4.6
Pyroxene group *24.2%*	13.7, 18.9	13.6, 18.9	13.7, 18.8	6.5, 4.7	6.5 4.7	6.5, 4.7

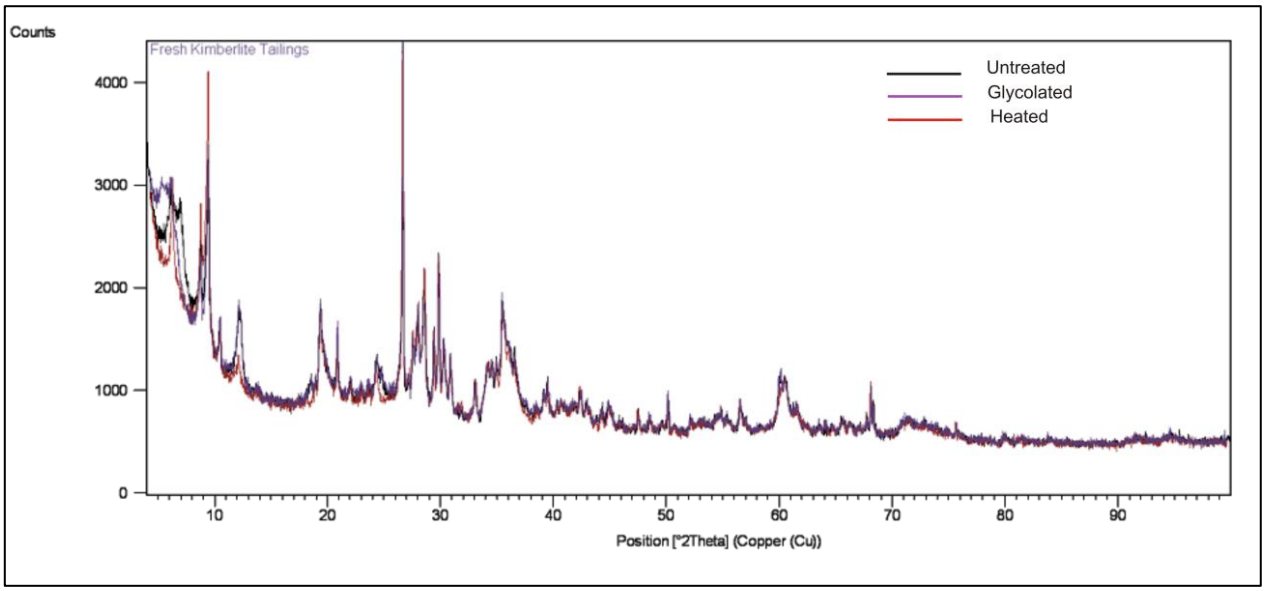

Figure 35: Mineralogical changes affected on XRD diffractogram of the Cullinan tailings by glycolation and heating, prior to leaching.

Table 9: Minerals present in the Cullinan kimberlite tailings as represented by the 4-20° 2Θ section of the diffractogram (Figure 35) prior to leaching.

MINERALS	***PEAK POSITION 2Θ***			***d-SPACING***		
CONTENT (weight %)	***Untreated***	***Glycolated***	***Heated***	***Untreated***	***Glycolated***	***Heated***
Clinochlore *0.1%*	6,4		6,3	13,9		14,1
	12,7		12,6	6,9		7,0
	19,1		18,9	4,6		4,7
Vermiculite *10%*	6,4	6,2		13,9	14,3	
	12,7	12,4		6,9	7,2	
	17,9			4,9		
	18,3	18,5		4,9	4,8	
	19,2	19,5		4,6	4,5	
Phlogopite *22.7%*	8,8	8,8	8,8	10,0	10,1	10,0
	17,6			5,0		
	19,5			4,6		
Talc *6.1%*	9,3	9,7	4,3	9,6	9,1	20,4
	13,2	13,4	7,4	6,7	6,6	11,9
	13,6	13,7	8,7	6,5	6,5	10,2
	16,8	16,9	10,9	5,3	5,2	8,1
	18,6		13,0	4,8		6,8
			14,9			5,9
			15,9			5,6
			16,7			5,4
Amphibole group *10.9%*	9,8	9,8	9,8	9,0	9,0	9,0
	10,5	10,5		8,4	8,4	
	17,4	17,3	17,3	5,1	5,1	5,1
	18,2	18,2		4,9		4,9

Table 9: (*cont.*) Minerals present in the Cullinan kimberlite tailings as represented by the 4-20° 2Θ section of the diffractogram (Figure 35) prior to leaching.

MINERALS	***PEAK POSITION 2Θ***			***d-SPACING***		
CONTENT (weight %)	***Untreated***	***Glycolated***	***Heated***	***Untreated***	***Glycolated***	***Heated***
Lizardite	12,2	12,2	12,1	7.3	7,3	7,3
20.1%		19,3	19,3		4,6	4,6
Pyroxene group	13,7	13,7	13,7	6,5	6,5	6,5
23.1%			19,9			4,5
		6,7			13,2	
		9,			9,5	
		9,9			8,9	
Labradorite		11,5			7,7	
0.4%		13,1			6,7	
		14,2			6,2	
		15,7			5,6	
		16,3			5,4	

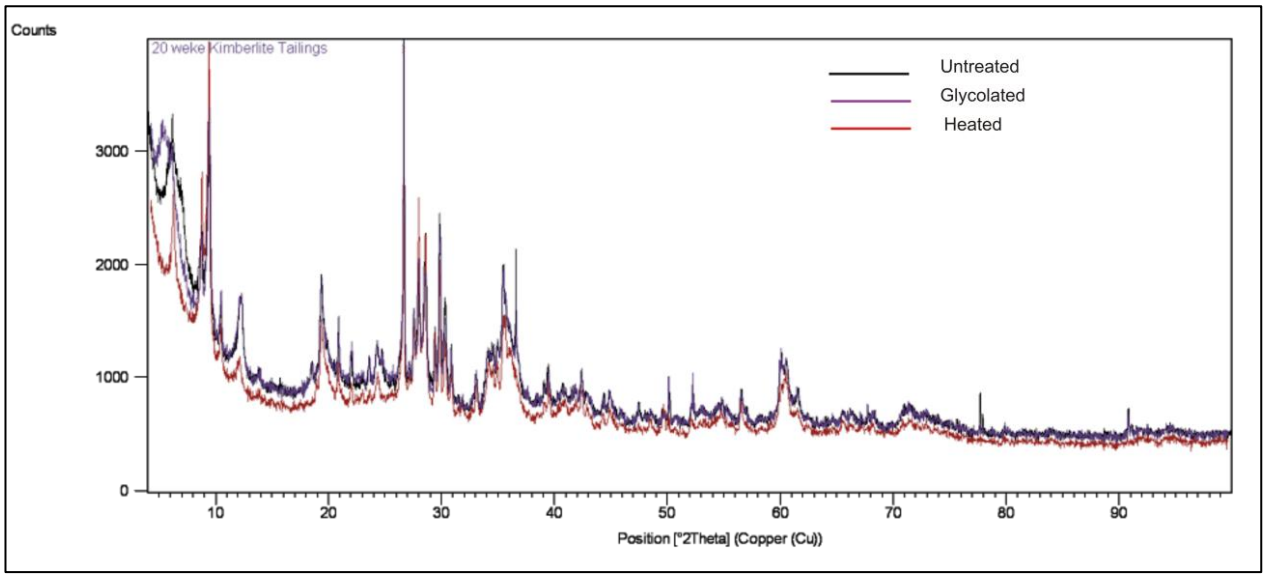

Figure 36: Mineralogical changes affected on the XRD diffractogram of the post-leaching Cullinan kimberlite tailings by glycolation and heating.

Table 10: Minerals present in the post-leaching Cullinan kimberlite tailings as represented by the 4-20˚ 2Θ section of the diffractogram (Figure 36) brought on by glycolation and heating (550 °C).

MINERAL CONTENT (weight %)	***PEAK POSITION °2Θ***			***d-SPACING***		
	Untreated	***Glycolated***	***Heated***	***Untreated***	***Glycolated***	***Heated***
Vermiculite *0.6%*	6,2 12,4 17,6 18,7			14,2 7,1 5,1 4,7		
Chlorite *20%*	6,2 12,4 18,7	6,1 9,5 11,1 15,2 16,8 18,5 19,6	6,4 12,7 19,1	14,2 7,1 4,7	14,4 9,3 7,9 5,8 5,3 4,8 4,5	13,8 6,9 4,7
Phlogopite *26%*	8,8 17,7	8,8 19,3	8,9	10,1 5,0	10,1 4,6	9,8
Talc *13.4%*	8,9 9,8 13,2 17,3 18,4	9,1 9,9	10,7 12,2 16, 18,7 19,2	9,9 9,0 6,7 5,1 4,8	9,7 8,9	8,3 7,2 5,5 4,7 4,6
Amphibole group *10.6%*	9,8 10,5 17,3 18,2	9,8 10,5 17,4 18,2	9,8 10,5 17,4	9,0 8,4 5,1 4,9	9,0 8,4 5,1 4,9	9,0 8,4 5,1
Pyroxene group *23.2%*	13,7 18,9	13,7	9,7 18,9 19,4	6,5 4,7	6,5	9,1 4,7 4,6
Lizardite *3.6%*			12,1 19,4			7,3 4,6

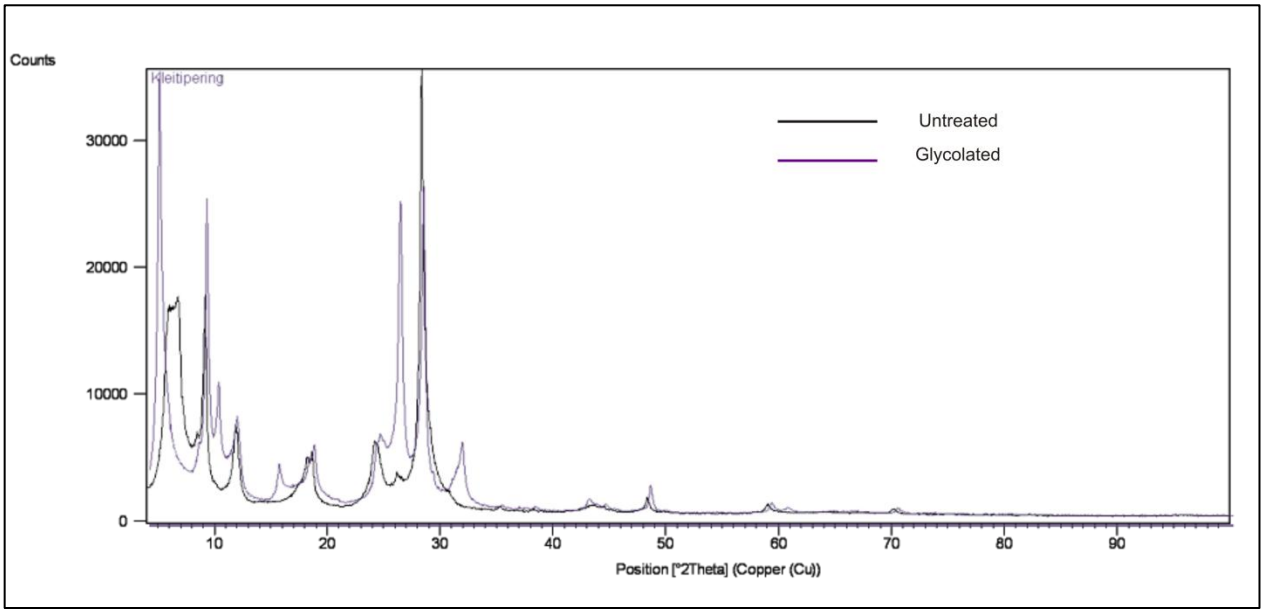

Figure 37: Mineralogical changes affected by glycolation on the XRD diffractogram of the Cullinan mine No 7 Dam clay, prior to treatment.

Table 11: Minerals present in the Cullinan mine No 7 Dam clay, as represented by the 4°-20° 2□ section of the diffractogram (Figure 37) before any treatment.

MINERAL	*PEAK POSITION °2Θ*		*d-SPACING*	
Composition (weight %)	*Untreated*	*Glycolated*	*Untreated*	*Glycolated*
Chlorite	6.3		14.1	
	12.5		7.1	
	18.6		4.8	
	19.3		4.6	
Montmorillonite-chlorite	6.1		14.5	
	9.1		9.7	
	12.2		7.3	
	18.3		4.9	
Saponite	5.7		15.5	
	11.4		7.7	
	17.3		5.1	
	19.4		4.6	
Nontronite		5.0		17.6
		10.3		8.6
		15.7		5.6

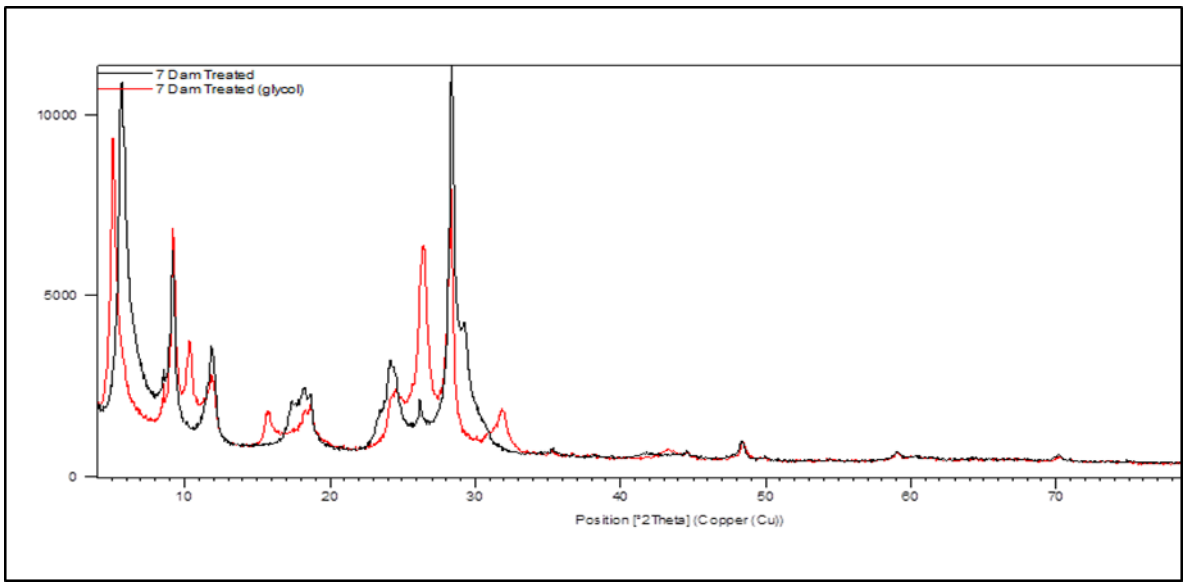

Figure 38: Mineralogical changes affected by glycolation, on the XRD diffractogram of the Cullinan mine No 7 Dam clay, after treatment.

Table 12: Minerals present in the No 7 dam clay, Cullinan mine, as represented by the 0°-20° 2□ section of the diffractogram (Figure 38) after treatment.

MINERAL	*PEAK POSITION °2Θ*	
Composition (weight %)	*Untreated*	*Glycolated*
Nontronite	X	X
Iron Phlogopite	X	X
Montmorillonite	X	

5.3 CHEMICAL CHARACTERISTICS OF THE KIMBERLITE ROCK, TAILINGS AND SUSPENDED CLAY

5.3.1 Contamination Index

Mitchell (1986) reported the crustal C.I. for the brown kimberlite (see Figure 5) as 2.02. The calculated C.I. for a composite XRF analysis from the three levels sampled was 1.853. This value indicates that the sample is only slightly contaminated. This confirms the findings of Wiethoff (2000) that contamination decreases with depth. From the XRF results below (**Error! Reference source not found.**), the enrichment in, not only SiO_2, Al_2O_3 and Na_2O, but also in K_2O, is clear.

$$C.I. = \frac{(SiO_2 + Al_2O_3 + Na_2O)}{(MgO + 2K_2O)}$$

$$= \frac{(40.86 + 4.491 + 0.874)}{\left(21.938 + (2 \times 1.503)\right)}$$

$$= 1.853$$

5.3.2 X-Ray Fluorescence

The following illustrated table (Fig 39) compares the elemental oxide composition as obtained by XRF. As expected Mg and Fe follows Si as most prominent constituents. Al concentrations are relatively higher that the average composition for Group I kimberlites. Ca values are significantly lower than expected for the tailings and kimberlite itself and even more so for the clay extracted from No 7 Dam. K and Na were confirmed to be somewhat higher than the average Group I kimberlite, as suggested by Frick (1970). K, Na and Ti each make up about 1% of the total composition (except Ti in the clay) for the respective materials. Compared to the kimberlite and tailings material, the clay appears to contain amply diluted amounts of the minor constituents Ti, Ba, Cr, Mn and P. The Ni content in the clay is more or less equal to that of both the kimberlite and tailings, which compares well to the average for Group I kimberlite. A slight increase/ accumulation of Na and SO_3 were observed in the clay.

The study by Miller *et al.* (2008) included some XRF analysis of the clay retrieved from different depth levels the No 7 Dam. At 10m depth they reported 1086 ppm Ni, 47544 ppm Fe, 786 ppm of Mn, 609 ppm of Cr, 3369 ppm Ti, 35344 ppm of Ca, 7622 ppm K, 439 204 ppm S as well as 758 ppm Ba and 105 ppm Te. In this study at 30m depth the following elemental abundances are reported: 988 ppm Ni, 41 026 ppm Fe, 587 ppm Mn, 429 ppm Cr, 1706 ppm Ti, 37 869 ppm Ca, 7137 ppm K, 680 380 ppm S, 612 ppm Ba and 55 ppm Te.

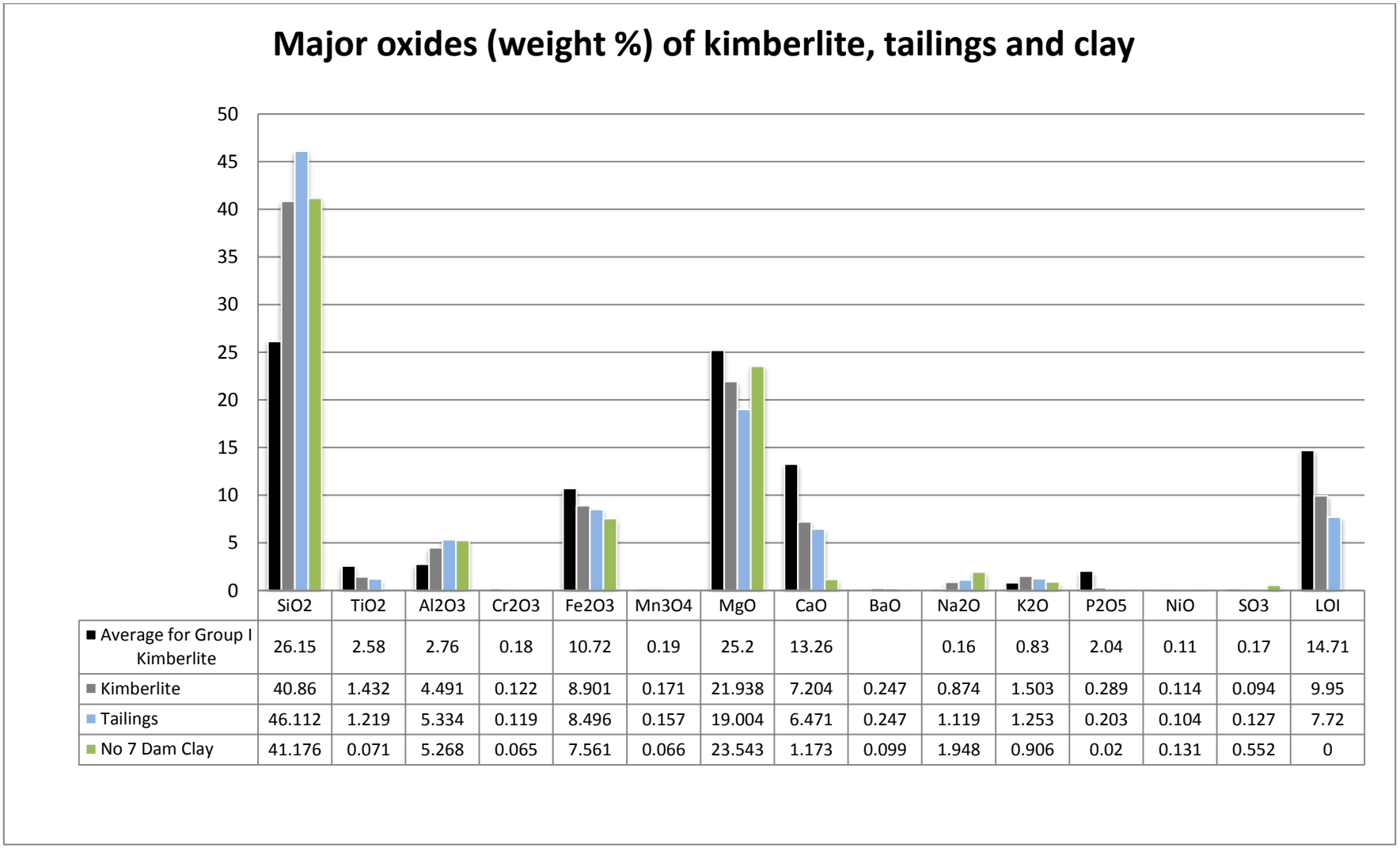

	SiO2	TiO2	Al2O3	Cr2O3	Fe2O3	Mn3O4	MgO	CaO	BaO	Na2O	K2O	P2O5	NiO	SO3	LOI
Average for Group I Kimberlite	26.15	2.58	2.76	0.18	10.72	0.19	25.2	13.26		0.16	0.83	2.04	0.11	0.17	14.71
Kimberlite	40.86	1.432	4.491	0.122	8.901	0.171	21.938	7.204	0.247	0.874	1.503	0.289	0.114	0.094	9.95
Tailings	46.112	1.219	5.334	0.119	8.496	0.157	19.004	6.471	0.247	1.119	1.253	0.203	0.104	0.127	7.72
No 7 Dam Clay	41.176	0.071	5.268	0.065	7.561	0.066	23.543	1.173	0.099	1.948	0.906	0.02	0.131	0.552	0

Figure 39: Comparison of major oxides present in the kimberlite rock, tailings and No 7 Dam clay. The averages for Group I kimberlite were calculated by Becker & Le Roex (2006), from selected South African kimberlite examples with minimal crustal contamination

There was no significant compositional change observed after the 20 cycles of leaching – see Appendix B.

Becker & Le Roex (2006) determined characteristic trace element patterns for South African Group I and II (on – and off-craton) kimberlites magmas represented in spider diagrams (also known as normalised multi-element diagrams) developed by Sun, Nesbit & Sharaskin (1979). In these diagrams the trace elemental abundances are usually normalised to some primitive mantle composition to even out the saw-tooth effect brought on by the uneven distribution of elements of odd- and even atomic number (known as Oddo-Harkins effect) (Winter, 2001). The work by Becker & Le Roex (2006) did not include the Cullinan kimberlite and therefore a spider diagram was constructed for the same set off elements, normalised to the same primitive mantle composition determined by Sun & McDonough (1989) for comparison. The clear trends seen in the shape of these diagrams allow for safe extrapolation of elements not determined as was done with dotted lines in the Figure 40 below (Winter, 2001).

The Cullinan kimberlite (and tailings material) clearly adheres to the pattern Becker & Le Roex (2006) developed for South African Group I kimberlites with little contamination. The smaller, more highly charged high field strength (HFS) incompatible elements (mostly on the right side of the diagram) occur at considerably lower concentrations than what Becker & Le Roex (2006) indicated (although it mostly follows the trend well). The trend persists for the No 7 Dam clay, but it retains significantly smaller concentrations of all the plotted trace elements. A noteworthy discrepancy does however occur for Nb (decreasing) / La (increasing) opposite to the kimberlite trend. Nb is a highly incompatible HFS element. Despite its ideal size for substitution, the high charge causes coordination with these elements (HFS's) to be energetically unfavourable. Nb is particularly immobile during weathering, insoluble and not well transported in aqueous solutions. La is a lithophilic rare earth element (REE) that have a preferred affinity toward silicate phases. Due to the higher valence (3+) and higher ionic potential (charge to ionic radius ratio) of La, it is readily coordinated by anions and therefore relatively insoluble in aqueous solutions (White, 1997). Due to the similar ionic radius but higher ionic potential La often substitute Na which could explain the increase observed for this element.

The clay was extracted by means of evaporation. It is recommended that this be compared to an analysis of the same clay minerals extracted by centrifugation. Evaporation can result in accumulation of dissolved constituents along with the suspended solids.

Table 13: Trace elements of the Cullinan kimberlite materials compared to the average trace elemental composition for Group I kimberlite as determined by Becker & Le Roex, (2006). Values determined for the bottom consolidated layers (at 30 m deep) are from Miller *et al.* (2008).

		AVERAGE FOR GROUP I KIMBERLITE[a]	KIMBERLITE	TAILINGS	NO 7 DAM CLAY	CONSOLIDATED SLIMES
				Concentration in ppm		
Alkali - & Alkaline-earth metals	**Rb**	*47*	96.8	58.3	58.2	61
	Sr	*1295*	408.3	303.4	137.7	284
	Cs		nd	nd	11.2	65
	Ba	*1308*				
Transition Metals	**Sc**	*17*	13.5	14.9	3.4	75
	V	*155*	92.4	95.9	28	144
	Cr	*1508*				461
	Co	*89*	67	72.6	40.1	356
	Ni	*935*				972
	Cu	*96*	43.3	38.7	19.6	62
	Zn		57.7	66.4	59	53
	Se		19.1	18.8	14.8	
	Br	*38*	18.7	16.5	32	
	Y	*20*	7.8	8.5	0.3	
	Zr	*371*	102.3	110.3	20.4	76
	Nb	*239*	74	48.5	3.3	
	Mo		1.8	0.9	7.2	10.8
	Pb	*10*	7	17.7	22.3	23
	Ag		nd	0.3	1.5	
	Cd		5.6	8.6	11.7	
	Hf	*7*	3.6	1.7	1.7	
	Ta	*12*	2.4	1.7	0.4	
	Hg		0	0.1	0	
	Th	*24*	16.4	11.6	8.2	
	Ga		4.6	5.2	6.4	
Other and Semi-metallics	**Ge**		nd	0.2	nd	
	As		67	64.3	51.3	
	Sn		7.7	10.3	10.9	21
	Sb		nd	nd	0.7	32
	Tl		23.4	21.2	15.6	
	Bi		31.1	29.7	23.8	
	La	*181*	38.7	28.1	3.8	
Lanthanides	**Ce**	*358*	45.1	52.8	7.8	
	Nd	*144*	28.5	30.5	8.2	
	Sm	*20*	2.6	0.9	nd	

nd = no detection

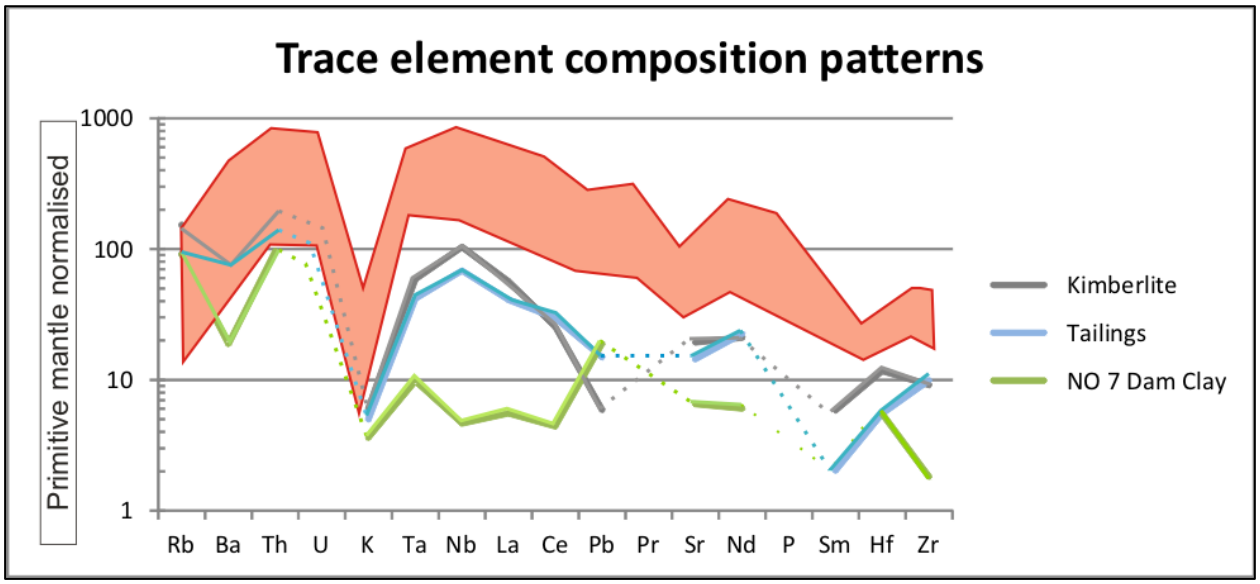

Figure 40: The trace element pattern (spider diagram) for the Cullinan kimberlite, tailings material and No 7 Dam clay, normalised to primitive mantle composition of Sun & McDonough (1989). The kimberlite and tailings materials follow the general trend of Group I kimberlites (red shaded area) developed by Becker & Le Roex (2006).

5.3.3 Alternative chemical parameters: CEC and exchangeable cations

The extracted clay of No. 7 dam has an unusually low CEC of 36.8 cmol/kg at pH 7 (but an S-value of 54.26 if adding all adsorbed cations together). According to Brady & Wel (2008) the pH dependent charges added in alkaline conditions will contribute about 5 % to the CEC in the case of smectite and up to 20 % in the case of non-swelling illite and chlorite. While both smectite clays and inerlayered illite occures in the NO 7 Dam water (see section 4.4.2), the determined CEC value resembles values typical of chlorites and fine grained micas (between 20 – 45 cmol/kg), more than that for smectite clay (typically around 80 – 100 cmol/kg) (Grondklassifikasiewerkgroep, 1991). This raises the question; to what extent has the transformation of mica to smectite (replacement of interlayer K) been completed? It has been found by Raussell-Colom *et al.* (1965) and Sanz & Stone (1979) that micas in which F replaces octahedral OH (such as phlogopite) binds interlayer K more strongly because of the electronegativity of F.

Both surface charges (permanent and pH dependent) and fixed interlayer charges contribute to the CEC of a clay. The detection of these charges can be influenced and vary according to the method used, incomplete ion exchange during sample preparation, and sample purity, as illustrated by Czímerová, Bujdák, & Dohrmann (2006) in their comparison of four different commonly used methods. Ideally, the surface charge distribution of a given sample will decrease in accordance with the ionic strength thereof since it will be energetically more difficult to accumulate surface charges in such conditions (Sparks, 2003). However, Kraepiel & Morel

(1998) found that surface charge distributions for clay minerals (kaolinite and montmorillonite were studied) behaved differently than ideal surface complexation models. Due to the porous nature (interlayer spaces) and fixed interlayer charges, a higher charge density is seen when the surrounding aqueous solution has a lower pH value and lower ionic strength. Figure 41 below shows the proportions of adsorbed cations that satisfy these surface charge sites while Figure 51 in sections 4.4.2 is an accurate indication of the extent thickness of the sorption double layer.

For the No. 7 Dam clay an ESP of the S-value was calculated as 39.8 % (58.75% when measured CEC is used). These values are extreme and not necessarily reliable due to the increased probability for analytical error at high Na concentrations. The SAR for a composite No 7 Dam water sample was given as 15 by Midvaal water. However, for the less dense top layer of the dam the SAR of 6 was calculated. This and declines to 3.5 for the more dense layer beneath it. The difference in SAR for the two layers is due to less dissolved (more adsorbed) ions being available in the lower layer (see section 5.4.1). After the mineral acid treatment the SAR of the cleared supernatant increased to 10 as dissolved Na and Ca increases (see Figure 49).. Acceptable SAR values specified in the DWA guidelines is 2.0 – 15 for irrigation (DWAF, 1996), depending on crop tolerance for Na. Irrigation water, with an SAR above 15 can have deconstructive effects on the structure of soils by inducing dispersion (Brady & Weil, 2008). For the leachate of both the kimberlite rock and tailings the SAR was also calculated as 3.5 (see appendix E).

Ca followed by Na, are removed from solution by preferential adsorption to the clay particles so that Mg and K are the prominent dissolved components (see Figure 41 and Figure 48).

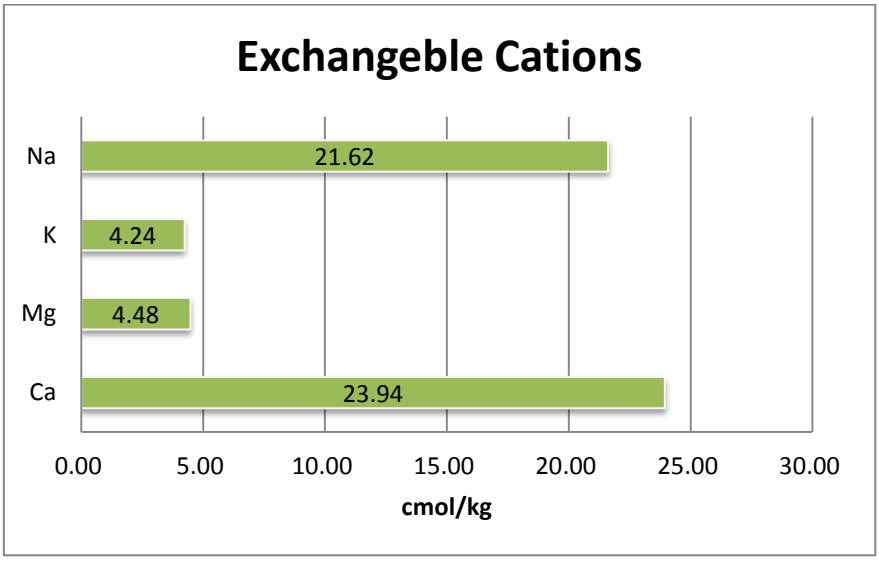

Figure 41: Ca and Na dominate the exchange sites on the clay particles of the Cullinan mine No. 7 Dam clay.

5.4 WATER QUALITY OF KIMBERLITE AND TAILINGS LEACHATE AS WELL AS THE NO 7 DAM BEFORE AND AFTER MINERAL ACID TREATMENT

5.4.1 Water quality of the kimberlite rock and tailings leachate

As expected of kimberlite, the pH_{H2O} of both the rock and tailings are fairly alkaline. Through the 20 weeks of accelerated weathering almost no change in the pH levels is observed (Figure 42). This is an indication of the buffer capacity provided by the weathering of alkali and carbonate minerals in the material (as explained in Equation 2 and Equation 3). The average pH of the No. 7 Dam is in the same range with no significant difference between the distinct layers. After the batch jar treatment (see section 5.4.3), the average of the decanted supernatant was 4.6. This is somewhat below the acceptable pH values specified in the DWAF guidelines for irrigation set at 6.5 to 8.4, (DWAF,1996) or between 5.5 and 9.5 as specified in the General and Special Effluent Standards of Gauteng (DWAF, 1984).

Small changes in pH have the potential to cause large changes in the concentration and types of dissolved ions and metallic complexes. It can lead to significant increases (or decreases) in the availability and toxicity of most metals, therefore the South African aquatic ecosystem guidelines cautions that pH values should not vary more than 5% (0.5 pH unit) from the range of the background pH values for a specific site (DWAF,1996).

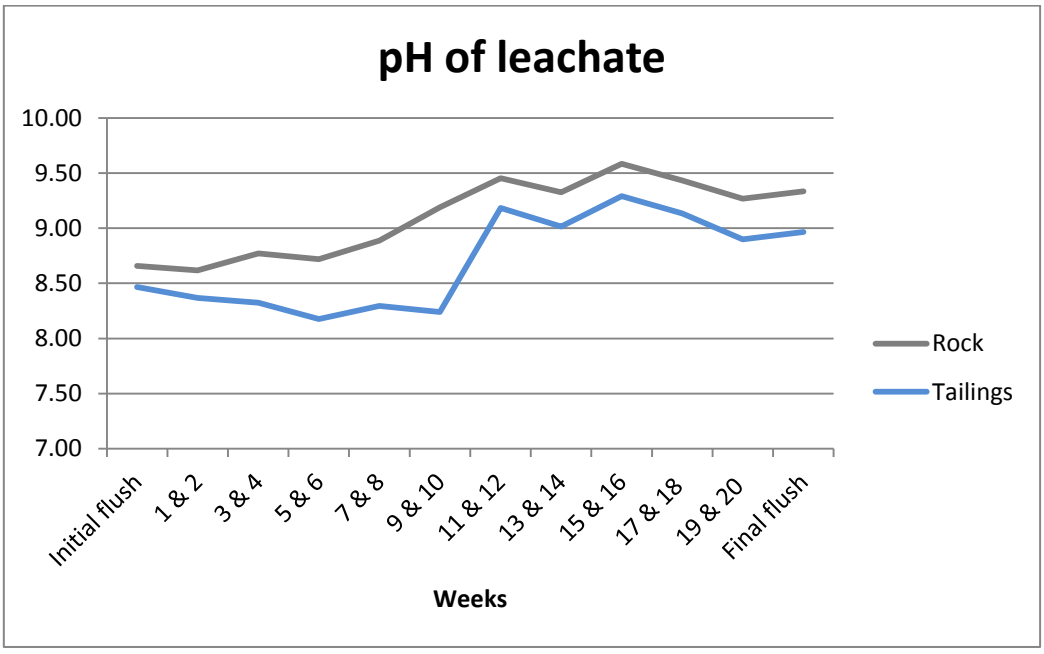

Figure 42: Only minor fluctuations in pH levels were observed for the leachate of the kimberlite rock and tailings during the 20 cycles of leaching.

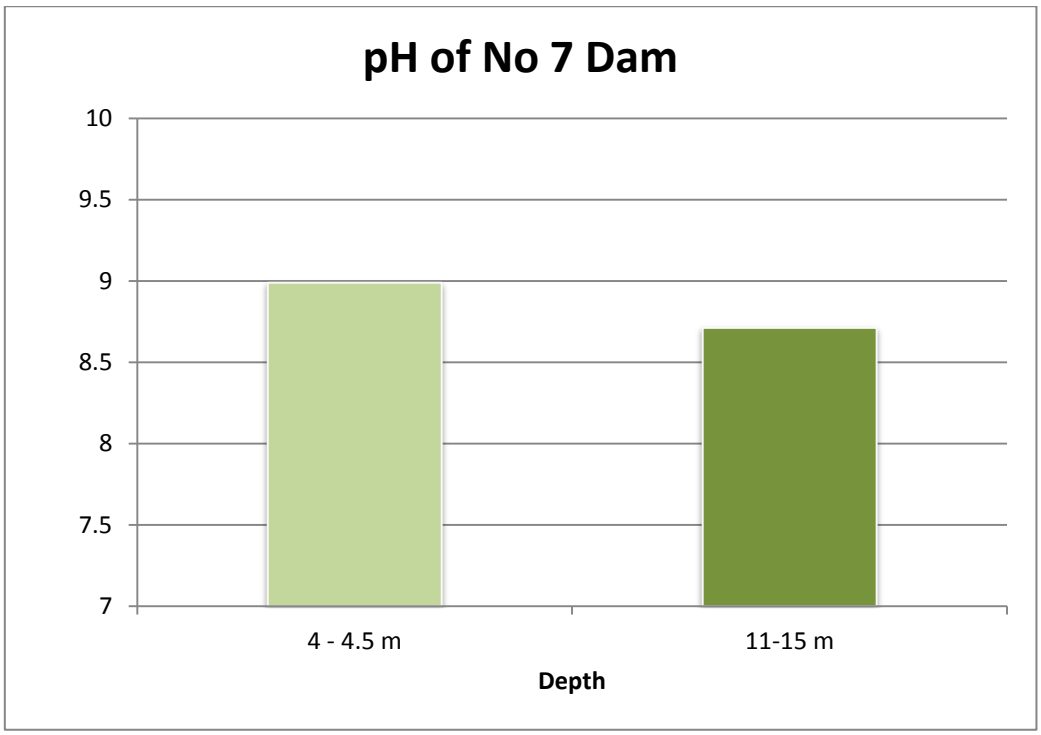

Figure 43: The pH measured for the less dense upper layer and the more dense lower part of the Cullinan mine No 7 Dam.

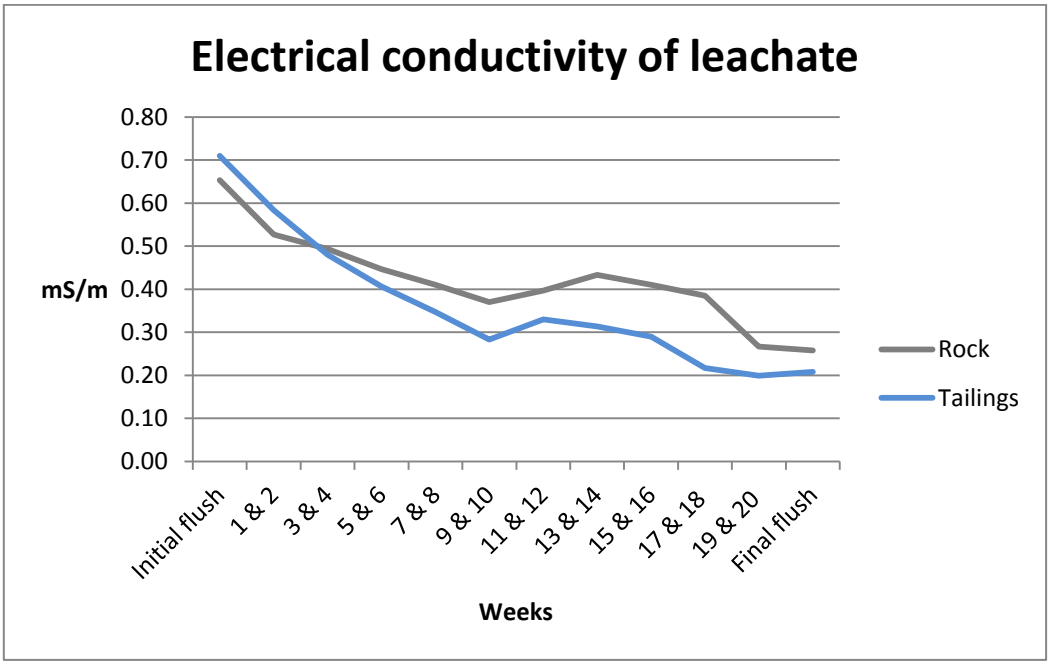

Figure 44: The EC measured in the leachate of the Cullinan kimberlite rock and tailings over the 20 cycles. The EC declined from 0.7 mS/m to 0.2 mS/m.

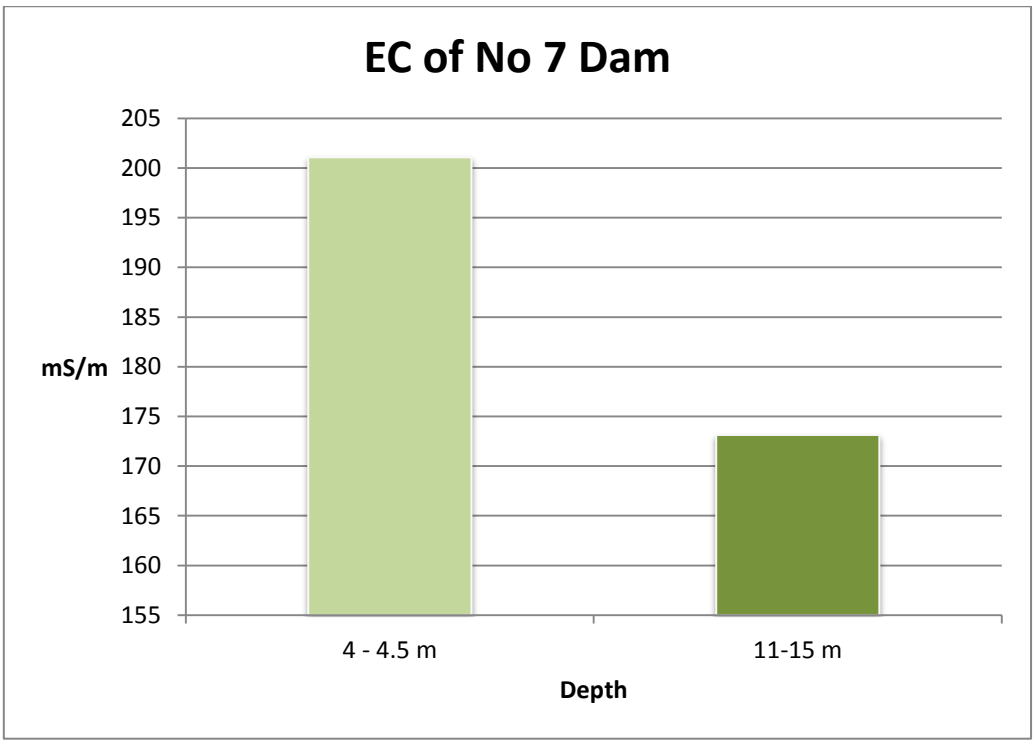

Figure 45: The EC measured in the Cullinan mine No 7 Dam shows quite a significant variation between the upper surface water and the denser subsurface layer.

The EC declined, as expected, during the 20 cycles of leaching (Figure 44). The higher initial EC is a function of adsorbed ions being displaced from the exchange sites and leached out. The dissociation (rate of weathering) of mineral constituents then provides dissolved ions to the leachate. Figure 46 and Figure 47 show that Mg and Ca, are quickly liberated and leached from the olivines, pyroxenes and amphiboles, in both the kimberlite rock and tailings material. There after dissolved concentrations of Na and K, $NO_{3,}$ F and Fe, essentially from the rock, all undergo a slight increase as the micas become susceptible to weathering, before returning to the trend of the tailings material. This trend is supported by the stability sequence of minerals in the weathering environment developed by Goldich (1938) (refer to Figure 9). The spike in dissolved constituents, observed at week 11-12, is not due to analytical error considering that the spike in EC (Figure 44) was observed at the same time whilst independently determined. The upper stratification in the No.7 Dam water, with an EC of 201 mS/m, contains significantly more dissolved salt than the more dense lower section where the EC was measured as 173 mS/m (Figure 45). With higher clay content in the lower stratification, more ions will be adsorbed onto the clay surfaces and the dissolved ion content, which affects EC, lower. The EC of the decanted supernatant following the batch jar trails, doubled to 415 mS/m to reach the critical point for coagulation (c_K).

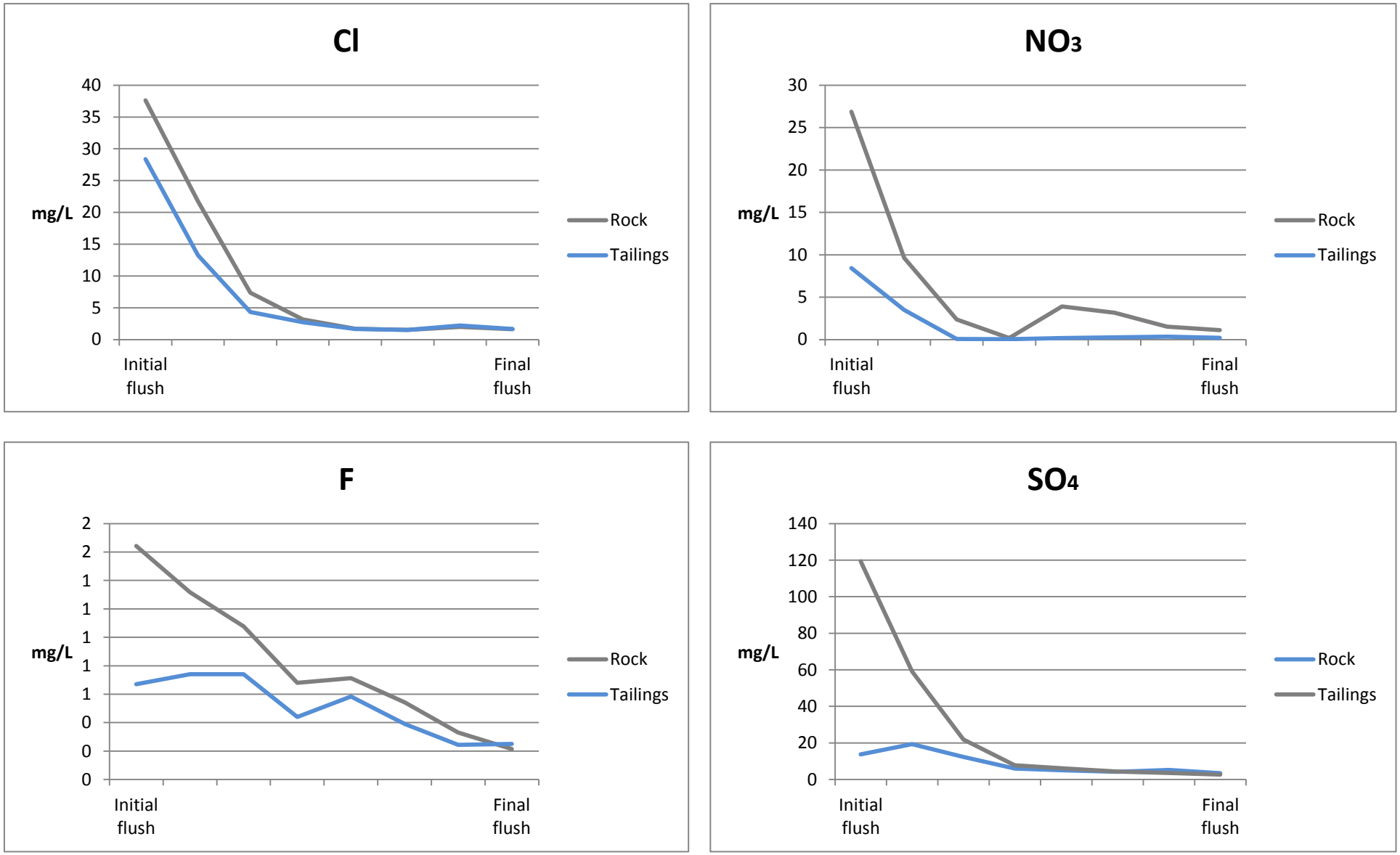

Figure 46: The changes observed in major dissolved anion concentrations in the kimberlite rock and tailings during the 20 cycles of leaching. Note that the scale of the vertical axes differ, to highlight changes that occurred.

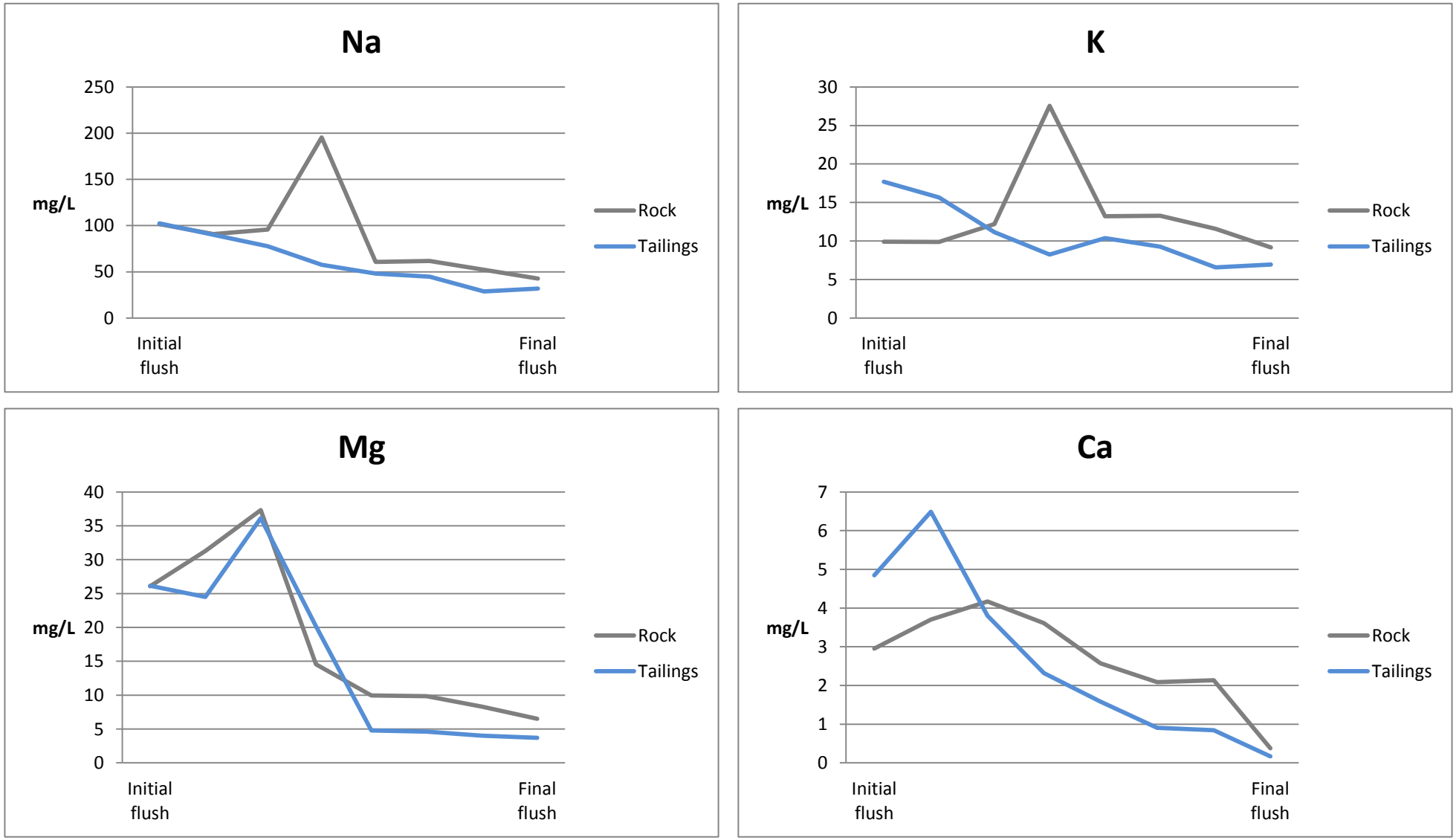

Figure 47: Dissolved cations leached from the kimberlite rock and tailings material during the 20 cycles of accelerated weathering. Again note the difference in vertical scale to emphasise similar trends at larger and smaller scales.

This is far above all recommended levels accept those for specified in the DWA guidelines for alternative use as irrigation water, which is acceptable between 40 – 540 mS/m, depending on crop tolerance. For domestic water tolerable values are 0 -150 mS/m and for discharge of treated effluent into a natural river the EC may not exceed the intake value with more than 15% and may not exceed 250 mS/m (DAWF, 1996). Brady & Weil (2008) however, warn that the specific combination of EC (415 mS/m) and TDS (2109 mg/l) of the treated supernatant can negatively affect water availability to plants due to the osmotic effect, should it be used as irrigation water. It is therefore not recommended. Dissolved solids in suspension may not exceed 10 or 25 mg/L according to the DWA guidelines (DWAF, 1996). The amount of suspended solids however, decreases from 19,437 mg/L in the No 7 Dam water to 24 mg/L after the batch jar treatment.

Figure 46 and Figure 47 show that all components leach from the rock in greater concentration than from the tailings material, except SO_4, K and Ca initially. The presence of NO_3 in the material can be from explosives used in the mining process or from anthropological influences, but because it follows the same trend as the above mentioned elements, it suggests that there are possible underlying interaction(s) with one, or some, of the components in the No 7 Dam that is not yet understood. Although the dissolved SO_4 content is considerably higher than the other dissolve anions, it is not unusual for kimberlite leachate and wastewater. Moncur & Smith (2012) reported dissolved sulphate concentrations of up to 6800 mg/L at the Diavik diamond mine in northern Canada. The review by Barker *et al.* (2003) lists minerals previously identified in kimberlite which can contribute to the dissolved SO_4 content to include pyrrhotite ($Fe_{(1-x)}S$), sphalerite ((Zn,Fe)S), pentlandite ($(Fe,Ni)_9S_8$), chalcopyrite ($CuFeS_2$), galena (PbS), marcasite (FeS_2) and millerite (NiS)and pyrite (FeS_2). Moncur and Smith (2012) reported that high SO_4 concentrations are restricted to the upper parts of tailings facilities where oxidation conditions are ideal. This explains why SO_4 content is leached from the tailings in higher concentrations than from the rock. The tailings material was sampled from the surface where conditions for oxidation are ideal. Deeper into the profile SO_4 concentration decrease in accordance with moisture and oxygen diffusion (Moncur & Smith, 2012), similar to the oxidation zone seen in a gold tailings storage facility where acid mine drainage is generated. However, any acid cations produced by sulphate mineral oxidation, illustrated by the oxidation of pyrite in Equation 16, are consumed and a change in pH buffered, as a result of the nature /composition of the material in combination with its high alkalinity. Consider for example the consumption of H^+ during the dissolution of phlogopite, a major component, in Equation 17.

$$2FeS_2 + 2H_2O + 7O_2 \rightarrow 2Fe^{2+} + 4(SO_4)^{2-} + 4H^+$$

Equation 16

$$K(Mg_2Fe)(AlSi_3O_{10}(OH)_2 + 5H^+ + 0.25O_2 + 3H_2O \rightarrow 0.5Al_2Si_2O_5(OH)_4 + Fe(OH)_3 + 2H_4SiO_4 + K^+ + 2Mg^{2+}$$

Equation 17

Ochieng, Harck & Peters (2009) determined the net neutralisation potential (NNP) of 135 different kimberlite samples. Despite some having considerably low Alkalinity (Alk):Ca molar ratio's, all of the samples were identified, by means of acid base accounting, as non-acid generating. They regarded the Alk:Ca molar ratio as an indication of the contribution of the calcite content of the sample to its total alkalinity. The Alk:Ca molar ratio for the No 7 Dam the was calculated as 0.1 and 0.2 for the top and subsurface layer respectively. This value was considered very low by Ochieng *et al.* (2009) which suggest the alkalinity and buffer capacity of the No 7 Dam arises from sources other than calcite.

The leaching of Na^+ and K^+ was used to evaluate the degree of weathering that in a specific sample if the kimberlite rock is considered to be the parent material. A leaching factor of 1 indicates no- weathering. After 20 cycles of HHAWK-tests the leaching factor for the weathered kimberlite rock was calculated as 0.976 whereas for the tailings material before the leaching cycles commenced the leaching factor was calculated as 0.878. After 20 cycles of leaching at 0.889 barely changed. The accumulation of element in the No 7 Dam is reflected by its leaching factor of 1.16.

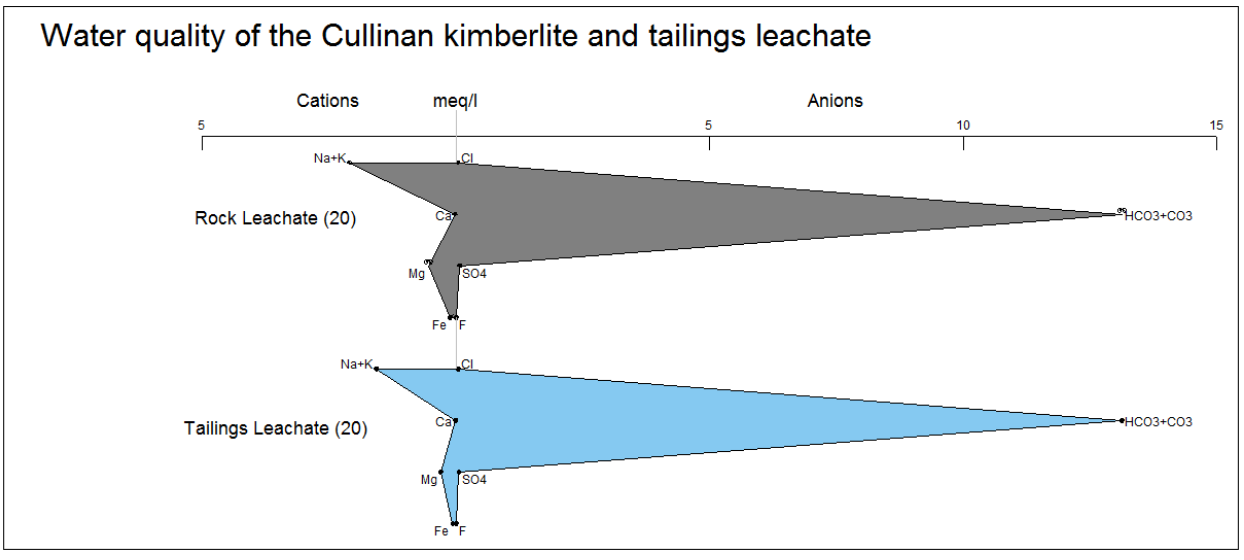

Figure 48: After 20 cycles of leaching, the leachate of the Cullinan kimberlite and tailings shows higher dissolved concentrations of Na and K than Mg, Ca or Fe. The high total alkalinity is observed.

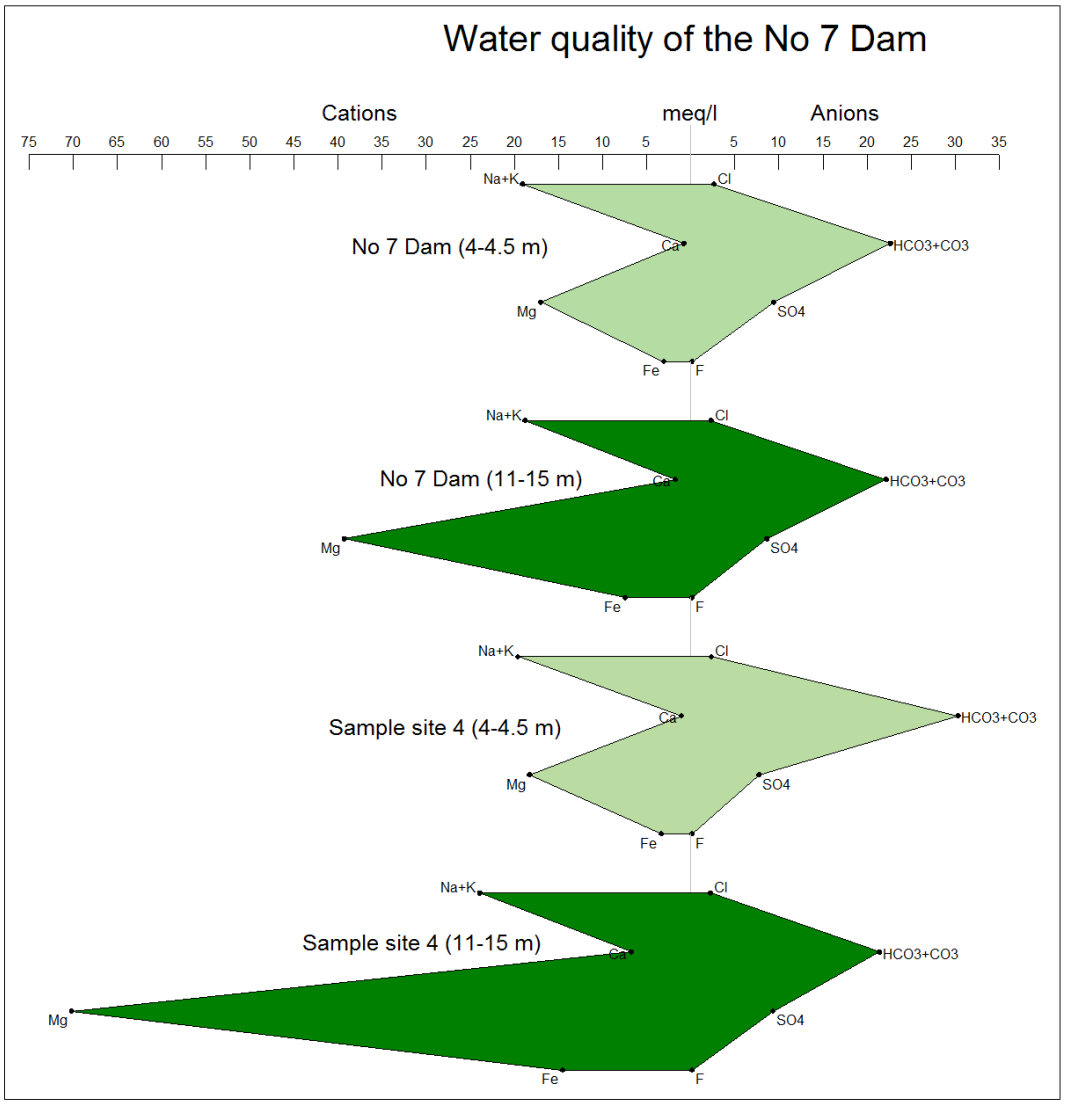

Figure 49: Dissolved constituents of the No 7 Dam water illustrate the effect of many years of concentration inside the dam. Differences are evident between the less dense upper (4-4.5 m) and denser lower (11-15 m) stratification.

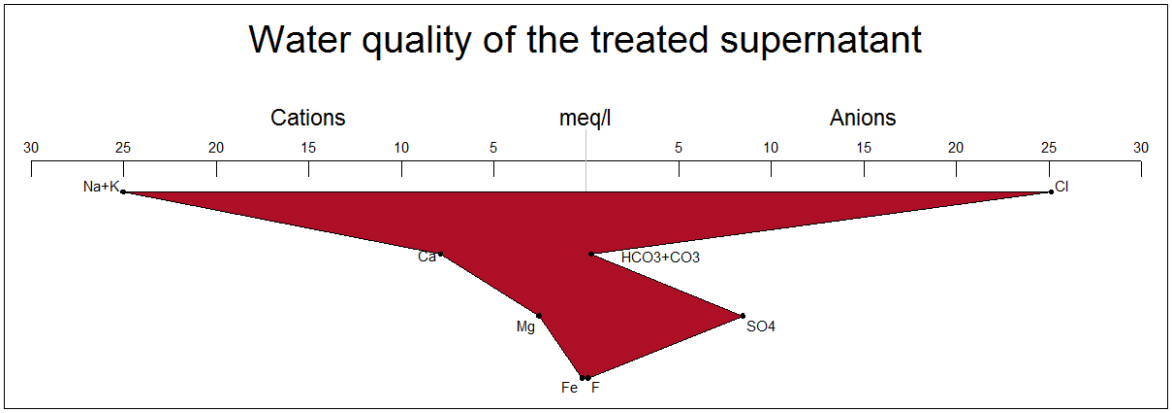

Figure 50: After mineral acid treatment the distribution pattern change reflects the change that occur within the system to obtain flocculation.

Table 14: Comparison of main water constituents of the kimberlite leachate and No 7 Dam, before and after treatment, compared to various national and international guidelines. The respective guidelines were taken from the following sources: a - Sparks (2003), b – WHO (2010), c – DWAF (1984), d - DWAF (1996a), e - DWAF (1996b). The risk ratio given here was calculated with the regards to *e.* A value greater than 1 indicates a potential risk.

ELEMENT	**KIMBERLITE LEACHATE*	*NO 7 DAM*		*[a]TYPICAL NATURAL GROUNDWATER*	*[b]DRINKING WATER*		*[c]GENERAL EFFLUENT STANDARDS GAUTENG*	*[d]AQUATIC ECOSYSTEMS (UM/L)*	*[e]ALTERNA-TIVE USE: IRRIGATION*	*RISK RATIO*
	mg/L									
		Before	*After treatment*		*Health concern*	*Accept-ability limit*				
Ca	3.7	38,7125	158	<500 (1.0 – 150)	-	-	-	-	-	
Chloride	21.7	85,5	890	<1000	-	200–300	0.1 remaining	-	-	
F	1.3	5,2625	3.3	0.1 – 5.0	1.5		1.0	***750***	0.2 - 15	0.22
Fe	8.42	147	6.240	0.01 – 10		0.3	0.3	+/- 10 % of the background dissolved iron concentration	5 - 20	0.3
K	15.64	77,0125	92	1.0 – 10	-	-	-	-	-	
Mg	24.5	391	1573	<400	-	-	-	-	-	
Na	90.7	406,25	521	<1000	-	200	<50 or <90 mg/L above intake water concentrations	-	70 – 460	1.1
N	9.63 (NO3)	2 (N)	2.5 (N)	0.2 -20 (NO^{3-})	-	NO^{2-} (0.2) & NO^{3-} (50) (for long term exposure)	1.5 or 10 as N	> 10	-	
SO_4	59.08	427,75	406	<2000	-	250 - 1000	-	-	-	
Sr	3.1		2.5	0.1 – 4.0	-	-	-	-	-	

*After 20 leaching cycles

Table 15: Minor dissolved constituents of the kimberlite leachate and No 7 Dam, as well as various guidelines for water. Note that only elements with concentrations exceeding 0.01 mg/l are given. Refer to Appendix G for the complete analyses of the various samples. The respective guidelines were taken from the following sources: a - Sparks (2003), b – DWAF (1984The risk ratio given here was calculated with the regards to *b.* A value greater than 1 indicates a potential risk.

TRACE ELEMENT	*KIMBERLITE LEACHATE*	*NO 7 DAM*		*[a]TYPICAL NATURAL GROUNDWATER*	*[b] GENERAL EFFLUENT STANDARDS GAUTENG*	*RISK RATIO*
		ppm				
		Before	After treatment			
Ag	<0.01	<0.01	<0.01	<5.0		
Al	-	76	3.11	<5.0 -1000		
B	-	1	0.56	20 - 1000	1.0	0.56
Co	<0.01	0.27	0.06	<10		
Cu	<0.01	0.2	0.03	<1.0 – 3.0	1.0	0.03
Ga	-	0.03	0.03	<2.0		
Li	-	0.03	0.003	1.0 – 150		
Mn	-	1.96	1.57	<10. – 1000	0.4	3.925
Mo		0.22	0.01	<1.0 -30		
Ni	0.06	3.73	0.63	<10 -50		
PO4		<0.08	2.3 (as P)	<100 – 1000	1 as P	2.3
Pb	-	0.09	0.002	<15	1	
Rb	0.03	0.28	0.45	<1.0		
Ti	-	0.18	0.13	<1.0 – 150		
Zn	-	0.2	0.86	<10 -2000	0.5	1.72

The Stiff diagrams show how the elements liberated during the kinetic testing (Figure 48) is concentrated in the No 7 Dam (Figure 48). The Stiff diagrams presented for the No 7 Dam in Figure 49 show the concentration of the elements liberated during kinetic testing (Figure 48). Dissolved Mg and Fe increase significantly from the surface water layer to the subsurface layer. The data for sample site four (see Figure 18) is presented separately as the water vegetation trap and physically accumulate the clay particles and associated dissolved ions. The effect of the chemical treatment of the No 7 Dam water is seen as the drastic change in the Stiff diagram constructed for the decanted supernatant (Figure 50). Both dissolved Na + K and Cl concentrations increase significantly and Ca goes into solution. Alkalinity is, as expected, almost completely consumed by the acid treatment. Dissolved Mg, Fe and F also decrease dramatically as these elements are adsorbed or become less soluble at the lower pH level. SO_4 concentrations are not affected.

5.4.2 Insights from the electrophoretic mobility of the suspension

Zeta potential investigation of the No 7 Dam suspension was based on the findings of Penner and Legally (2001) that identified the smallest c_K value at which flocculation was induced in their laboratory prepared 2 % montmorillonite suspension, with the addition of HCl as coagulant. The ζ auto titrations were intended to find the pH level at which the ionic strength of the solution is ideal (lowest possible salt concentration) for the DDL to be thin enough (all surface charges are optimally satisfied) for the clay particles to approach and attract each other so that coagulation can occur.. PHREEQC modelling also distinguished HCl to be suitably effective, amongs the various mineral acids considered, in decreasing the pH of the No 7 Dam water (see Figure 22 and Figure 23). The batch (incremental) reactions run with the dissolved load of the No 7 Dam water and various concentrations of HCl, indicated that a concentration of 0.1M HCl was suitable to reach a pH of around 5 if 13 ml of HCL is added to 100 ml of the No 7 Dam water.

The outcomes predicted by the software considered only the dissolved components in solution. The interactions of the suspended solids with the components in solution and consequent buffering capacity, was not accounted for.

Changes occur in the system as the pH decreases. This would include the shape, the size, the surface charge and the mobility of the particles. The decrease in ζ indicates that particles are becoming less mobile, therefore larger. The No 7 Dam suspension has an initial ζ of -44 mV at pH 9. The titration down to pH 2 spanned two hours and consumed 2.71 ml of 0.1 M HCl. At this pH level the ζ only reached -32 mV. No IEP/PZC was determined for the suspension.

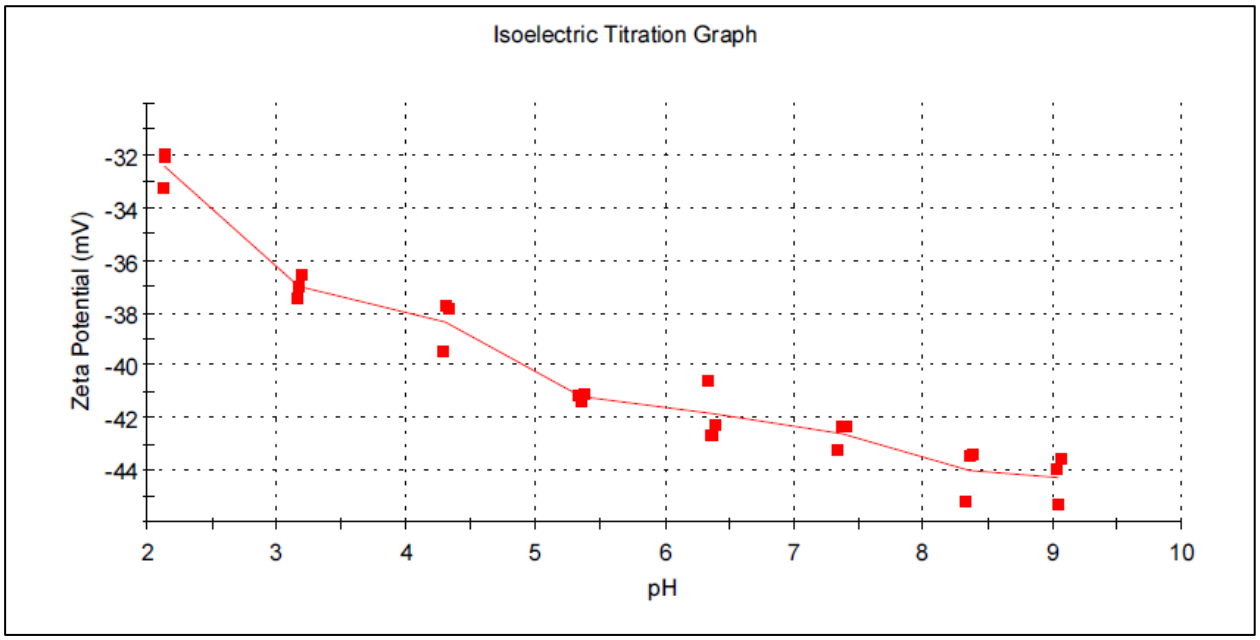

Figure 51: Isoelectric titration curve of the No 7 Dam suspension from pH 9 to 2 with 0.1 M HCl.

At this potential the system is expected to still be moderately stable as a suspension (see Figure 13). The highly negative measured ζ reflects a large diffuse double layer and therefore also inter-particular repulsion (Brady & Weil, 2008).

The PZC of the clay suspension is therefore dependent on both the pH (influences charge and charge density; Kraepiel & Morel, 1998) and the ionic strength of the solution (influences the thickness of the double layer). Niriella & Carnahan (2006) confirms this observation with their study on the behaviour of bentonite in different concentrations of various salt solutions versus distilled water. In the water suspension, a change in pH (from 10 to 4) had a marked effect decreasing the negativity of the ζ. When the pH reached 6 to 8 (depending on the amount of clay in suspension) the ζ stabilized at approximately -10mV. However, for the various low concentration salt solutions (0.001M and 0.1 M), the change in pH (from 10 to 4) effected very little change in ζ. The cation type had a greater influence in increasing the ζ than the pH (as seen earlier from Penner & Legally, 2001, as well). In highly concentrated solutions no charge (PZC) was observed throughout. It therefore seems that, contrary to previous thought (Porgieter & Green, 2003; Janse van Rensburg & van Blerk, 2007; Miller *et al.,* 2008,) the ionic strength of the No 7 Dam is too low to reach the PZC in the measured pH range.

As expected the EC of the No 7 Dam suspension increases slightly from 210 mS/m to 230 mS/m during this titration, as pH decrease and H^+ replaces other ions on the surface exchange sites of the clay particles and the available pH dependent charges decrease.

5.4.3 Mineral Acid Batch Jar Tests

Since the results from the zeta potential analysis were inconclusive regarding pH, the batch jar tests were conducted in a systematic and exploratory manner based on visual observations. The results in the table below (Table 16) are presented for a 48 hour observation time.

For the 48 hour observation period, coagulation was observed in all the batches, although not to the same extend. In the batches where acidification was the only modification (see nr 1 and 3 in Table 16), signs of coagulation occurred only at extremely low pH levels and after considerable periods of time. In the 48 hour observation period, only minimal and incomplete sedimentation was observed (see Figure 52). In all cases, signs of coagulation were considered to be; the formation and escape of small air bubbles, followed by an increase in viscosity, the adhering of solution to sides of the glass container, and lastly the formation of visible disordered flocks. The sedimentation time was taken as the moment when the first layer of clear supernatant was observed at the top of the sediment column.

In all the batches where the specified amount of No 7 Dam water was added to acid digested tailings material (see all no 4 batches – Table 16), coagulation was immediate and sedimentation followed shortly after. Digesting the finer fraction of tailings aided flocculation by providing alternative nucleation sites as suggested by van Duuren (1997). However, the sensitivity to electrical conductivity observed from the batch jar tests proves that the salt concentration (ionic strength) of the solution to be a main determining factor in combination with (and not solely) the pH level of the solution. For example, the EC of the batch no 3B (Table 16) was measured as 228 mS/m when the pH was 5 and flocculation for this solution was only observed at pH 1.8 when the measured EC was 676 mS/m compared to the immediate coagulation and flocculation observed for batch 4G (Table 16) where the measured EC was 357 mS/m at pH 4.14.

In the above mentioned set of batch jar tests, the combination in 4 G (Table 16) was the lowest dissolved salt concentration at which sufficient flocculation occurred. It can therefore be assumed to be the closest to the c_K for the No 7 Dam solution. It is recommended that the batch jar test be extended and refined to determine the exact c_K value which could possibly be at a lower EC value, as immediate coagulation (but poor sedimentation) was observed when the EC was as low as 60mV (batch 4 C – Table 16).

Table 16: pH, EC and flocculation observations for the various batches of jar tests using the water of the Cullinan mine No 7 Dam,

BATCH NR.	*ADDITIVE(S)*			*pH*	*EC (mS/m)*	*COAGULATION*	*SEDIMENTATION*
	HCl	**No7 Dam Water**	**Solids**				
1	6ml 0.5M	500 ml	-	5		No flocculation observed	Not observed
2	Inconclusive						
3	A 23ml 0.5M	500 ml		2.1	-	Slight increase in viscosity.	Initiated: Not observed Completed: Not observed
	B 14 ml 1M			1.83	676	Suspension starts to adhere to glass jar surface.	Initiated: 3h17min Completed: Not observed
4	A 3 ml 1 M	100 ml	5 g	2.13	640	Immediate flocculation	Initiated: 7min Completed:> 4 hours
	B 2 ml 1 M	100 ml	3 g	2.7	528	Immediate flocculation	Initiated: 13 min Completed: > 4 hours
	C 1 ml 1 M	100 ml	2 g	5.6	144	Immediate flocculation	Initiated: 1h26 min Completed: Not observed
	D 5 ml 0.5M	150 ml	5 g	2.5	578	Immediate flocculation	Initiated: 11 min Completed: < 4 hours
	E 5 ml 0.5M	250 ml	5 g	4	381	Immediate flocculation	Initiated: 9 min Completed: < 4 hours
	F 10 ml 0.5M	300 ml	10 g	5.5	165	Immediate flocculation	Initiated: 6 min Completed: < 3 hours
	G 12 ml 0.5 M	400 ml	20 g	4.14	357	Immediate flocculation	Initiated: 4 min Completed: < 3 hours
	H 30 ml 0.5 M	1 L	50 g	3.7	415.2	Immediate flocculation	Initiated: 8 min Completed: < 4 hours

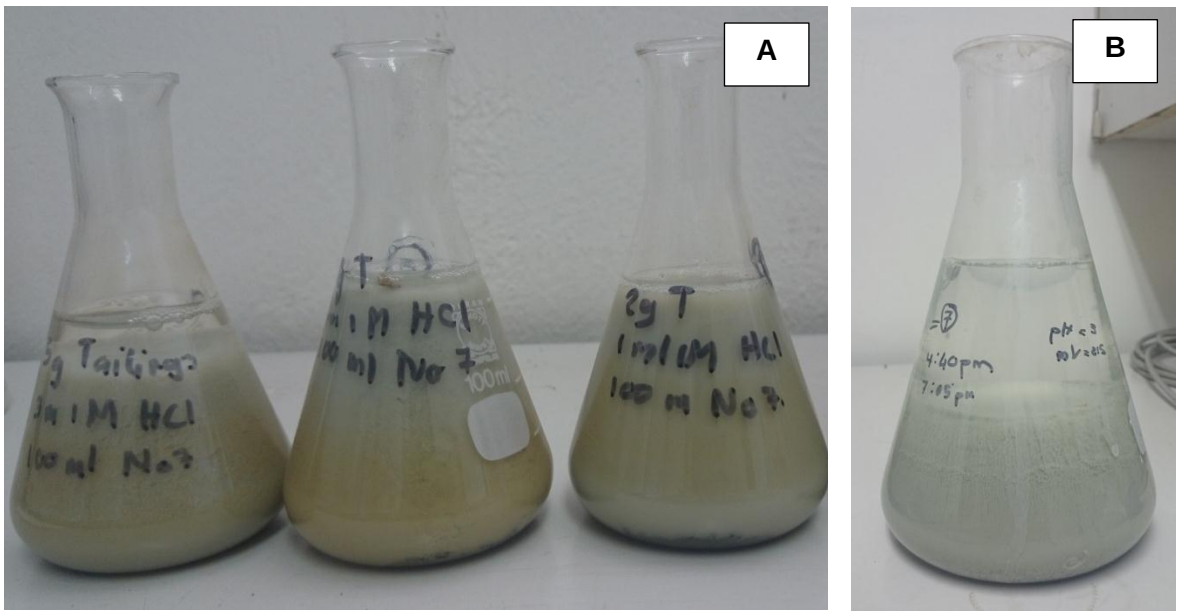

Figure 52: In photograph A examples of three of the batch jar tests just after mixing, are displayed. In photograph B the extent of completed sedimentation in an example of batch 4H (Table 16), is clear.

During the batch jar tests, the No 7 dam suspension illustrated a significant buffering capacity as the pH level often fluctuated during acidification. In some cases the measured pH level increased again if gently stirred and left to equilibrate for a few minutes especially for those that reached lowest pH levels.

The importance of the ionic strength of the solution was confirmed through three more jar tests where the same coagulating effect was achieved by the addition of highly concentrated solutions of $MgCl_2$, NaCl and KCl respectively.

CHAPTER 6

SYNTHESIS

6.1 CONCLUSION

This study was undertaken to firstly develop a better understanding of the origin of the suspended clays in the No 7 wastewater dam at the Cullinan Diamond mine and of what causes the clay mineral weathering products of the in the dam to remain in a dispersed state. The following conclusions could be drawn from the more detailed characterization of the material in various stages of weathering (rock tailings, clay mineral weathering products and constituents dissolved in the wastewater):

- The Cullinan kimberlite is mainly composed of the minerals phlogopite, pyroxene, chlorite, lizardite and talc. Vermiculite appears in the post HHAWK-test kimberlite material as the phlogopite component decrease and the chlorite mineral content increase. The chlorite mineral content in the tailings material is drastically less which suggests that it could have been washed out of the tailings material to the No 7 Dam or nearly all of it has been transformed. However the chlorite content in the post HHAWK-test tailing sample return to levels similar to the post HHAWK-test kimberlite sample.

- It was confirmed that the Cullinan kimberlite material is enriched in Na_2O, K_2O compared to the average South African on-craton kimberlite. It contains less CaO, MgO, TiO and Fe2O3 in comparison to the average and has been contaminated (higher SiO2 and Al2O3) by wall rock inclusions. The trace element pattern of the Cullinan kimberlite does mirror the average but at slightly lower concentrations.

- The dissolved salt (the major components Ca, Mg, Na, K, Fe, SO_4, Cl, F, were investigated) and suspended solid content of the No 7 Dam results from the concentration of mineral weathering products over many years to reach a TDS of around 1600 mg/L and TSS of up to 120000 mg/L. The transformation of major mineral components olivine (lizardite), pyroxene and phlogopite are important contributors to the formation of the clay minerals.

- The breakdown process of the kimberlite material, as observed in high HHAWK-test, bring on a loss of volume of material in the leaching columns as the PSD decrease during the 20 leaching cycles. During the weathering process, the kimberlite rock and tailings material transform to chlorite, vermiculite, interlayered montmorillonite-chlorite, possibly illite–smectite and finally to nontronite and saponite that dominate in the No 7 Dam. These flaky clay mineral particles vary in size and shape from a few nm to µm in diameter but are extremely thin in comparison.

  The interstratifications of the clay minerals in the No 7 Dam (especially the fine-grained mica and trioctahedral Mg-rich smectite) result in unusually low surface charges.The CEC of the Extracted No & Dam clay was 36.8 cmol/kg. This indicate weaker surface interactions implying a thicker DDL and resulting repulsion rather than attraction between particles.

- The dissolution of the silicate minerals, in particular olivine (lizardite), pyroxene and phlogopite, provides dissolved elements to the surrounding aqueous solution which influences the interactions between particles as well as between the particles and the weathering solution. Along with high pH (8.5 to 9.5) and EC (175 to 200 mS/m) levels, the suspension illustrates a significant buffering capacity which results from the silicate and carbonate mineral weathering. The HHAWK-test leachate illustrates the same dissolved load/species composition but at much smaller concentrations than what was measured for the No 7 Dam solution. The maximum EC measured for the leachate however, was 0.7 mS/m. From the week 9 and 10 composite analysis to the week 11 and 12 composite analysis, there was a marked spike in most dissolved constituents (and EC) which indicate the possible collapse (and subsequent release of elements) of one or more mineral species in the rock and tailings material. The cations Mg^{2+}, Na^{+}, K^{+}, and to a lesser extend Fe along with the anions HCO_3^{-} and CO_3^{2-}, SO_4^{2-} and Cl^{-} were found to be predominant in the weathering solution. Ca^{2+} and Na^{+} were the prevalent exchangeable cations adsorbed to the suspended clay minerals. The SAR calculated of the No 7 Dam varied between 15 and 3.5 between sample sites while the ESP for the extracted clay exceeded 50%. This result however is not regarded as reliable.

- Although the Na content in the No 7 Dam (adsorbed > dissolved) is high compared to common local and international guidelines, it is not the sole cause

of non-settlement of the dispersed fine clay minerals. The cause of this phenomenon is confirmed to be the result of a combination of factors listed here. The (1) significantly large DDL (-44 mV zeta-potential) measured for the smectite particles in suspension, which is a function of both the (2) composition and ionic strength of the solution and (3) low surface reactivity (low CEC) on the (4) large negatively charged faces and excessively small positively charged edges of the flaky interlayered clay particles as well as (5) the consequent poor interparticular attraction between clay particles.

Secondly the study also aimed to develop a laboratory treatment to separate the fine clay minerals from the solution by means of chemical coagulation, flocculation and gravitational sedimentation, for the No 7 Dam suspension based on the specific characteristics of the material. Of the various causes mentioned above, the ionic strength and composition of the solution (nr 2) is most easily changed. A simple mineral acid coagulation treatment was developed from relevant literature and tested on a small scale by means of batch jar tests. The following conclusions summarize the outcomes of the proposed mineral acid treatment of the No 7 Dam solution.

- HCl was identified as the mineral acid with the smallest c_K for montmorillonite clay suspensions. This means that compared to other mineral acids, the addition of HCL results in the lowest critical salt concentration (ionic strength) of the relevant solution at which coagulation will initiate.

- The addition of HCl (various amounts and concentration as specified in section 5.4.3) did not achieve the expected result because of the buffer capacity of the No 7 Dam suspension. To increase the ionic strength of the solution sufficiently, a small amount of the kimberlite tailings material was pre-digested in the HCl and then added to the No 7 Dam suspension. This resulted in immediate coagulation and flocculation of the clay minerals.

- Many variation of this specific combination were considered in the batch jar tests where after the following was identified as the most effective with regard to the time for gravitational sedimentation to conclude as well as amount and concentration of HCl added and amount of tailings material digested.

- To add to 1 lL of No 7 Dam suspension, 50 g of fine tailings material were digested in 30 ml of 0.5 M HCl. After four hours ? ml of low turbidity (10 NTU) supernatant with a pH of 4.6 could be decanted.

- After the mineral acid treatment the EC increased to 415 mS/m, the TSS decreased to 24 mg/L but the TDS increased somewhat to 2 100 mg/L. The SAR was calculated as 10 since Na+, K+ and Cl- followed by Ca2+ were now the predominant dissolved components. The high total alkalinity was reduced to < 5 mg/L. Dissolved SO4 remained constant but dissolved Mg2+, Fe and F were effectively reduced

The cleared supernatant is suitable to use as irrigation water. Slight to moderate restriction do apply due to the current TDS. If used as irrigation water, the soil salt balance should be monitored carefully. However the pH level and dissolved Na, Cl, constituents bare some environmental risk with regards to irrigation.

Tambo (1990) stated that: “If man can categorise impurities which are effectively removed by coagulation, then water purification can be designed rationally”.

6.2 RECOMMENDATIONS FOR FUTURE RESEARCH

Following the current research, the first step ahead would be a feasibility study to modify and scale the mineral acid treatment of the No 7 Dam suspension to a pilot plant. If successful, one can proceed to large scale implementation.

Some recommendations were made throughout the text regarding interesting observations that can extend the current research and contribute to the understanding of the system interactions. These were:

- The effect and interactions of the established reed population near sample site 4 on the No 7 Dam water composition.
- Refining the mineral acid treatment

Further studies that evolve from the present research can also consider

- Alternative use for the separated clay minerals clay. Previous studies have considered kimberlite waste material as soil ameliorants.

- Means to further improve the water quality of the supernatant with regards to the Na and Cl content – possibilities to consider include amongst other (1) re-equilibration with $CaCO_3$ or $BaCO_3$ as indicated in the text, (2) evaporation, (3) reverse osmosis
- Alternatives to chemical flocculation – electrochemical methods can be considered since the dispersion is partially charge dependent. This will exclude the need for alternative additives and the associated costs.

LIST OF REFERENCES

APPELO, C.A.J. & POSTMA, D. 2005. *Geochemistry, groundwater and pollution.* London: CRC Press Taylor & Francis Group.

ASTM D2035. 2008. Standard practice for Coagulation-Flocculation Jar Test of Water. In: *Annual Book of ASTM Standards*, ASTM International.

ASTM. D422. 1998. Standard Test Method for Particle Size Analysis of Soils. In: *Annual book of ASTM Standards*, ASTM International.

ASTM D5744. 1996. Standard Test Method for Accelerated Weathering of Solid Materials using a Modified Humidity Cell. In: *Annual Book of ASTM Standards*, ASTM International.

BACH, W., PAULICK, H., GARRIDO, C. J., ILDEFONSE, B., MEURER, W. P. & HUMPHRIS, S. E. (2006). Unraveling the sequence of serpentinization reactions: petrography, mineral chemistry and petrophysics of serpentinites from MAR158N (ODP Leg 209, Site 1274). *Geophysical Research Letters*, 33 (L13306).1-4.

BAKER, M.J., BLOWES, D.W., LOGSDON, M.J.& JAMBOR, J.L. 2003. Environmental geochemistry of kimberlite materials: Diavik Diamond Project, Lac de Gras, Northwest Territories, Canada. Exploration Mining. *Geology,* 10, 155-163.

BALAN, E. CALAS, G & BISH, D.L., 2014 Kaolin-Group Minerals: From Hydrogen-Bonded Layers to Environmental Recorders. *ELEMENTS*, 10, 183–188

BANDFIELD, J.F. JONES, B.F. & VEBLEN, D.R. 1991. An AEM-TEM study of weathering and diagenesis, Albert Lake, Oregon: I. Weathering reactions in the volcanics . *Geochim.Cosmochim*, 55, 2781-93.

BANFIELD, J.F. & MURAKAMI, T. 1998. Atomic-resolution transmission electron microscope evidence for the mechanism by which chlorite weathers to 1:1 semi-regular chlorite-vermiculite. *American Mineralogist,* 83, 348–357.

BARNES, I. & O'NEIL, J. R. (1969). The relationship between fluids in some fresh alpine-type ultramafics and possible modern serpentinization. *Geological Society of America Bulletin*, 80, 1947-1960.

BARTLETT, P.J. 1998. Premier Mine. Seventh International Kimberlite Conference – Large Mines Field Excursion. Cape Town: 7IKC Organising Committee, 39-49.

BARTLOW, E. & PETERSON, B. 1928. Effect of Salts on the Rate of Coagulation and Optimum Preccipitation of Alum Floc . *Ind. Eng. Chem,* 20, 52.

BEARD, J.S., FROST, B.R., FRYER, P., McCAIG, A. SEARLE, R., ILDEFONSE, B., ZININ, P. & SHARMA, S.K. 2009. Onset and Progression of Serpentinization and Magnetite Formation in Olivine-richTroctolite from IODP Hole U1309D. *Journal of Petrology*, Jan, 1-17.

BECKER, M. & LE ROEX, A. P. 2006. Geochemistry of South African On- and Off craton, Group I and Group II Kimberlites: Petrogenesis and Source Region Evolution. *Journal of Petrology*, 47(4), 673-703.

BELL, F.G. 2007. *Engineering Geology*. 2nd ed. London, Elsevier.

BOSHOFF, E.T., MORKEL, J., VERMAAK, M.K.G. & PISTORIUS, P.C. 2007. Kimberlite degradation: The role of cation type. *Minerals Engineering,* 20(Sep), 1351-1359.

BOUZAHZAH, H., BENZAAZOUA, M., BUSSIèrE, B. 2010. A modified protocol of the ASTM normalized humidity cell test as laboratory weathering method of concentrator tailings. *Mine Water and Innovative Thinking, IMWA*. 567-570.

BRADY, N.C. & WEIL, R.R. 2008. *The Nature and Propperties of Soils.* 14th ed. Upper Saddle River: New Jersey: Pearson Prentice Hall.

BRENER, EK & BRENER, R.A. 1996. *Global environment: Water, Air and Geochemical Cycles.* Upper Saddle River, NJ: Prentice Hall Inc.

BROUWER, P. 2003. *Theory of XRF: Getting acquainted with the principles.* The Netherlands: PANalytical BV.

BROWN, G.E. & CALAS, G. Environmental Mineralogy – Understanding element behavior in ecosystems. *Comptes Rendus Geoscience*, 343(Mar), 90-112.

CAS, R.A.F. & HAYMAN, P.C. 2011. Criteria for interpreting kimberlite as coherent: insights from the Muskox and Jericho kimberlites (Nanavut, Canada). *Bulletin of Volcanology,* 73(8), 1005 -1027.

CAS, R.A.F., PORRITT, L., PITTARI, A. AND HEYMAN, P.C.2009. A practical guide to terminology for kimberlite facies: A systematic progression from descriptive to genetic, including a pocket guide. *Lithos,* 112, 183-190.

CLEMENT, C.R. 1982. A comparative geology study of some major kimberlite pipes in the Northern Cape and Orange Free State. PhD –Thesis, University of Cape Town, South Africa

COLMAN, S.M. 1982. Chemical weathering of basalts and andesites: Evidence from weathering rinds. *US Geological Survey,* Prof. Pap. no 1246, 51.

CRESCIMANNO G., IOVINO M. AND PROVENZANO G. 1995. Influence of salinity and sodicity on soil structural and hydraulic characteristics. *Soil Science Society of America,* 59, 1701 - 1708CZÍMEROVÁ, A., BUJDÁK, J. & DOHRMANN, R. 2006. Traditional and novel methods for estimating the layer charge of smectites. *Applied Clay Science,* 34, 2–13.

DAWSON, J.B. 1980. *Kimberlites and teir Xenoliths.* Berlin: Springer-Verlag.

DEAT. 2006. *South Africa Environment Outlook: A report on the state of the environment*. Department Environmental Affairs and Tourism, Pretoria.

DECARREAU, A. 1982. Etude expérimentale de la cristallo-genese des smectites." Etat : Univ. Orsay (France).

DOUGLAS, L.A. 1989. Vermiculites. In: DIXON, J.B. & WEED, S.B. eds. *Minerals in Soil Environments*. Wisconsin, USA: Soil Science Society of America, 635 -674.

DREVER, J.I. 1969. The separation of clay minerals by continuous particle electrophoresis. *The American Mineralogist,* 54(May), 937-942.

DUZGORIN-AYDIN, N.S., AYDIN, A & MALPAS, J. 2002. Re-assessment of chemical weathering indices: case study of pyroclastic rocks of Hong-Kong. *Engineering Geology,* 63, 99-119.

DWAF. 1984. General and Specific Effluent Standards for Gauteng. Department of Water Affairs and Forestry.

DWAF. 1996. *South African Water Quality Guidelines, Volume 4 (Irrigation),* Department of Water Affairs and Forestry.

DWAF.1996 *South African Water Quality Guidelines* Volume *7 (Aquatic ecosystems).* Department of Water Affairs and Forestry.

EBY, N.G. 2004. *Principles of Environmental Geochemistry.* United States: Brooks/Cole Cengage Learning.

EBY, N.G. 2004. *Principles of Environmental Geochemistry.* United States: Brooks/Cole Cengage Learning.

EGGLER, D.H. 1989. Kimberlites: How do they form? *GSA Special publication*, 489 - 501.

FAIRBAIRN, P.E. & ROBERTSON, R.H.S. 1966. Stages in the tropical weathering of kimberlite. *Clay Minerals,* (6), 351-370.

FANNING, D.S., KERAMIDAS, V.Z. & EL-DESOKY, M.A. 1989. Micas. In: DIXON, J.B. & WEED, S.B. eds. *Minerals in Soil Environments*. Wisconsin, USA: Soil Science Society of America, 550-634.

FESQ, H.W., KABLE, E.D.J. AND GURNEY, J.J. 1975. Aspects of the geochemistry of kimberlites from the Premier Mine and other South African occurences, with particular reference to the rare earth elements. *Physics and Chemistry of the Earth,* 9, 686-707.

FIELD, M., STIEFEHOFER, J., ROBEY, J. & KURSZLAUKIS, S. 2008. Kimberlite-hosted diamond deposits of southern Africa: A review. *Ore Geology Reviews*, 34(Apr): 33-75.

FRICK, C. 1970. The mineralogy and petrology of kimberlite and its related inclusions, with special reference to Premier Mine. Doctoral thesis, University of Pretoria, Gauteng Province, South Africa.

FROST, B.R. & BEARD, J.S. (2007). On silica activity and serpentinization. *Journal of Petrology,* 48, 1351-1368.

FROSTAD, S., KLEIN, B. & LAWRENCE, R.B. 2002. Evaluation of laboratory kinetic test methods for measuring rates of weathering. *Mine water and the Environment, IMWA*, 21, 183-192.

GERBER, F.A. & HARMSE, J.H.VON M. 1987. Proposed procedure for identification of dispersive soils by chemical testing. *Die Siviele Ingeneur in Suid Afrika,* (Okt), 397-399.

GILCHREST, I.C.R. & HUNT.M.S. 1988. The recovery of water from a Colloidal Stable Kimberlite Suspension. *International Mine Water Association Proceedings*. In: International Mine Water Association. 2012.

GOLDICH, S.S. 1938. A study in rock weathering. *Journal of Geology*, 46, 17-58.

GOLDING H.G, BAYLISS P (1968) Compact chlorite associated with lizardite from New South Wales, Australia. *Mineral Mag*, 36:825–831.

GOMEZ- ARIAS, A. CASTILLO, J. POSTHUMUS, J & VAN HEERDEN, E. 2014 Evidence for the effective treatment of alkaline mine drainage using a matrix of $BaCO_3$ and wood chips: solution for in-situ passive treatment. Paper presented at *21st General Meeting of the International Mineralogical Association,* 1 – 5 September, Johannesburg, South Africa.

GRONDKLASSIFIKASIEWERKGROEP. 1991. *'n Taksonomiese sisteem vir Suid Afrika.* Pretoria: Department of Agriculture and Development.

HILLEL, D. 2004. *Introduction to Environmental Soil Physics.* London: Elsevier Academic Press.

HORNBERGER, R.J. & BRADY, K.B.C. 1998. Kinetic (leaching) tests for the prediction of mine drainage quality. In: Brady, K.B.C. ed. *Coal mine drainage prediction and pollution prevention in Pennsylvania*. Pennsylvania Department of Environmental Protection. p 7-1 to 7-54.

HUDSON, H.E. & WAGNER, E.G. 1981. Conduct and Uses of Jar Tests. *American Water Works Association,* 73(4), 218-223.

JACKSON, M.L., HSEUNG, Y., COREY, R.B. EVANS, E.J. & VANDEN HEUWEL, R.C. 1952. Weathering of clay size minerals in soils and sediments. *Soil Science Society of America Proceedings*, 16, 3-6.

JANSE VAN RENSBURG, H. & VAN BLERK, J.J. 2007. Cullinan Diamond Mine: Establishment of a Preliminary Groundwater Flow and Mass Transport Numerical Model. Unpublished project report , Aquisim Consulting, Petra Diamonds.

JANSE, A.J.A. & SHEAHAN, P.A. 1995. Catalogue of world wide diamond and kimberlite occurrences: a selective and annotative approach. *Journal of Geochemical Exploration* 53: 73 - 111.

JENNY, H. 1941. *Factors of Soil Formation: A System of Quantitative Pedology.* New York: Dover Publications Inc.

KARGBO, D. M. AND HE, J,. 2004. A simple accelerated rock weathering method to predict acid generation kinetics. *Environmental Geology*, 46(Jul), 775-783.

KIM, W., LUDWIG, H.F. & BISHOP, W.D. 1965. Cation-Exchange Capacity and pH in the Coagulation Process. *American Water Works Association*, 57(3), 327-348.

KLUG, H.P. & ALEXANDER, L.E. 1974. *X-Ray Diffraction procedures*. 2nd ed. New York; John Wiley & Sons..

KRAEPIEL, A.M.L & MOREL, F.M.M. 1998. The influence of internal charge on the sorption properties of clays. *Goldschmidt Conference Toulouse, Mineralogical Magazine, 62, 809-8010.*

LAPIDUS, D.F. & WINSTANLEY, I. eds. 1990. *Collins Dictionary of Geology.* Glasgow: Omnia Books Limited.

LEGALY, G. 1989. Principles of flow of Kaolin and Bentonite dispersions. *Applied Clay Science,* 4, 105-123.

LEGALY, G. & ZEISMER, S. 2003. Colloid chemistry of clay minerals: the coagulation of montmorillonite dispersions. *Advances in Colloid and Interface Science,* 100-102, 105-128.

LEONG, Y.-K., TEO, J., TEH, E., SMITH, J., WIDJAJA, J. LEE, J.-X., FOURIE, A., FAHEY, M. & CHEN, R. 2012. Controlling attractive interparticular forces via small anionic and cationic additives in kaolin slurries. *Chemical Engineering Research and Design,* 90, 658-666.

LEOPOLD, P & FREESE, S.D. 2009. *A Simple Guide to Chemistry,selection and Chemicals for Water and Wastewater Treatment.* Report (No 405/09) to the Water Research Commission, Water Science. WRC.

M. MELLINI, M., RUMORI, EC & VITI, EC. 2005. Hydrothermally reset magmatic spinels in retrograde serpentinites: formation of ‘‘ferritchromit’’ rims and chlorite aureoles. *Contributions to Mineral Petrology,*149, 266–275.

MA, M., BRUCKARD, W.J. & MCCALLUM, D. 2012. Role of Water Structure-Making/Breaking Ions in the Cationic Flotation of Kaolinite: Implications for Iron Ore Processing. *International Journal of Mining Engineering and Mineral Processing*, 1(1), 17-20.

MAGGI, F. 2005. Flocculation dynamics of cohesive sediment. Doctoral Thesis, Delft University of Technology. Delft, Netherlands.

MALVERN INSTRUMENTS Ltd. 2004. *Zetasizer Nano Series Usermanual: Man 0317.* Issue 2.1. United Kingdom: Malvern Instruments Ltd.

MARCHUK, A & RENGASAMY, P. 2011. Clay behaviour in suspension is related to the ionicity of clay-cation bonds. *Applied clay science,* 53(Jul), 754-759.

MASOMERA, W., EKOSSE, G.E. &NGOLE.V.M. 2011. The potential of clay based soil ameliorants in soil remediation: a review. In: *Conference proceedings of the 1st ICCCM& 2nd ICGSA.* 168-176.

MILLER, W. R., VAN DEN BOSSCHE, P. & SLOGROVE, D.J. 2008. Geophysical Survey of the Cullinan Diamond Mine No. 7 Slimes Dam. Unpublished project report, Marine GeoSolutions, Petra Diamonds.

MITCHELL, R.H. 1986. *Kimberlites: Mineralogy, Geochemistry and Petography.* New York: Plenum Press.

MITCHELL, R.H., SKINNER, E.M.W & SCOTT SMITH, B.H. 2008. Tuffisitic Kimberlites: Mineralogical Characteristics Relevant to their Formation. *Extended abstracts of the 9th International Kimberlite Conference*, No. 9IKC-A-00054.

MONCUR, M.C. & SMITH, L.J.D. 2012 Processed Kimberlite Porewater Geochemistry from Diavik Diamonds Mines, Inc. In: PRICE, W.A. ed. *Proceedings from the 9th International Conference Acid Rock drainage*, May,20-26 Ottawa, Ontario, Canada.

MOORE, D.M. & REYNOLDS, R.C. 1997. *X-Ray diffraction and the identificationand Analysis of Clay Minerals.* 2nd ed. New York: Oxford University Press,

MORKEL, J. 2006. Kimberlite weathering: Mineralogy and mechanisms. Doctoral Thesis, University of Pretoria, South Africa.

MORKEL, J., KRUGER, S.J. & VERMAAK, M.K.G. 2006. Characterization of clay mineral fractions in tuffisitic kimberlite breccia. *The Journal of The South African Institute of Mining and Mettalurgy,* 106 (Jun), 397-406.

NIRIELLA, D & CARNAHAN, R.P. 2006. Comparison Study of Zeta Potential Values of Bentonite in Salt Solutions. *Journal of Dispersion Science and Technology,* 27,123–131.

NORRISH, K. 1973. Factors in the weathering of mica to vermiculite. In: SERRATOSA, J.M. ed. *Proceedings of the International Clay Conference*. Madrid: Div. de Ciencias. 417-432.

OCHIENG, L., HARK.,T & PETERS, M. 2009. Net neutralisation potential (NNP) in Kimberley diamond tailings and slimes waste material. In: *Abstracts of the international mine water conference.* Pretoria, Document Transformation Technologies*. 910-916.*

OHTA, T & ARIA, H. 2007.Statistical empirical index of chemical weathering in igneous rocks: A new tool for evaluating the degree of chemical weathering. *Chemical Geology,* 240, 280-297.

PECKHAM, R.F. 1962. The Coagulation Process II - Effect of pH on the precipitation of Aluminu Hydroxide. *Journal of Applied Chemistry* , 12, 564.

PENNER, D. & LEGALY, G. 2001. Influence of anions on the rheological properties of clay mineral dispersions. *Applied Clay Science*, 19, 131-142.

PETRA DIAMONDS LIMITED. 2014.*Cullinan.* Available from: http://www.petradiamonds.com/operations/operating-mines/cullinan.aspx. [Accessed January 13, 2014].

POTGIETER, J. H. & GREEN, C. 2006. A. novel application of phosphogypsum: Treatment of a diamond mine's slimes tailings. *Water SA,* 32(4): 489-497.

POURBAIX, M. 1974. *Atlas of electrochemical equilibria in aqueous solutions*. 2d English ed. 1974, Houston: National Association of Corrosion Engineers.

PRINCE, W. A. 1997. *Guidelines and recomended methods for the prediction of metal leaching and acid rock drainage at mine site in British Columbia*. Draft report, Energy and Minerals Div, Minestry of Employment and Investment, British Columbia, Canada,

PUTNIS, C.V. & RULZ-AGUDO, E. 2013. The Mineral-Water Interface: Where Minerals React with the Environment. *Elements,* 9(Jun):177-182.

RAMAMOHANA RAO, N.V., RAO, N., SURYA PARKASH RAO,K &SCHUILING, R.D. 1993. Fluorine distribution in waters of Nalgonda District, Andhra Pradesh, India. *Environmental Geology*, 21,84-89.

RAUSSELL-COLOM, J.A., SWEATMAN, T.R., WELLS, C.B. & NORISH, K. 1965. Studies in the artificial weathering of mica. In: HALLSWORTH, E.G. & CRAWFORD, D.V. eds. *Experimental Pedology*. London: Butterworths, 40-72.

REARDON, E.J. & WANG, Y. 2000. A Limestone Reactor for Fluoride removal from Wastewaters. *Environmental Science & Technology, 34, 3247-3253.*

SANZ, J. & STONE, W.E.E. 1979. NMR study of mica: Distribution of Fe^{2+}, F^{-}, and OH^{-} in the octahedral sheet of phlogopites. *American mineralogist*, 64, 119-126.

SAPSFORD, D.J., BOWELL, R.J., DEY, M., & WILLIAMS K.P. 2009. Humidity cell tests for the prediction of acid rock drainage. *Minerals Engineering,* 22 (May), 25 - 36.

SCHOEMAN, A. 2012. Photo produced 6 March.

SCHOFIELD, R.K. 1949. Effect of pH on electric charges charges carried by clay particles. *Journal of Soil Science, 1, 1-8.*

SHERVAIS, J.W., KOLESAR, P. & ANDREASEN, K. (2005). A field and chemical study of serpentinizationçStonyford, California: chemical flux and mass balance. *International Geology Review* ,47, 1-28.

SIFFERT, B. 1962. Quelques reactions de la silice en solution; la formation de argiles. *Mémoir Service Carte Géol Alsace Lorraine*, 21, 86.

SINGER, A. & GALAN, E. 1984. Paligorskite - s*epiolite: occurrences, genesis and uses.* Amsterdam, Elsevier.

SKINNER, E.M.W. & MARSH, J.S. 2004. Distinct kimberlite pipe classes with contrasting eruption processes. *Lithos,*76 (Jun), 183-200.

SKINNER, E.M.W.& TRUSWELL, J.F. 2006. Kimberlites. In: . Johnson, M. R., Anhauser, C.R. and Thomas, R.J., eds. *The Geology of South Africa.* Pretoria: Geological Scociety of South Africa/Council for Geoscience, 651-659.

SKOOG, D. A., HOLLER, F. J. & CROUCH, S. R. 2007. Electron-Stimulated Mycroanalysis Methods. In: *Principles of Instrumental Analysis*. Belmont USA: Brooks/Cole Cengage Learning, 607-613.

SPARKS, D. L. 2003. *Environmental Soil Cemistry.* 2nd ed. San Diego: Elsevier.

STIFF, H.A. 1951. THE INTERPRETATION OF CHEMICAL WATER ANALYSIS BY MEANS OF PATTERNS. *Journal of Petroleum Technology,* 3, 15-17.

SUN, S.-S. & MCDONOUG, W.F. 1989. Chemical and isotopic systematics of oceanic basalts: implications for mantle composition and processes. *Geological Society, London, Special Publications,* 42, 313-345.

SUN, S.-S., NESBITT, R.W. & SHARASKIN, A.Y. 1979. Geochemical characteristics of mid-ocean ridge basalts. *Earth and Planetary Science Letters*, 46 (3), 462.

TAMBO, N. 1990. Basic concepts and innovative turn of coagulation/flocculation. *IWSAf - IAWPRC Joint Specialised Conference.* Jonkoping, 1-10.

TASSEL, A. 2012. Petra implements the C-Cut at Cullinan. *Modern Mining*, (Jan): 70-75.

THERIALUT, E.J. & CLARK, W.M. 1923. An expeirmental stydy of the relation of H+ concentration on the formation of floc in Alum Solution. *Public Health Reports,* 38, 181.

VAN DEVENTER, A. 2013. Photo produced 23 Jan. Frame number IMG_4637.

VAN DEVENTER, A. 2014. Verbal communication with Cullinan mine SHE manager on February 17th.

VAN DEVENTER, P.W. 2003. Buffer capacity and requirement of neutralising agent on slimes material. Unpublished project report, Envirogreen, Petra Diamonds.

VAN DUUREN, F.A. ed. 1997.*Water purification works design.* Republic of South Africa: Water Research Commission.

VELDE, B. 1985. Clay Minerals: A Physio-Chemical Explanation of their occurrence. In: *Developments in Sedimentology.* Vol. 40. Amsterdam: Elsevier..

VELDE, B. & MEUNIER, A. 2008. *The origin of Clay Minerals in Soils and Weathered Rocks.* Berlin: Springer-Verlag.

VERWOERD, W.J. 2006. The Pilanesberg Alkaline Province. In: . Johnson, M. R., Anhauser, C.R. and Thomas, R.J., eds. *The Geology of South Africa.* Pretoria: Geological Scociety of South Africa/Council for Geoscience, 381-393.

WAGNER, P.A. 1914. *The diamond fields of South Africa.* Johannesburg: The Transvaal Leader..

WEISBURD, S. 1986. Rooting for continental roots. *Seience News* 130(24), 380-382.

WENK, H.-R. & BULAKH, A. 2004. *Minerals: Their Constitution and Origin.* New York: Cambridge University Press.

WHITE, W.M. 1997. *Geochemistry*. Ithaca, New York: Cornell University.

WHO. 2010. *WHO Guidelines for Drinking Water Quality.* Geneva: World Health Organization Press.

WIETHOFF, A. 2000. Geochemistry and Petrology of the Premier Kimberlite Pipe. Unpublished honnors dissertation, Rhodes University, Grahamstown, South Africa.

WILLIAMS, A.F. 1932. *The genesis of diamonds.* London: Ernest Benn Ltd.

WINTER, J.D. 2001. Continental Alkaline Magmatism. In: *An Introduction to Igneous and Metamorphic Petrology*. New Jersey: Prentice-Hall Inc , 362-400.

WU, F.Y., MITCHELL, R.H., LI, Q.L., LIU, C.Z. & YANG, T.H. 2013. In situ U\Pb age determination and Sr\Nd isotopic analysis of perovskite from the Premier (Cullinan) kimberlite, South Africa. *Chemical Geology*, 353 (Jun), 83-95.

ANNEXURES

A: PARTICLE SIZE DISTRIBUTION DATA

Table 17: Data obtained by mechanical sieve analysis for the compilation of the PSD graph (fig 25 and 26)

	Tailings material (800g)		Kimberlite after leaching (817g)		Tailings after leaching (809g)	
Sieve diameter (µm)	% Retained on sieve	Cumulative % passing	% Retained on sieve	Cumulative % passing	% Retained on sieve	Cumulative % passing
10000	0	100.00	0	100	0	100
7000	19.60	80.40	2.94	97.06	4.45	95.55
4000	20.35	60.05	28.89	68.18	19.78	75.77
1700	24.40	35.65	28.27	39.90	19.16	56.61
1400	11.76	23.89	4.28	35.62	3.34	53.28
1000	2.40	21.49	3.92	31.70	4.33	48.95
700	2.28	19.22	8.81	22.89	14.96	33.99
600	2.91	16.31	3.30	19.58	6.43	27.56
500	1.90	14.41	1.96	17.63	3.83	23.73
425	1.52	12.90	2.33	15.30	2.97	20.77
315	2.65	10.24	2.94	12.36	5.56	15.20
212	2.78	7.46	3.06	9.30	4.82	10.38
180	1.14	6.32	1.35	7.96	1.98	8.41
75	3.29	3.03	3.92	4.04	5.07	3.34
Bowl	3.03	0.00	4.04	0.00	3.34	0.00
	100.00		100.00		100	

B: COEFFICIENT OF LINEAR EXTENSIBILITY

Table 18: Data used to calculate the COLE for the clay extracted from Cullinan mine No 7 Dam before and collected after the mineral acid treatment of the wastewater.

Repititions No 7 Dam Clay	Weight (g) bar	Weight (g) bar and saturated soil	Weight (g) saturated soil (PL)	Weight (g) bar and dry soil	Weight (g) dry soil		COLE		Mass (g) water present
1	26.3	45.62	19.32	33.42	7.12		63.14699793		12.2
2	26.26	44.99	18.73	32.98	6.72		64.12172985		12.01
3	26.3	45.43	19.13	32.47	6.17		67.74699425		12.96
4	26.26	43.96	17.7	31.93	5.67		67.96610169		12.03
5	26.3	44.82	18.52	33.36	7.06		61.87904968		11.46
	Averages		18.68		6.42		65.63169165		12.3
	Standard deviation		0.565791481		0.5536569		2.140437668		
No 7 Dam Clay After treatment									
1	26.3	41.16	14.86	30.32	4.02		72.94751009		10.84
2	26.3	40.87	14.57	30.31	4.01		72.47769389		10.56
3	26.2	41.52	15.32	30.4	4.2		72.5848564		11.12
4	26.3	41.2	14.9	30.3	4		73.15436242		10.9
5	26	41	15	29.89	3.89		74.06666667		11.11
	Averages		15		4.024				10.906
	Standard deviation		0.241826384		0.0997196				0.205679362

C: X-RAY FLUORESCENCE DATA

C1 : Oxide species

Table 19: Table 19: Weight % of oxides identified in the Cullinan mine materials with the assistance of Mrs Belinda Venter at the NWU.

Oxide (%)	Kimberlite	Kimberlite after 10 leachings	Kimberlite after 20 leachings	Tailings material	Tailings after 10 leachings	Tailings after 20 leachings	No 7 Dam Clay
SiO_2	40.86	40.736	39.873	46.112	44.681	45.427	41.176
TiO_2	1.432	1.543	1.428	1.219	1.429	1.356	0.071
Al_2O_3	4.491	4.396	4.387	5.334	5.105	5.162	5.268
Cr_2O_3	0.122	0.129	0.129	0.119	0.118	0.116	0.065
Fe_2O_3	8.931	8.931	8.917	8.496	8.804	8.451	7.561
Mn_3O_4	0.171	0.175	0.189	0.157	0.162	0.156	0.066
MgO	21.938	21.999	21.58	19.004	19.629	19.202	23.543
CaO	7.204	7.475	8.12	6.471	6.423	6.222	1.173
BaO	0.247	0.262	0.135	0.247	0.323	0.162	0.099
Na_2O	0.874	0.795	0.807	1.119	0.98	1.114	1.948
K_2O	1.503	1.491	1.473	1.253	1.282	1.202	0.906
P_2O_5	0.289	0.305	0.316	0.203	0.195	0.201	0.02
NiO	0.114	0.128	0.118	0.104	0.108	0.101	0.131
SO_3	0.094	0.092	0.09	0.127	0.151	0.133	0.552
V_2O_5	0.025	0.013	0.013	0.018	0.011	0.022	0.007
SrO	0.048	0.048	0.05	0.03	0.026	0.033	0.009
ZnO	0.006	0.007	0.005	0.004	0.007	0.009	0.005
ZrO_2	0.008	0.004	No detection	0.005	0.006	0.001	No detection
LOI	9.95	9.97	10.48	7.72	10.09	7.19	Not enough sample.

C2: Trace elements

Table 20: Components that occur in trace amounts in the Cullinan mine materials as identified by mean of XRF at the NWU by Mrs Belinda Venter.

Trace element	FRESH ROCK 0 WKS	FRESH ROCK 10 WKS	FRESH ROCK 20 WKS	TAILINGS 0 WKS	TAILINGS 10 WKS	TAILINGS 20 WKS	NO 7 DAM CLAY
			Concentration ppm				
Sc	13.5	15.6	16.7	14.9	15.3	13.3	3.4
V	92.4	93.3	90.3	95.9	101.3	97.3	28
Co	67	70.8	68.8	72.6	71	75.9	40.1
Cu	43.3	48.9	48.3	38.7	39.6	44.2	19.6
Zn	57.7	55.5	58	66.4	75.2	74.2	59
Ga	4.6	4.5	5.7	5.2	6.1	5.2	6.4
Ge	nd	nd	nd	0.2	0.4	nd	nd
As	67	73.7	57.8	64.3	68.4	64.5	51.3
Se	19.1	20.6	18.6	18.8	20.3	18.5	14.8
Br	18.7	18.2	16.7	16.5	18.6	15.3	32
Rb	96.8	98	92.6	58.3	64.3	56.6	58.2
Sr	408.3	397.4	400.7	303.4	307.9	293	137.7
Y	7.8	6.7	7.1	8.5	7.6	8.8	0.3
Zr	102.3	95.1	93.4	110.3	104.1	108.1	20.4
Nb	74	79	83.2	48.5	53.8	51.7	3.3
Mo	1.8	0.8	0.9	0.9	1.6	0.9	7.2
Ag	nd	nd	1	0.3	nd	nd	1.5
Cd	5.6	8.4	10.4	8.6	5.6	6.6	11.7
Sn	7.7	11.1	13.2	10.3	6.9	16.1	10.9
Sb	nd	nd	nd	nd	nd	7.9	0.7
I	15.9	12.4	13.3	13.2	14.6	9.8	12.2
Cs	nd	nd	nd	nd	nd	nd	11.2
La	38.7	29.9	41.4	28.1	29.1	29.2	3.8
Ce	45.1	65	62.3	52.8	46.8	48.7	7.8
Nd	28.5	33.2	32	30.5	23	19.6	8.2
Sm	2.6	7.1	nd	0.9	4.8	nd	nd
Hf	3.6	1.6	3.2	1.7	1.5	0.5	1.7
Ta	2.4	1.1	1.7	1.7	1.2	nd	0.4
W	67.9	64.7	63.3	126.5	98.7	108.9	45.1
Hg	0	0	0	0.1	0.1	0.1	0
Tl	23.4	26.5	21.9	21.2	25.1	20.9	15.6
Pb	7	6.9	7.2	17.7	18.2	23.3	22.3
Bi	31.1	32.6	29.5	29.7	31.2	30.9	23.8
Th	16.4	16.1	16.9	11.6	16	15	8.2

Table 21: Trace element composition in ppm of the primitive mantle given by Sun & McDonough (1989). The values were used for normalisation of the relevant trace elements in Error! Reference source not found. **to use in the compilation of Figure 40 that show the trace element pattern of the Cullinan mine materials.**

Relevant ement	ppm
Rb	0.635
Ba	6.989
Th	0.085
U	0.021
K	250
Ta	0.041
Nb	0.713
La	0.687
Ce	1.775
Pb	0.185
Pr	0.276
Sr	21.1
Nd	1.354
P	95
Sm	0.444
Hf	0.309
Zr	11.2

D: ADSORBED CATIONS

Table 22: Laboratory report from Eco-Analytica that give the cations and exchange capacity for the clay extracted from the No 7 Dam wastewater. These values were used in the compilation of Figure 41.

NORTH-WEST UNIVERSITY
ECO-ANALYTICA

Eco Analytica
P.O. Box 19140
NOORDBRUG 2522
Tel: (018) 293 3900

JESSICA STRYDOM

23/5/2014

Nutrient Status

Sample no.	Ca	Mg	K	Na	P
	(mg/kg)				
No 7 CLAY	4797.5	544.5	1652.5	4972.5	

Exchangeable cations

Sample no.	Ca	Mg	K	Na	CEC	S-value
	(cmol(+)/kg)					
No 7 CLAY	23.94	4.48	4.24	21.62	*****36.8	54.28

HANDBOOK OF STANDARD SOIL TESTING METHODS FOR ADVISORY PURPOSES

Exchangeable cations: 1M NH_4-Acetate pH=7
CEC: 1 M Na-Acetate pH=7
Extractable, Exchangeable micro-elements: 0.02M $(NH_4)_2$ EDTA.H_2O
EC: Saturated Extraction
pH H_2O/KCl: 1:2.5 Extraction
Phosphorus: P-Bray 1 Extraction

This laboratory participates in the following quality control schemes:
1. Agricultural Laboratory Association of Southern Africa.
2. International Soil-Analytical Exchange (ISE), Wageningen, Nederland.

No responsibility is accepted by North-West University for any losses due to the use of this data

*****CEC determined by Mr Dries Bloem of Geolab, Potchefstroom.

E: SODIUM ADSORPTION RATIO

Table 23: Calculation of the SAR for the various water samples.

Laboratory	Midvaal water	Waterlab					Leachate (Eco-Analytica)	
Sample name	No 7 Dam 8 - 15 m	No 7 Dam 4 - 4.5 m	No 7 Dam 11-15 m	Site 4 (4.5 m)	Site 4 (11-15 m)	No 7 Dam After treatment	Rock (20 weeks)	Tailings (20 weeks)
	mg / L							
Na^+	279	402.3	385.33	412	475.00	521	42.85	32.01
Ca^{2+}	11	15.96	35.2	21.2	135	158	0.38	0.17
Mg^{2+}	9.2	206.66	477.66	222	853	31	6.52	3.70

Laboratory	Midvaal water	Waterlab					Leachate (Eco-Analytica)	
Sample name	No 7 Dam 8 - 15 m	No 7 Dam 4-4.5m	No 7 Dam 11-15 m	Site 4 (4.5 m)	Site 4 (11-15 m)	No 7 Dam After treatment	Rock (20 weeks)	Tailings (20 weeks)
	mmol / L							
Na^+	12.18	17.56	16.82	17.99	20.74	22.75	1.87	1.39
Ca^{2+}	0.27	0.39	0.87	0.52	3.36	3.93	0.0094	0.0041
Mg^{2+}	0.3786008	8.5030515	19.653021	9.13392	35.095659	1.269697593	0.268202702	0.1521498
SAR	**14.6**	**5.9**	**3.4**	**5.8**	**3.2**	**9.9**	**3.5**	**3.5**

Atomic weight	
Na	22.9
Ca	40.08
Mg	24.305

F: HIGH HUMIDITY ACCELERATED WEATHERING KINETIC TESTING

F1: pH

Table 24: pH of the leachate of three repetitions of Cullinan kimberlite rock and tailings material as determined with a 3-point calibrated Hannah HI9828 multi-parameter meter

	TAILINGS			Averages	ROCK			Averages
Weeks	1	2	3		1	2	3	
Initial flush	8.3	8.27	8.83	8.47	8.4	8.72	8.85	8.66
1 & 2	8.2	8.36	8.54	8.37	8.79	8.5	8.56	8.62
3 & 4	8.26	8.3	8.41	8.32	9.37	8.53	8.41	8.77
5 & 6	8.06	8.07	8.4	8.18	8.7	8.97	8.49	8.72
7 & 8	8.32	8.47	8.09	8.29	9.08	8.55	9.03	8.89
9 & 10	8.09	8.62	8.01	8.24	8.58	9.37	9.62	9.19
11 & 12	9.06	9.27	9.22	9.18	9.35	9.52	9.49	9.45
13 & 14	9.05	8.93	9.06	9.01	9.25	9.33	9.4	9.33
15 & 16	9.26	9.24	9.37	9.29	9.51	9.67	9.57	9.58
17 & 18	9.1	9	9.3	9.13	9.4	9.6	9.3	9.43
19 & 20	8.9	8.8	9	8.90	9.2	9.4	9.2	9.27
Final flush	8.9	8.9	9.1	8.97	9.3	9.3	9.4	9.33

F2: EC

Table 25: EC of the leachate of three repetitions of Cullinan kimberlite rock and tailings material as determined with a 3-point calibrated Hannah HI9828 multi-parameter meter

	TAILINGS			Averages	ROCK			Averages
Weeks	1	2	3		1	2	3	
Initial flush	0.74	0.65	0.74	0.71	0.72	0.6	0.64	0.65
1 & 2	0.62	0.59	0.54	0.58	0.54	0.52	0.52	0.53
3 & 4	0.48	0.47	0.49	0.48	0.53	0.47	0.48	0.49
5 & 6	0.41	0.41	0.4	0.41	0.42	0.46	0.46	0.45
7 & 8	0.33	0.37	0.34	0.35	0.41	0.36	0.46	0.41
9 & 10	0.29	0.29	0.27	0.28	0.33	0.37	0.41	0.37
11 & 12	0.37	0.3	0.32	0.33	0.38	0.38	0.43	0.40
13 & 14	0.32	0.31	0.31	0.31	0.44	0.47	0.39	0.43
15 & 16	0.29	0.28	0.3	0.29	0.36	0.45	0.42	0.41
17 & 18	0.201	0.191	0.259	0.22	0.489	0.396	0.27	0.39
19 & 20	0.197	0.189	0.211	0.20	0.262	0.313	0.225	0.27
Final flush	0.192	0.186	0.246	0.21	0.239	0.287	0.248	0.26

F3: Leachate analysis

Table 26: Change in major dissolved anion species concentrations as determined by Eco-Analytica for the 20 cycles of the HHAWK-test.

Major components in ROCK				
	Cl	**NO_3**	**F**	**SO_4**
	mg/l			
Initial flush	37.62	26.88	1.64	13.74
1 & 2	21.72	9.63	1.32	19.32
3 & 4	19.27	8.04	1.25	18.07
5 & 6	7.38	2.38	1.08	12.33
7 & 8	3.16	0.20	0.68	5.92
9 & 10	6.70	0.31	0.65	5.90
11 & 12	1.71	3.92	0.71	4.95
13 & 14	1.65	3.53	0.65	4.63
15 & 16	1.52	3.16	0.54	4.22
17 & 18	1.99	1.52	0.33	5.22
19 & 20	1.63	1.13	0.21	3.48
Final flush	1.62	1.13	0.19	3.32
Major components in TAILINGS				
	Cl	**NO_3**	**F**	**SO_4**
	mg/l			
Initial flush	28.36	8.43	0.67	119.35
1 & 2	13.26	3.50	0.74	59.08
3 & 4	15.08	2.59	0.74	50.32
5 & 6	4.34	0.08	0.74	21.83
7 & 8	2.71	0.04	0.44	7.70
9 & 10	2.46	0.06	0.45	5.80
11 & 12	1.67	0.20	0.58	5.92
13 & 14	1.55	0.30	0.52	4.61
15 & 16	1.54	0.27	0.39	4.30
17 & 18	2.20	0.35	0.24	3.51
19 & 20	1.66	0.22	0.25	2.69
Final flush	1.63	0.23	0.21	2.64

Table 27: Change in major dissolved cation species concentration as determined by Eco-Analytica for the 20 cycles of the HHAWK-test.

	Major components in ROCK				
	Na	**K**	**Mg**	**Ca**	**Fe**
	mg/l				
Initial flush	101.64	9.91	26.06	2.95	8.49
1 & 2	90.82	9.90	31.28	3.70	10.18
3 & 4					
5 & 6	95.80	12.20	37.31	4.17	11.70
7 & 8	195.37	27.54	14.57	3.61	4.53
9 & 10					
11 & 12	60.68	13.23	9.97	2.57	6.01
13 & 14					
15 & 16	61.70	13.28	9.86	2.09	5.62
17 & 18	52.34	11.58	8.31	2.13	4.52
19 & 20	42.85	9.17	6.52	0.38	3.21
Final flush					
	Major components in TAILINGS				
	Na	**K**	**Mg**	**Ca**	**Fe**
	mg/l				
Initial flush	102.35	17.69	26.16	4.85	8.21
1 & 2	90.07	15.64	24.50	6.49	8.42
3 & 4					
5 & 6	77.84	11.16	36.11	3.80	10.79
7 & 8	57.68	8.23	20.17	2.32	6.17
9 & 10					
11 & 12	48.15	10.38	4.80	1.58	2.72
13 & 14					
15 & 16	44.77	9.27	4.62	0.91	2.41
17 & 18	28.78	6.59	4.03	0.84	2.07
19 & 20	32.01	6.95	3.70	0.17	1.85
Final flush					

F4: Leaching factor

Table 28: Recalculation of oxide weight % to the leaching factors (degree of weathering) for the various Cullinan mine materials with the kimberlite rock considered as parent material.

Molecular values (oxide percentage from XRF / molecular weight)							
	No 7 Dam Clay	**20wk Tailings**	**10wk Tailings**	**tailings**	**20wk Rock**	**10wk Rock**	**Rock**
NiO	0,001747	0,001346667	0,00144	0,0014	0,0015733	0,0017067	0,00152
Fe2O3	0,047256	0,05281875	0,055025	0,0531	0,0557313	0,0558188	0,0556313
CaO	0,020946	0,111107143	0,114696429	0,1156	0,145	0,1334821	0,1286429
K2O	0,009638	0,012787234	0,013638298	0,0133	0,0156702	0,0158617	0,0159894
SiO2	0,686267	0,757116667	0,744683333	0,7685	0,66455	0,6789333	0,681
Al2O3	0,051647	0,050607843	0,05004902	0,0523	0,0430098	0,043098	0,0440294
MgO	0,588575	0,48005	0,490725	0,4751	0,5395	0,549975	0,54845
Na2O	0,031419	0,017967742	0,015806452	0,018	0,0130161	0,0128226	0,0140968

	ba1 value ((K+Na)/Al)	**ba2 value ((Ca+Mg)/Al)**
No 7 Dam Clay	0,794965941	11,80166775
20wk Tailings	0,607711652	11,68113688
Tailings	0,60003258	11,2948377
20wk Rock	0,666972159	15,91497607
Rock	0,683319052	15,37819448

Leaching factor (assesses loss of monovalent cations through leaching) B=ba leached/ba parent			
	ba1		**ba2**
Tailings to Rock	0,8781148		0,734471
20 wk Rock to Rock	0,9760772		1,0349054
Clay to Rock	1,1633891		0,7674287

G: WATER QUALITY OF THE NO 7 DAM

G1: On-site measurements

Table 29: Parameters measured on site at the Cullinan mine No 7 wastewater dam with a Hannah HI9828 multi-parameter meter in May 2014 to distinguish between the upper less dense and deeper more dense stratification that occurs in the Dam.

4 - 4.5 m deep (A)						11 - 15 m deep (B)				
Sample no	**1A**	**2A**	**3A**	**4A**		**Sample no**	**1B**	**2B**	**3B**	**4B**
Depth (m)	4.5	4	4.5	4.5		**Depth (m)**	11	11	12	15
pH	9.18	8.9	8.8	9.08		**pH**	9.09	8.9	7.8	9.06
EC (µS/cm)	2014	2025	2018	1987		**EC (µS/cm)**	1790	1868	1700	1568
DO	4.45	4.88	4.6	3.95		**DO**	2.93	3.6	3.3	2.05
ORP	-9.7	-3.6	-5.4	-8.4		**ORP**	-8	-4.8	-8.9	-7.5
SAL	1.03	1.03	1.03	1.04		**SAL**	0.9	0.95	0.85	0.81
Temp	16.7	16.3	17	17		**Temp**	18.9	16	18.5	18.9

G2: Alkalinity to Calcite Ratio

Table 30: Calculation of the alkalinity to calcite ratio of the various Cullinan mine No 7 Dam samples to indicate the contribution of the calcite mineral content to the total alkalinity of the water.

	Ca	**Alk ($CaCO_3$)**			**Ca**	**Alk ($CaCO_3$)**		**Alk:Ca**
	mg/L				**mmol/L**			**Molar ratio**
Average Site 1-3 (4-4.5 m)	15.96	448		**Average Site 1-3 (4-4.5 m)**	0.39	4.48		0.09
Average Site 1-3 (11-15 m)	35.2	438.66		**Average Site 1-3 (11-15 m)**	0.87	4.39		0.20
Site 4 (4-4.5 m)	21.2	600		**Site 4 (4-4.5 m)**	0.52	6.01		0.09
Site 4 (11-15 m)	135	424		**Site 4 (11-15 m)**	3.36	4.24		0.79

Molecular weight	
Ca	40.08
CaCO3	99.79

G3: Laboratory reports of the No 7 Dam water quality

Table 31: Laboratoy report from Midvaal Water Company for a composite sample of the Cullinan mine No 7 Dam.

MIDVAAL Water Company

sanas Testing Laboratory T0132

SCIENTIFIC SERVICES

PO Box 31, Stilfontein, 2550 ♦ Farm Buffelsfontein 443 IP, District Klerksdorp
Tel: 018 482 9500 ♦ Fax: 086 698 4740
lab@midvaalwater.co.za ♦ www.midvaalwater.co.za

TEST REPORT

Submitter:	NWU	**Sample type:**	Water sample
	PO Box 2675	**Date Received:**	2014-03-03
	2520 Potchefstroom	**Debit Number:**	DEP004
		Certificate Number:	2014-13478

Analyses Results

Sample number			13478
Sample date			2014-02-28
Identification on container			7 Dam
Determinand	**Unit**	**Method Number**	
Physical, Aesthetic and Calculated Determinands			
Bicarbonate**	Ca(HCO3)2		633
Calcium precipitation potential**	mg/L CaCO3		9
Carbonate**	CaCO3		42
Electrical Conductivity	mS/m	WL2	203
Hardness Calcium**	mg/L CaCO3		26
pH	pH units	WL1	8.98
pHs**	-		7.85
Sodium Adsorption Ratio**	-		15
Stability index**	-		6.72
Suspended Solids at 105°C	mg/L	WL5	6 058
Total Dissolved Solids at 180°C	mg/L	WL6	1 635
Turbidity	NTU	WL3	15 220
Chemical - Macro Determinands			
Alkalinity - p**	mg/L CaCO3	WL 8-A	21
Alkalinity Total	mg/L CaCO3	WL 8-A	675
Ammonia	mg/L N	GL 7-1	<0.5
Calcium Dissolved	mg/L Ca	ICP1	11
Chloride	mg/L Cl-	GL 7-5	99
Fluoride	mg/L F-	GL 4	5.9
Magnesium Dissolved	mg/L Mg	ICP1	9.2
Nitrate & Nitrite	mg/L N	GL 7-2	2.5
Orthophosphate**	mg/L P	CFA - 1B	<0.05
Potassium Dissolved	mg/L K	ICP1	35
Sodium Dissolved	mg/L Na	ICP1	279
Sulphate	mg/L SO4	GL 7-4	409
Zinc Dissolved	mg/L Zn	ICP1	0.02

Chemical analyses commenced on 2014-03-04 and completed on 2014-03-31.
If a test is marked ** in this report it is not included in the SANAS Schedule of Accreditation for this laboratory.

J W D Pietersen:_____ (All methods)
Date of issue: 2014-04-07
This test report is only valid if signed by technical signatories. Refer to Schedule of Accreditation.
This report relates only to the samples supplied to Midvaal Water Company Scientific Services.
This signed test report shall not be reproduced, except in full, without the written approval of the Technical Signatory.
SS025 Ver:009 Implementation date: 2012-07-24

Page 1 of 2 Certificate number: 2014-13478

Table 31: (*cont.)* Laboratoy report from Midvaal Water Company for a composite sample of the Cullinan mine No 7 Dam.

Sample number			13478
Sample date			2014-02-28
Identification on container			7 Dam
Determinand	Unit	Method Number	
Chemical - Micro Determinands			
Aluminium Dissolved	mg/L Al	ICP1	1.2
Antimony Dissolved	mg/L Sb	ICP1	0.01
Arsenic Dissolved	mg/L As	ICP1	0.02
Barium Dissolved	mg/L Ba	ICP1	1.2
Beryllium Dissolved	mg/L Be	ICP1	<0.10
Boron Dissolved	mg/L B	ICP1	0.73
Cadmium Dissolved	mg/L Cd	ICP1	<0.005
Chromium 6+	mg/L Cr	GL 7-6	0.03
Chromium Dissolved	mg/L Cr	ICP1	0.03
Cobalt Dissolved	mg/L Co	ICP1	<0.01
Copper Dissolved	mg/L Cu	ICP1	0.04
Cyanide Dissolved - CFA**	mg/L CN	CFA - 1D	<0.02
Gold Dissolved	mg/L Au	ICP1	<0.02
Iron Dissolved	mg/L Fe	ICP1	1.6
Lead Dissolved	mg/L Pb	ICP1	<0.01
Lithium Dissolved	mg/L Li	ICP1	<0.02
Manganese Dissolved	mg/L Mn	ICP1	<0.10
Mercury Dissolved	mg/L Hg	ICP1	0.02
Molybdenum Dissolved	mg/L Mo	ICP1	0.30
Nickel Dissolved	mg/L Ni	ICP1	0.05
Selenium Dissolved	mg/L Se	ICP1	<0.01
Silver Dissolved	mg/L Ag	ICP1	<0.02
Strontium Dissolved	mg/L Sr	ICP1	0.18
Tin Dissolved	mg/L Sn	ICP1	<0.07
Titanium Dissolved	mg/L Ti	ICP1	0.07
Uranium Dissolved	mg/L U	ICP1	0.016
Vanadium Dissolved	mg/L V	ICP1	0.01
Chemical - Organic and Related Determinands			
Oil & grease**	mg/L	WL11	1
Total Phosphorus	mg/L P	N8	3.3

Chemical analyses commenced on 2014-03-04 and completed on 2014-03-31.
If a test is marked ** in this report it is not included in the SANAS Schedule of Accreditation for this laboratory.

J W D Pietersen:_____ (All methods)
Date of issue: 2014-04-07
This test report is only valid if signed by technical signatories. Refer to Schedule of Accreditation.
This report relates only to the samples supplied to Midvaal Water Company Scientific Services.
This signed test report shall not be reproduced, except in full, without the written approval of the Technical Signatory.
SS025 Ver:009 Implementation date: 2012-07-24

Table 32: Laboratory report on the water quality of the top less dense (A) and deeper more dense (B) layers Cullinan mine No 7 Dam wastewater.

WATERLAB

WATERLAB (Pty) Ltd
Reg. No.: 1963/009165/07 V.A.T. No.: 4130107891

Building D
The Woods
41 De Havilland Cresent
Persequor Techno Park
Meiring Naudé Drive
Pretoria

P.O. Box 283
Persequor Park, 0020
Tel: +2712 – 349 – 1066
Fax: +2712 – 349 – 2064
e-mail: admin@waterlab.co.za

SANAS Accredited Testing Laboratory No. T0391

CERTIFICATE OF ANALYSES
GENERAL WATER QUALITY PARAMETERS

Date received: 2014 - 06 - 02 **Date completed:** 2014 - 06 – 26

Project number: 248 **Report number: 46276** **Order number: -**

Client name: North-West University (NWU) **Contact person: Me. J. Strydom**

Address: Faculty of Natural Science, Geology
Private Bag X6001, Potchestroom, 2531
e-mail: Jessica.strydom@nwu.ac.za
e-mail: 21212627@nwu.ac.za

Telephone: 018 299 1089 **Facsimile: 018 299 2370** **Mobile: 076 876 6247**

Analyses in mg/ℓ (Unless specified otherwise)	Method Identification	Sample Identification	
		1A	1B
Sample Number		7932	7933
pH – Value at 25°C	WLAB001	8.8	8.9
Electrical Conductivity in mS/m at 25°C	WLAB002	201	187
Total Dissolved Solids at 180°C (Calculated) *	WLAB003		
Suspended Solids at 105°C *	WLAB004	23 894	99 018
Turbidity in N.T.U	WLAB005	379	680
Total Alkalinity as $CaCO_3$	WLAB007	448	456
Chloride as Cl	WLAB046	88	79
Sulphate as SO_4	WLAB046	440	414
Fluoride as F	WLAB014	6.1	4.5
Nitrate as N	WLAB046	2.5	1.0
Nitrite as N	WLAB046	<0.1	<0.1
Total Phosphate as P *	WLAB031	0.4	0.7
Ortho Phosphate as P	WLAB046	<0.2	<0.2
Dissolved Organic Carbon as C [s]	---	3.0	1.7
Oxygen Absorbed as O_2 (4-hour) *	WLAB019	203	204
Oil & Grease *	WLAB034	6	10
Free & Saline Ammonia as N	WLAB046	<0.2	<0.2
ICP-MS Scan [s]	---	See Attached Report: 46276-A	
% Balancing	---		

Technical Signatory

Table 32: (*cont.)* Laboratory report on the water quality of the top less dense (A) and deeper more dense (B) layers Cullinan mine No 7 Dam wastewater.

WATERLAB

WATERLAB (Pty) Ltd
Reg. No.: 1963/009165/07 V.A.T. No.: 4130107891

Building D
The Woods
41 De Havilland Cresent
Persequor Techno Park
Meiring Naudé Drive
Pretoria

P.O. Box 283
Persequor Park, 0020
Tel: +2712 – 349 – 1066
Fax: +2712 – 349 – 2064
e-mail: admin@waterlab.co.za

sanas Testing Laboratory
SANAS Accredited Testing Laboratory No. T0391

CERTIFICATE OF ANALYSES
GENERAL WATER QUALITY PARAMETERS

Date received: 2014 - 06 - 02 **Date completed:** 2014 - 06 – 26

Project number: 248 **Report number: 46276** **Order number: -**

Client name: North-West University (NWU) **Contact person: Me. J. Strydom**

Address: Faculty of Natural Science, Geology **e-mail: Jessica.strydom@nwu.ac.za**
Private Bag X6001, Potchestroom, 2531 **e-mail: 21212627@nwu.ac.za**

Telephone: 018 299 1089 **Facsimile: 018 299 2370** **Mobile: 076 876 6247**

Analyses in mg/ℓ (Unless specified otherwise)	Method Identification	Sample Identification	
		2A	2B
Sample Number		7934	7935
pH – Value at 25°C	WLAB001	8.9	9.0
Electrical Conductivity in mS/m at 25°C	WLAB002	202	189
Total Dissolved Solids at 180°C (Calculated) *	WLAB003		
Suspended Solids at 105°C *	WLAB004	2 360	122 670
Turbidity in N.T.U	WLAB005	330	679
Total Alkalinity as $CaCO_3$	WLAB007	440	420
Chloride as Cl	WLAB046	94	89
Sulphate as SO_4	WLAB046	459	442
Fluoride as F	WLAB014	5.2	4.9
Nitrate as N	WLAB046	2.5	0.8
Nitrite as N	WLAB046	0.1	0.5
Total Phosphate as P *	WLAB031	0.5	0.6
Ortho Phosphate as P	WLAB046	<0.2	<0.2
Dissolved Organic Carbon as C [s]	---	3.8	3.1
Oxygen Absorbed as O_2 (4-hour) *	WLAB019	202	201
Oil & Grease *	WLAB034	9	34
Free & Saline Ammonia as N	WLAB046	<0.2	<0.2
ICP-MS Scan [s]	---	See Attached Report: 46276-A	
% Balancing	---		

Technical Signatory

Table 32: (*cont.)* Laboratory report on the water quality of the top less dense (A) and deeper more dense (B) layers Cullinan mine No 7 Dam wastewater.

WATERLAB

WATERLAB (Pty) Ltd
Reg. No.: 1983/009165/07 V.A.T. No.: 4130107891

Building D
The Woods
41 De Havilland Cresent
Persequor Techno Park
Meiring Naudé Drive
Pretoria

P.O. Box 283
Persequor Park, 0020
Tel: +2712 – 349 – 1066
Fax: +2712 – 349 – 2064
e-mail: admin@waterlab.co.za

sanas Testing Laboratory
SANAS Accredited Testing Laboratory No. T0391

CERTIFICATE OF ANALYSES
GENERAL WATER QUALITY PARAMETERS

Date received: 2014 - 06 - 02 **Date completed:** 2014 - 06 – 26

Project number: 248 **Report number: 46276** **Order number: -**

Client name: North-West University (NWU) **Contact person: Me. J. Strydom**

Address: Faculty of Natural Science, Geology
Private Bag X6001, Potchestroom, 2531

e-mail: Jessica.strydom@nwu.ac.za
e-mail: 21212627@nwu.ac.za

Telephone: 018 299 1089 **Facsimile: 018 299 2370** **Mobile: 076 876 6247**

Analyses in mg/ℓ (Unless specified otherwise)	Method Identification	Sample Identification	
		3A	3B
Sample Number		7936	7937
pH – Value at 25°C	WLAB001	8.9	8.9
Electrical Conductivity in mS/m at 25°C	WLAB002	203	172
Total Dissolved Solids at 180°C (Calculated) *	WLAB003		
Suspended Solids at 105°C *	WLAB004	24 816	156 908
Turbidity in N.T.U	WLAB005	649	1 835
Total Alkalinity as $CaCO_3$	WLAB007	456	440
Chloride as Cl	WLAB046	96	77
Sulphate as SO_4	WLAB046	458	390
Fluoride as F	WLAB014	5.3	5.6
Nitrate as N	WLAB046	2.2	<0.2
Nitrite as N	WLAB046	0.1	<0.1
Total Phosphate as P *	WLAB031	0.7	0.7
Ortho Phosphate as P	WLAB046	<0.2	<0.2
Dissolved Organic Carbon as C [s]	---	1.8	4.4
Oxygen Absorbed as O_2 (4-hour) *	WLAB019	195	186
Oil & Grease *	WLAB034	7	18
Free & Saline Ammonia as N	WLAB046	<0.2	<0.2
ICP-MS Scan [s]	---	See Attached Report: 46276-A	
% Balancing	---		

Technical Signatory

Table 32: (*cont.)* Laboratory report on the water quality of the top less dense (A) and deeper more dense (B) layers Cullinan mine No 7 Dam wastewater.

WATERLAB

WATERLAB (Pty) Ltd
Reg. No.: 1983/009165/07 V.A.T. No.: 4130187891

Building D
The Woods
41 De Havilland Cresent
Persequor Techno Park
Meiring Naudé Drive
Pretoria

P.O. Box 283
Persequor Park, 0020
Tel: +2712 – 349 – 1066
Fax: +2712 – 349 – 2064
e-mail: admin@waterlab.co.za

SANAS Accredited Testing Laboratory
No. T0391

CERTIFICATE OF ANALYSES
GENERAL WATER QUALITY PARAMETERS

Date received: 2014 - 06 - 02 **Date completed:** 2014 - 06 – 26

Project number: 248 **Report number: 46276** **Order number: -**

Client name: North-West University (NWU) **Contact person: Me. J. Strydom**

Address: Faculty of Natural Science, Geology **e-mail: Jessica.strydom@nwu.ac.za**
Private Bag X6001, Potchestroom, 2531 **e-mail: 21212627@nwu.ac.za**

Telephone: 018 299 1089 **Facsimile: 018 299 2370** **Mobile: 076 876 6247**

Analyses in mg/ℓ (Unless specified otherwise)	Method Identification	Sample Identification	
		4A	4B
Sample Number		7938	7939
pH – Value at 25°C	WLAB001	8.9	8.9
Electrical Conductivity in mS/m at 25°C	WLAB002	201	169
Total Dissolved Solids at 180°C (Calculated) *	WLAB003		
Suspended Solids at 105°C *	WLAB004	26 676	261 238
Turbidity in N.T.U	WLAB005	674	>4 000
Total Alkalinity as $CaCO_3$	WLAB007	600	424
Chloride as Cl	WLAB046	82	79
Sulphate as SO_4	WLAB046	372	447
Fluoride as F	WLAB014	5.3	5.2
Nitrate as N	WLAB046	2.0	<0.2
Nitrite as N	WLAB046	0.1	<0.1
Total Phosphate as P *	WLAB031	1.6	14
Ortho Phosphate as P	WLAB046	<0.2	<0.2
Dissolved Organic Carbon as C [s]	---	2.5	2.9
Oxygen Absorbed as O_2 (4-hour) *	WLAB019	185	172
Oil & Grease *	WLAB034	19	Insufficient Sample
Free & Saline Ammonia as N	WLAB046	<0.2	<0.2
ICP-MS Scan [s]	---	See Attached Report: 46276-A	
% Balancing	---		

*** = Not SANAS Accredited**
Tests marked "Not SANAS Accredited" in this report are not included in the SANAS Schedule of Accreditation for this Laboratory.

[s] = Analyses performed by a Sub-Contracted Laboratory
Results marked "Subcontracted Test" in this report are not included in the SANAS Schedule of Accreditation for this Laboratory

Technical Signatory

Table 33: Dissolved components of the top less dense (A) and deeper more dense (B) layers Cullinan mine No 7 Dam wastewater as determined by IC-PMS scan.

WATERLAB (PTY) LTD

CERTIFICATE OF ANALYSIS

Project Number : 248
Client : North-West University (NWU)
Report Number : 46276-A

Sample Origin	Sample ID	Note: all results in parts per million (ppm) unless specified otherwise											
		Ag	Al	As	Au	B	Ba	Be	Bi	Ca	Cd	Ce	Co
		mg/l	mg/l	mg/l	mg/l	mg/l	mg/l	mg/l	mg/l	mg/l	mg/l	mg/l	mg/l
Lowest Reported Concentration		<0.01	<0.01	<0.01	<0.01	<0.01	<0.01	<0.01	<0.01	<0.01	<0.01	<0.01	<0.01
1A	7932	<0.01	40.6	0.038	<0.01	0.715	0.167	<0.01	<0.01	14.6	<0.01	<0.01	0.092
1B	7933	<0.01	79.3	0.037	<0.01	0.712	0.340	<0.01	<0.01	24.7	<0.01	0.015	0.271
2A	7934	<0.01	36.2	0.037	<0.01	0.736	0.149	<0.01	<0.01	13.1	<0.01	0.005	0.083
2B	7935	<0.01	80.4	0.038	<0.01	0.734	0.343	<0.01	<0.01	24.4	<0.01	0.014	0.294
3A	7936	<0.01	61.2	0.036	<0.01	0.772	0.255	<0.01	<0.01	20.2	<0.01	0.011	0.142
3B	7937	<0.01	158	0.031	<0.01	0.748	0.648	<0.01	<0.01	56.5	<0.01	0.052	0.746
4A	7938	<0.01	49.6	0.038	<0.01	0.775	0.262	<0.01	<0.01	21.2	<0.01	0.011	0.136
4B	7939	<0.01	155	0.013	<0.01	0.701	0.310	<0.01	<0.01	135	<0.01	0.123	1.36

Sample Origin	Sample ID												
		Cr	Cs	Cu	Dy	Er	Eu	Fe	Ga	Gd	Ge	Hf	Hg
		mg/l	mg/l	mg/l	mg/l	mg/l	mg/l	mg/l	mg/l	mg/l	mg/l	mg/l	mg/l
Lowest Reported Concentration		<0.01	<0.01	<0.01	<0.01	<0.01	<0.01	<0.01	<0.01	<0.01	<0.01	<0.01	<0.01
1A	7932	0.446	0.029	0.098	<0.01	<0.01	<0.01	75.6	0.014	<0.01	<0.01	<0.01	<0.01
1B	7933	0.874	0.045	0.178	<0.01	<0.01	<0.01	151	0.028	<0.01	<0.01	<0.01	<0.01
2A	7934	0.431	0.026	0.089	<0.01	<0.01	<0.01	68.1	0.014	<0.01	<0.01	<0.01	<0.01
2B	7935	0.931	0.048	0.190	<0.01	<0.01	<0.01	152	0.030	<0.01	<0.01	<0.01	<0.01
3A	7936	0.665	0.042	0.149	<0.01	<0.01	<0.01	113	0.022	<0.01	<0.01	<0.01	<0.01
3B	7937	2.112	0.090	0.422	<0.01	<0.01	<0.01	321	0.055	<0.01	<0.01	<0.01	<0.01
4A	7938	0.533	0.042	0.154	<0.01	<0.01	<0.01	93.6	0.018	<0.01	<0.01	<0.01	<0.01
4B	7939	2.45	0.082	0.810	<0.01	<0.01	<0.01	406	0.002	<0.01	<0.01	<0.01	<0.01

Sample Origin	Sample ID												
		Ho	Ir	K	La	Li	Lu	Mg	Mn	Mo	Na	Nb	Nd
		mg/l	mg/l	mg/l	mg/l	mg/l	mg/l	mg/l	mg/l	mg/l	mg/l	mg/l	mg/l
Lowest Reported Concentration		<0.01	<0.01	<0.01	<0.01	<0.01	<0.01	<0.01	<0.01	<0.01	<0.01	<0.01	<0.01
1A	7932	<0.01	<0.01	61.1	<0.01	0.013	<0.01	185	0.591	0.297	402	<0.01	<0.01
1B	7933	<0.01	<0.01	73.5	<0.01	0.030	<0.01	355	1.91	0.188	383	<0.01	<0.01
2A	7934	<0.01	<0.01	59.7	<0.01	0.012	<0.01	164	0.556	0.328	402	<0.01	<0.01
2B	7935	<0.01	<0.01	73.5	<0.01	0.029	<0.01	356	2.09	0.198	383	<0.01	<0.01
3A	7936	<0.01	<0.01	64.6	<0.01	0.019	<0.01	271	0.982	0.261	403	<0.01	<0.01
3B	7937	<0.01	<0.01	89.7	0.029	0.068	<0.01	722	5.603	0.064	390	<0.01	0.014
4A	7938	<0.01	<0.01	66.0	<0.01	0.016	<0.01	222	0.936	0.280	412	<0.01	<0.01
4B	7939	<0.01	<0.01	128	0.069	0.068	<0.01	853	9.15	0.008	475	<0.01	<0.01

Sample Origin	Sample ID												
		Ni	Os	P	Pb	Pd	Pr	Pt	Rb	Re	Ru	Sb	Sc
		mg/l	mg/l	mg/l	mg/l	mg/l	mg/l	mg/l	mg/l	mg/l	mg/l	mg/l	mg/l
Lowest Reported Concentration		<0.01	<0.01	<0.80	<0.01	<0.01	<0.01	<0.01	<0.01	<0.01	<0.01	<0.01	<0.01
1A	7932	1.698	<0.01	<0.80	0.045	<0.01	<0.01	<0.01	0.195	<0.01	<0.01	<0.01	<0.01
1B	7933	3.705	<0.01	<0.80	0.084	<0.01	<0.01	<0.01	0.275	<0.01	<0.01	<0.01	<0.01
2A	7934	1.478	<0.01	<0.80	0.039	<0.01	<0.01	<0.01	0.193	<0.01	<0.01	<0.01	<0.01
2B	7935	3.942	<0.01	<0.80	0.093	<0.01	<0.01	<0.01	0.291	<0.01	<0.01	<0.01	<0.01
3A	7936	2.599	<0.01	<0.80	0.071	<0.01	<0.01	<0.01	0.238	<0.01	<0.01	<0.01	<0.01
3B	7937	8.952	<0.01	<0.80	0.216	<0.01	<0.01	<0.01	0.480	<0.01	<0.01	<0.01	0.015
4A	7938	2.400	<0.01	<0.80	0.075	<0.01	<0.01	<0.01	0.245	<0.01	<0.01	<0.01	<0.01
4B	7939	14.486	<0.01	<0.80	0.364	<0.01	0.010	0.000	0.711	<0.01	<0.01	<0.01	0.014

Table 33: *(cont.)* Dissolved components of the top less dense (A) and deeper more dense (B) layers Cullinan mine No 7 Dam wastewater as determined by IC-PMS scan.

Sample Origin	Sample ID	Se	Si	Sm	Sn	Sr	Ta	Tb	Te	Th	Ti	Tl	Tm
		mg/l	mg/l	mg/l	mg/l	mg/l	mg/l	mg/l	mg/l	mg/l	mg/l	mg/l	mg/l
Lowest Reported Concentration		<0.01	<0.01	<0.01	<0.01	<0.01	<0.01	<0.01	<0.01	<0.01	<0.01	<0.01	<0.01
1A	7932	<0.01	57.2	<0.01	<0.01	0.517	<0.01	<0.01	<0.01	<0.01	0.147	<0.01	<0.01
1B	7933	<0.01	92.3	<0.01	<0.01	0.870	<0.01	<0.01	<0.01	<0.01	0.214	<0.01	<0.01
2A	7934	<0.01	58.7	<0.01	<0.01	0.466	<0.01	<0.01	<0.01	<0.01	0.149	<0.01	<0.01
2B	7935	<0.01	82.0	<0.01	<0.01	0.862	<0.01	<0.01	<0.01	<0.01	0.189	<0.01	<0.01
3A	7936	<0.01	73.3	<0.01	<0.01	0.693	<0.01	<0.01	<0.01	<0.01	0.189	<0.01	<0.01
3B	7937	<0.01	122	<0.01	<0.01	2.01	<0.01	<0.01	<0.01	<0.01	0.208	<0.01	<0.01
4A	7938	<0.01	60.1	<0.01	<0.01	0.779	<0.01	<0.01	<0.01	<0.01	0.157	<0.01	<0.01
4B	7939	<0.01	129	<0.01	<0.01	3.93	<0.01	<0.01	<0.01	<0.01	0.089	<0.01	<0.01

Sample Origin	Sample ID	U	V	W	Y	Yb	Zn	Zr
		mg/l	mg/l	mg/l	mg/l	mg/l	mg/l	mg/l
Lowest Reported Concentration		<0.01	<0.01	<0.01	<0.01	<0.01	<0.01	<0.01
1A	7932	<0.01	0.067	<0.01	<0.01	<0.01	<0.01	<0.01
1B	7933	<0.01	0.102	<0.01	<0.01	<0.01	<0.01	<0.01
2A	7934	<0.01	0.064	<0.01	<0.01	<0.01	<0.01	<0.01
2B	7935	<0.01	0.103	<0.01	<0.01	<0.01	<0.01	<0.01
3A	7936	<0.01	0.079	<0.01	<0.01	<0.01	<0.01	<0.01
3B	7937	<0.01	0.265	<0.01	<0.01	<0.01	0.217	<0.01
4A	7938	<0.01	0.083	<0.01	<0.01	<0.01	<0.01	<0.01
4B	7939	<0.01	0.383	<0.01	0.015	0.003	0.404	<0.01

G5: Post mineral acid treatment water quality

Table 34: Table 35: Laboratory report for water quality of the Cullinan mine wastewater after the mineral acid treatment (two repetitions).

WATERLAB (Pty) Ltd

Reg. No.: 1993/009165/07 V.A.T. No.: 4130107591

Building D
The Woods
41 De Havilland Cresent
Persequor Technopark
Meiring Naudé Drive
Pretoria

P.O. Box 283
Persequor Park, 0020
Tel: +2712 – 349 – 1066
Fax: +2712 – 349 – 2064
e-mail: admin@waterlab.co.za

SANAS Accredited Testing Laboratory No. T0391

CERTIFICATE OF ANALYSES
GENERAL WATER QUALITY PARAMETERS

Date received: 2014 - 11 - 25 Date completed: 2014 - 12 – 11

Project number: 248 Report number: 49244 Order number: -

Client name: North-West University (NWU) Contact person: Me. J. Strydom

Address: Faculty of Natural Science, Geology e-mail: Jessica.strydom@nwu.ac.za

Private Bag X6001, Potchefstroom, 2531 e-mail: 21212627@nwu.ac.za

Telephone: 018 299 1089 Facsimile: 018 299 2370 Mobile: 076 876 6247

Analyses in mg/ℓ (Unless specified otherwise)	Method Identification	Sample Identification	
		7.3	7.4
Sample Number		21612	21613
pH – Value at 25°C	WLAB001	4.6	3.7
Electrical Conductivity in mS/m at 25°C	WLAB002	415	412
Total Dissolved Solids (Calculated) *	WLAB003	2 109	2 098
Suspended Solids at 105°C *	WLAB004	24	28
Turbidity in N.T.U	WLAB005	10	4.7
Total Alkalinity as $CaCO_3$	WLAB007	<5	<5
Chloride as Cl	WLAB046	890	926
Sulphate as SO_4	WLAB046	406	395
Fluoride as F	WLAB014	3.3	2.7
Nitrate as N	WLAB046	2.5	3.0
Nitrite as N	WLAB046	0.1	<0.1
Total Phosphate as P *	WLAB031	1.9	9.0
Ortho Phosphate as P	WLAB046	1.3	5.4
Total Organic Carbon as C *	WLAB060	**	**
Dissolved Organic Carbon as C *	WLAB060	**	**
Oxygen Absorbed as O_2 (4-hour) *	WLAB019	**	**
Oil & Grease *	WLAB034	**	**
Free & Saline Ammonia as N	WLAB046	0.3	0.2
ICP-MS Scan [s]	---	See Attached Report: 49244-A	
% Balancing	---	97.8	98.2

*** = Not SANAS Accredited**
Tests marked "Not SANAS Accredited" in this report are not included in the SANAS Schedule of Accreditation for this Laboratory.

** Insufficient sample.

[s] = Analyses performed by a Sub-Contracted Laboratory
Results marked "Subcontracted Test" in this report are not included in the SANAS Schedule of Accreditation for this Laboratory

A. van de Wetering

Technical Signatory

Page 1 of 1

Table 35: Dissolved components of the for water quality of the Cullinan mine wastewater after the mineral acid treatment as determined by IC-PMS scan (two repetitions).

WATERLAB (PTY) LTD

CERTIFICATE OF ANALYSIS

Project Number : **248**
Client : **North West University**
Report Number : **49244-A**

Sample Origin	Sample ID	Ag (mg/L)	Al (mg/L)	As (mg/L)	Au (mg/L)	B (mg/L)	Ba (mg/L)	Be (mg/L)	Bi (mg/L)	Ca (mg/L)	Cd (mg/L)	Ce (mg/L)	Co (mg/L)
7.3	21612	0.000	3.11	0.016	0.001	0.561	0.170	0.000	0.000	158	0.001	0.002	0.063
7.4	21613	0.000	5.90	0.031	0.001	0.567	0.393	0.000	0.000	161	0.000	0.010	0.059

Sample Origin	Sample ID	Cr (mg/L)	Cs (mg/L)	Cu (mg/L)	Dy (mg/L)	Er (mg/L)	Eu (mg/L)	Fe (mg/L)	Ga (mg/L)	Gd (mg/L)	Ge (mg/L)	Hf (mg/L)	Ho (mg/L)
7.3	21612	0.004	0.018	0.028	0.000	0.000	0.000	6.240	0.026	0.000	0.000	0.000	0.000
7.4	21613	0.016	0.021	0.037	0.001	0.000	0.000	12.960	0.060	0.001	0.000	0.000	0.000

Sample Origin	Sample ID	In (mg/L)	Ir (mg/L)	K (mg/L)	La (mg/L)	Li (mg/L)	Lu (mg/L)	Mg (mg/L)	Mn (mg/L)	Mo (mg/L)	Na (mg/L)	Nb (mg/L)	Nd (mg/L)
7.3	21612	0.000	0.000	92	0.001	0.003	0.000	31	1.573	0.010	521	0.000	0.000
7.4	21613	0.000	0.000	93	0.007	0.003	0.000	22	1.343	0.011	488	0.000	0.000

Sample Origin	Sample ID	Ni (mg/L)	Os (mg/L)	P (mg/L)	Pb (mg/L)	Pd (mg/L)	Pt (mg/L)	Rb (mg/L)	Rh (mg/L)	Ru (mg/L)	Sb (mg/L)	Sc (mg/L)	Se (mg/L)
7.3	21612	0.634	0.000	2.3	0.002	0.000	0.000	0.459	0.000	0.000	0.004	0.000	0.000
7.4	21613	0.466	0.000	7.1	0.017	0.000	0.000	0.453	0.000	0.000	0.006	0.000	0.003

Sample Origin	Sample ID	Si (mg/L)	Sm (mg/L)	Sn (mg/L)	Sr (mg/L)	Ta (mg/L)	Tb (mg/L)	Te (mg/L)	Th (mg/L)	Ti (mg/L)	Tl (mg/L)	Tm (mg/L)	U (mg/L)
7.3	21612	7.0	0.000	0.000	2.5	0.000	0.000	0.000	0.000	0.134	0.001	0.000	0.000
7.4	21613	5.3	0.001	0.000	2.6	0.000	0.000	0.000	0.000	0.138	0.001	0.000	0.002

Sample Origin	Sample ID	V (mg/L)	W (mg/L)	Y (mg/L)	Yb (mg/L)	Zn (mg/L)	Zr (mg/L)
7.3	21612	0.005	0.000	0.000	0.000	0.086	0.000
7.4	21613	0.024	0.000	0.003	0.000	0.112	0.002

H: ZETA-POTENTIAL ANALYSIS

Table 36: Measurement made during the zeta potential auto titrations by Dr Albrecht Truter at Micron Scientific.

Sample Name	General Notes	Measurement Date and Time	T (°C)	ZP (mV)	Mob (µmcm/Vs)	Cond (mS/cm)	pH
N7 Dam Suspensie		31/10/2014 10:42	25				
N7 Dam Suspensie 1		31/10/2014 10:43	25	-43.9	-3.443	2.16	9.02
N7 Dam Suspensie 2		31/10/2014 10:45	25	-45.3	-3.549	2.17	9.03
N7 Dam Suspensie 3		31/10/2014 10:46	25	-43.5	-3.411	2.17	9.05
N7 Dam Suspensie 4		31/10/2014 10:53	24.9	-45.2	-3.539	2.18	8.32
N7 Dam Suspensie 5		31/10/2014 10:55	25	-43.4	-3.402	2.18	8.34
N7 Dam Suspensie 6		31/10/2014 10:57	25	-43.3	-3.397	2.18	8.38
N7 Dam Suspensie 7		31/10/2014 11:32	25	-43.2	-3.384	2.18	7.33
N7 Dam Suspensie 8		31/10/2014 11:34	25	-42.3	-3.316	2.17	7.36
N7 Dam Suspensie 9		31/10/2014 11:36	25	-42.3	-3.313	2.17	7.4
N7 Dam Suspensie 10		31/10/2014 12:15	24.9	-40.6	-3.179	2.18	6.33
N7 Dam Suspensie 11		31/10/2014 12:17	25	-42.6	-3.343	2.17	6.35
N7 Dam Suspensie 12		31/10/2014 12:19	25	-42.2	-3.308	2.17	6.39
N7 Dam Suspensie 13		31/10/2014 12:30	25.1	-41.1	-3.222	2.18	5.32
N7 Dam Suspensie 14		31/10/2014 12:32	24.9	-41.3	-3.241	2.18	5.35
N7 Dam Suspensie 15		31/10/2014 12:33	25	-41	-3.216	2.18	5.37
N7 Dam Suspensie 16		31/10/2014 12:39	25	-39.5	-3.093	2.2	4.28
N7 Dam Suspensie 17		31/10/2014 12:41	25	-37.7	-2.958	2.19	4.3
N7 Dam Suspensie 18		31/10/2014 12:42	25	-37.8	-2.964	2.19	4.33
N7 Dam Suspensie 19		31/10/2014 12:46	25	-37.4	-2.933	2.36	3.15
N7 Dam Suspensie 20		31/10/2014 12:47	25	-37	-2.897	2.34	3.17
N7 Dam Suspensie 21		31/10/2014 12:49	25	-36.5	-2.863	2.34	3.18